UCRL9588

UNIVERSITY OF CALIFORNIA

Ernest O. Lawrence Radiation Laboratory

THE POSITIVE COLUMN IN A LONGITUDINAL MAGNETIC FIELD

TWO-WEEK LOAN COPY

This is a Library Circulating Copy which may be borrowed for two weeks. For a personal retention copy, call Tech. Info. Division, Ext. 5545

DISCLAIMER

This document was prepared as an account of work sponsored by the United States Government. While this document is believed to contain correct information, neither the United States Government nor any agency thereof, nor the Regents of the University of California, nor any of their employees, makes any warranty, express or implied, or assumes any legal responsibility for the accuracy, completeness, or usefulness of any information, apparatus, product, or process disclosed, or represents that its use would not infringe privately owned rights. Reference herein to any specific commercial product, process, or service by its trade name, trademark, manufacturer, or otherwise, does not necessarily constitute or imply its endorsement, recommendation, or favoring by the United States Government or any agency thereof, or the Regents of the University of California. The views and opinions of authors expressed herein do not necessarily state or reflect those of the United States Government or any agency thereof or the Regents of the University of California.

UCRL-9588
UC-20 Controlled Thermonuclear Processes
TID-4500 (16th Ed.)

UNIVERSITY OF CALIFORNIA
Lawrence Radiation Laboratory
Berkeley, California

Contract No. W-7405-eng-48

THE POSITIVE COLUMN IN A LONGITUDINAL MAGNETIC FIELD

George A. Paulikas

(Ph.D. Thesis)

February 27, 1961

Printed in USA. Price $2.25. Available from the
Office of Technical Services
U. S. Department of Commerce
Washington 25, D.C.

THE POSITIVE COLUMN IN A LONGITUDINAL MAGNETIC FIELD

Contents

Abstract 3

I. Introduction and Purpose 5

A. List of Symbols 8

II. Theory of the Positive Column in a Longitudinal Magnetic Field

A. The Classical Theory 9

B. Theory of Ecker 12

C. Analyses of Stability 14

III. Apparatus and Procedure 21

IV. Results

A. The Longitudinal Electric Field and the Critical Magnetic Field 31

B. The Radial Potential Distribution 47

C. Properties of the Instability 48

V. Summary and Conclusions 74

Acknowledgments 76

Appendices

A. Curves of Measurements of the Longitudinal Electric Field 77

B. Curves of Measurements of the Radial Potential Distribution 87

References 97

THE POSITIVE COLUMN IN A LONGITUDINAL MAGNETIC FIELD

George A. Paulikas

Lawrence Radiation Laboratory
University of California
Berkeley, California

February 27, 1961

ABSTRACT

The positive column of a glow discharge is shown to become hydromagnetically unstable when immersed in a longitudinal magnetic field of the order of 1 kilogauss. The instability transforms the azimuthally symmetric column into a constricted, rotating, helical state; neither this new steady state nor its properties are predicted by classical theories. The critical magnetic field, B_c, describing the onset of the instability, varies approximately inversely as the tube radius and directly as the square root of the ion mass; e.g., in a helium discharge at a pressure of 1 mm Hg and in a 0.9-cm-radius tube we find $B_c = 2.4$ kilogauss. For $B > B_c$ the longitudinal electric field increases with magnetic field and indicates particle losses in excess of classical predictions. The occurrence of this instability explains the previously mysterious "anamolous diffusion" observed by Lehnert.

The properties of the helical state have been measured in H_2, D_2, He, and Ne as functions of gas pressure and tube radius. For the above example we find the angular frequency of rotation of the luminous spiral to be 0.8×10^5 sec^{-1} with a wave length of about 40 cm. Frequency decreases with increasing pressure, increasing tube radius, and increasing ion mass. The wave length is found to decrease with increasing pressure. These dependences, as well as the values of B_c are in good agreement with predictions of the perturbation theory of Kadomtsev and Nedospasov. The onset of instability as predicted by the entirely different sheath-instability theory of Hoh is not in as good agreement with the experimental results;

Hoh's theory does not include a description of the nature or build-up of the presumed instability. A comparison of measurements of radial potential distributions with the theory of Ecker indicates the absence of anamolous effects for $B < B_c$.

I. INTRODUCTION AND PURPOSE

The low-pressure glow discharge (10^{-2} to 10 mm Hg) has been extensively studied for the past half century.[1] A schematic diagram of the spatial distribution of the dark and luminous zones and the longitudinal electric field E_z is presented in Fig. 1.

Bounded at one end by the Faraday dark space and at the other by the anode dark space is the positive column— "positive" because its electrical potential lies above that of the various glows and dark spaces near the cathode. The constant longitudinal electric field and the slowly varying radial field indicate that in the column $n_+ \approx n_- = n$. Electron densities are typically of the order of 10^9 to 10^{11} per cm^3. Electron temperatures of several electron volts are also typical, with ion temperatures considerably lower than this. Thus the Debye length[1a] is a small fraction of the dimensions of the vessel and we are dealing with a quasi-neutral, weakly ionized plasma.

Relatively few authors have investigated the behavior of such a plasma in a longitudinal magnetic field. The early experiments of Cummings and Tonks,[2] Rohklin,[3] and Reichrudel and Spivak,[4] although limited by the rather low available magnetic fields and complicated by end effects, were found to give results consistent with the theories of Tonks,[5] Langmuir and Tonks,[6] and Schottky.[7]

Bohm and collaborators measured the electron densities in the vicinity of a short low-pressure arc in a magnetic field and concluded that the charged particle losses were much more rapid than would be predicted by assuming ambipolar diffusion.[8] This led to speculation about the possibility of enhanced diffusion, perhaps due to electrical oscillations in the plasma. Simon, however, showed theoretically that the diffusion across the field need not be ambipolar if the discharge is short, because the large anisotropy in the conductivity of the plasma permits end effects to short circuit the flow of electrons across the magnetic field.[9] Such a modified picture of the particle losses explained the results of Bohm, as well as the experiment of Neideigh.[10]

Although the experiments of Bohm were not carried out in the glow discharge, they nevertheless prompted Bickerton and von Engel[11]

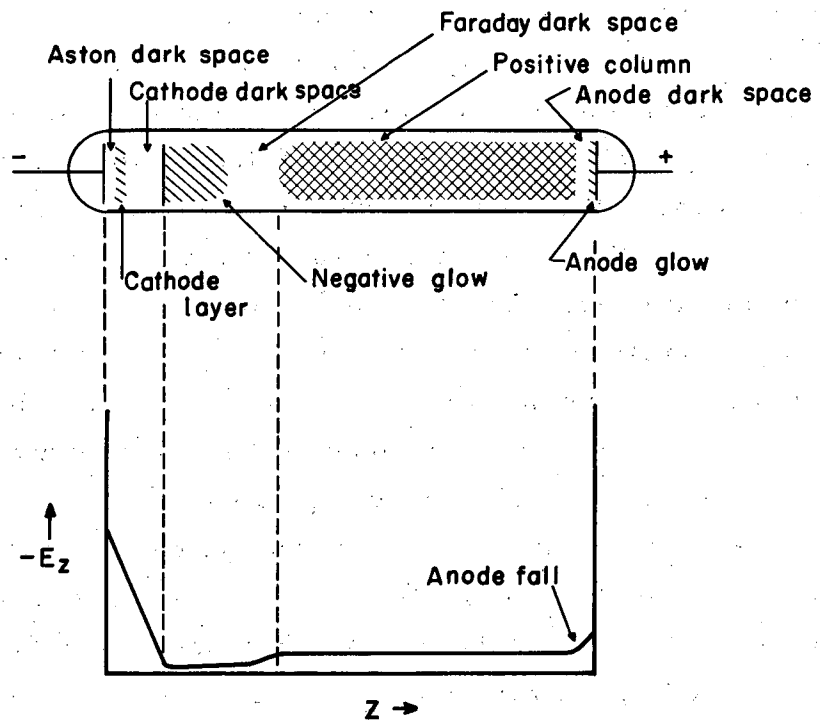

MU-22915

Fig. 1. Schematic diagram of spatial distribution of dark and luminous zones and longitudinal field E_z in a glow discharge.[1]

to re-examine the positive column in an experiment which avoided the end effects discussed by Simon. Their measurements of the electric fields, as well as the charged-particle distribution as functions of a longitudinal magnetic field up to 600 gauss, were in good agreement with the classical theories of the positive column. No evidence of an increase of particle losses was observed. This work has been extended by Lehnert[12] and Hoh and Lehnert[13] to considerably stronger magnetic fields and in geometries designed to eliminate end effects. Measurements of the longitudinal electric field as a function of the applied magnetic field show that above some critical magnetic field B_c, the losses of particles no longer decrease with increasing magnetic field, as predicted, but rather increase with higher magnetic fields.

A number of other magnetically confined plasmas, widely differing in geometry, temperature, and percentage of ionization, also show losses considerably in excess of theoretical prediction.[14-16] These results have revived interest in the possibility of enhanced diffusion and a spate of papers has appeared discussing the problem in terms of microscopic and macroscopic instabilities.[17-21]

Study of the positive column has shown that at B_c a macroscopic instability appears in the column. The observed increase in particle losses is associated with the formation of a new azimuthally asymmetric steady state.[22] This work is an experimental investigation of the development and the properties of this anomalous steady state of the positive column, as well as a search for possible enhanced losses preceding the large-scale instability. Studies of the onset and parameters of the instability are presented and compared with the theories of Hoh[20] and Kadomtsev and Nedospasov.[21]

A. List of Symbols

B	Magnetic field.
D_a	Ambipolar diffusion coefficient at field B.
$D_{\mp}$	Diffusion coefficients of electrons or ions.
E_z	Axial electric field.
$\Gamma_{\mp r}$	Radial particle flux of electrons or ions.
J_0, J_1	Bessel functions of order zero, order one.
$\vec{j}$	Electric current density.
κ	Boltzmann constant.
$k = \frac{2\pi}{\lambda}$	Wave number.
$\Lambda \pm$	Mean free path of ions or electrons.
λ	Wave length.
$\mu_{\mp}$	Electron or ion mobilities.
$m_{\mp}$	Electron or ion masses.
$n_{\mp}$, n	Particle densities of electrons or ions.
ν_i	Number of ionizations per second per electron.
$\Omega_{\mp}$	Electron or ion cyclotron frequencies.
p	Neutral gas pressure (reduced to $0^{\circ}C$).
R	Discharge tube radius.
$T_{\mp}$	Electron or ion temperature.
$\tau_{\mp}$	Mean time between collisions of electron or ion with neutral particle.
$U(r)$	Radial potential distribution
$v_{\mp}$, $v_{\mp r}$, z	Electron or ion drift velocities and components.
v_+	Ion thermal velocity.

II. THEORY OF THE POSITIVE COLUMN IN A LONGITUDINAL MAGNETIC FIELD

A. The Classical Theory

The stable positive column is a quasi-neutral, weakly ionized plasma whose properties can be adequately predicted by considering the particle and energy balances in a given geometry.[7] When the positive column is formed, the rapid diffusion of electrons creates at the tube wall a region of negative charge several Debye lengths thick (typically 10^{-2} cm), the wall sheath. Only the fastest electrons can overcome this potential barrier; the flow of electrons is reduced, the flow of ions to the wall is increased. Thus unequal mobilities produce space-charge effects which couple the flow of positive and negative carriers so that no net electrical current reaches the insulating wall, i.e., $\Gamma_{+r} = \Gamma_{-r}$ for singly charged ions. The particle losses in the presence of a longitudinal magnetic field B are then described by the ambipolar diffusion coefficient[23]

$$D_a(B) = \frac{D_+\mu_- + D_-\mu_+}{\mu_+ + \mu_-} \cdot \frac{1}{1 + \mu_+ \mu_- B^2} , \qquad \text{(II-1)}$$

where $D_\pm$, $\mu_\pm$ are the diffusion coefficients and mobilities at $B = 0$. Volume recombination is neglected; however, Pahl has shown that the inclusion of this loss mechanism does not materially affect the behavior of the column.[24] In the noble gases, as well as hydrogen and deuterium, it is also permissible to neglect electron attachment. With these simplifying assumptions, the particle balance is described by

$$\nabla^2 n(\vec{r}) + \frac{\nu_i}{D_a} n(\vec{r}) = 0 , \qquad \text{(II-2)}$$

where ν_i is the number of ion pairs produced per second per electron. In a long cylindrical geometry, provided ν_i is independent of n, the solution of Eq. (II-2) is

$$n(r) = n(0) \; J_0 \left(\sqrt{\frac{\nu_i}{D_a}} \; r \right) , \qquad \text{(II-3)}$$

where r is the radial coordinate. From the boundary conditions we can then obtain expressions relating the ionization rate and hence the electron temperature T_- to the parameters of the discharge for the two pressure regions of interest,[11] described by the average mean free path Λ:

$$\nu_i = \left(\frac{2.4}{R}\right)^2 D_a \qquad \text{for } \Lambda << R , \tag{II-4a}$$

$$\frac{4D_a}{Rv_+} = \frac{1}{x}\frac{J_0(x)}{J_1(x)} , \qquad x = \left(\frac{\nu_i}{D_a}\right)^{1/2} R \qquad \text{for } \Lambda \approx R. \tag{II-4b}$$

The form of $\nu_i(T_-)$ depends strongly upon the behavior of the ionization cross section near threshold as well as upon assumptions of the shape of the electron-velocity distribution, which is not necessarily Maxwellian. Measurements of the electron-velocity distributions in a discharge with standing striations show that a distinct high-energy group is present.[25] Since the usual "uniform" column almost invariably contains moving striations,[26] a similar high-energy group may be present and contribute significantly to ν_i.

Either of Eqs. (II-4) may be solved for T_- as a function of the magnetic field for a given pressure and radius, although an additional assumption regarding ion temperatures is necessary for solution of (II-4b). If quadratic ionization processes are included, i.e., ionizations from excited atomic states, the plasma-balance equations cannot be reduced to the simple form of Eqs. (II-4); the result of this modification is to depress electron temperture slightly.[27]

The longitudinal electric field is determined by the power input required to maintain the electron distribution at a temperature T_- determined from Eqs. (II-4). If $X(T_-)$ denotes the fractional energy lost by an electron in a collision, including elastic, inelastic, and wall losses, the electric field is found to be

$$E_z = \left(\frac{64}{\pi}\right)^{1/4} (X(T_-))^{1/2} \frac{\kappa T_-}{\Lambda_- e} \text{ volts/cm}, \qquad \text{(II-5)}$$

where Λ_- is the mean free path of the electron.[28] The effect of the longitudinal magnetic field will be to decrease the electron temperature, by decreasing particle losses, and this will be reflected in a diminished longitudinal field. This has been confirmed experimentally at low magnetic fields by the experiment of Bickerton and von Engel.[11] A departure from the monotonic decrease of E_z with increasing B, such as found by Lehnert and Hoh at fields in the kilogauss range, may consequently be taken as an indication of a change in the particle loss.[12,13] Ecker has pointed out, however, that the longitudinal electric field is a rather insensitive measure of the particle loss; large changes in the diffusion coefficient near the wall are required to alter E_z noticeably.[29]

The radial potential distribution in a cylindrical column, if one assumes ambipolar diffusion and neglects ion-electron interactions, is found from the equation of motion to be

$$\frac{eU(r)}{\kappa T_-} = \frac{1 + \mu_+\mu_- B^2\left(\frac{\mu_+}{\mu_-} - \frac{T_+}{T_-}\right)}{1 + \mu_+\mu_- B^2} \ln\left[J_0\left(\frac{2.4r}{R}\right)\right], \qquad \text{(II-6)}$$

which exhibits a monotonic increase or decrease with radius depending on the relations between μ_+, μ_-, T_+, T_-. The reduction of the radial field with increasing magnetic field as predicted by Eq. (II-6) has been confirmed experimentally[11]; however, the results display curious asymmetries, probably due to the perturbing effects of the probes used in the measurements.

B. Theory of Ecker

The generalization of the analysis of the radial potential distribution to include an arbitrary electron-ion interaction term η, perhaps describing microinstabilities,[17, 18, 19] yields the expression[29]

$$\frac{eU(r)}{\kappa T_-} = \frac{1+\mu_+\mu_- B^2\left(\frac{\mu_+}{\mu_-} - \frac{T_+}{T_-}\right)}{1+\mu_+\mu_- B^2} \ln\left[J_0\left(\frac{2.4r}{R}\right)\right]$$

$$+ \frac{\mu_+\mu_- B^2\left(1+\frac{T_+}{T_-}\right)}{1+\mu_+\mu_- B^2} \ln \frac{1+\frac{\sigma_{0+}+\sigma_{0-}}{1+\mu_+\mu_- B^2} J_0\left(\frac{2.4\,r}{R}\right)}{1+\frac{\sigma_{0+}+\sigma_{0-}}{1+\mu_+\mu_- B^2}} \tag{II-7}$$

$$\sigma_{0\pm} = e\eta\,\mu_\pm\, n(0)$$

If the second term on the right of the equation is appreciable, the shape of the U(r) vs r curve is noticeably modified and develops a minimum as shown in Fig. 2. Accurate determination of the radial potential distribution can thus be used as a rather sensitive measure of the presence or absence of any enhanced interaction.

The radial potential may also serve as an indicator of deviations from ambipolar diffusion. "Simon" diffusion presupposes no radial flow of electron, i.e., $\Gamma_{-r} = 0$. The equation for the radial potential, in the absence of any enhanced interaction, takes the simple form

$$\frac{eU(r)}{k\,T_-} = \ln\left[J_0\left(\frac{2.4\,r}{R}\right)\right], \tag{II-8}$$

which is independent of the magnetic field. Inclusion of the interaction parameter η yields

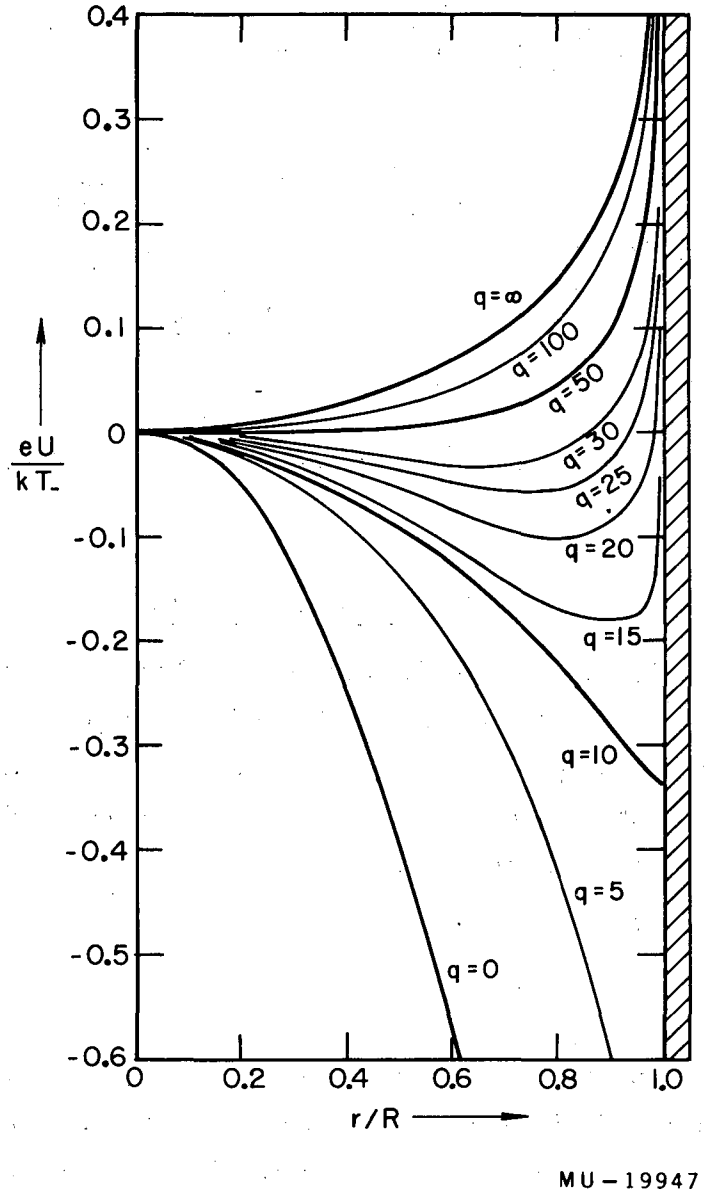

Fig. 2. The ambipolar radial potential distribution from the theory of Ecker[29] plotted as a function of the relative radial distance r/R for values of the parameter $q = \mu_+\mu_- B^2 \cdot \sigma_{0+} + \sigma_{0-} = 5$; $T_-/T_+ = 10$.

$$\frac{eU(r)}{\kappa T_-} = \ln\left[J_0\left(\frac{2.4r}{R}\right)\right] - \left(1 + \frac{T_+}{T_-}\right)\sigma_{0+}\left(1 - J_0\left(\frac{2.4r}{R}\right)\right)$$

$$+\left(1 + \frac{T_+}{T_-}\right)\mu_+^2 B^2 \ln \frac{1 + \dfrac{\sigma_{0+} + \sigma_{0-}}{1 + \mu_+^2 B^2} J_0\left(\dfrac{2.4r}{R}\right)}{1 + \dfrac{\sigma_{0+} + \sigma_{0-}}{1 + \mu_+^2 B^2}} . \qquad \text{(II-9)}$$

A plot of a family of curves derived from Eq. (II-9) is shown in Fig. 3.

C. Analyses of Stability

Recently Hoh[20] and Kadomtsev and Nedospasov[21] have theoretically investigated the stability of the positive column from two differing standpoints. Hoh starts with the criterion, due to Bohm, for the stability of the sheath surrounding the plasma.[8] The radial ion velocity at the sheath must satisfy

$$v'_{+r} \geqslant \left(\frac{\kappa T_-}{m_+}\right)^{1/2} , \qquad \text{(II-10)}$$

where T_- is the electron temperature and m_+ ionic mass. By considering the effect of the magnetic field upon the radial drift velocity of the ions, he is able to show that Eq. (II-10) is not satisfied for magnetic fields

$$B \geqslant B_c = \frac{1}{(\mu_{+1}\mu_{-1})^{1/2}} \left\{ 2.4 \frac{g'}{R} p - p^2 \right\}^{1/2}$$

(II-11)

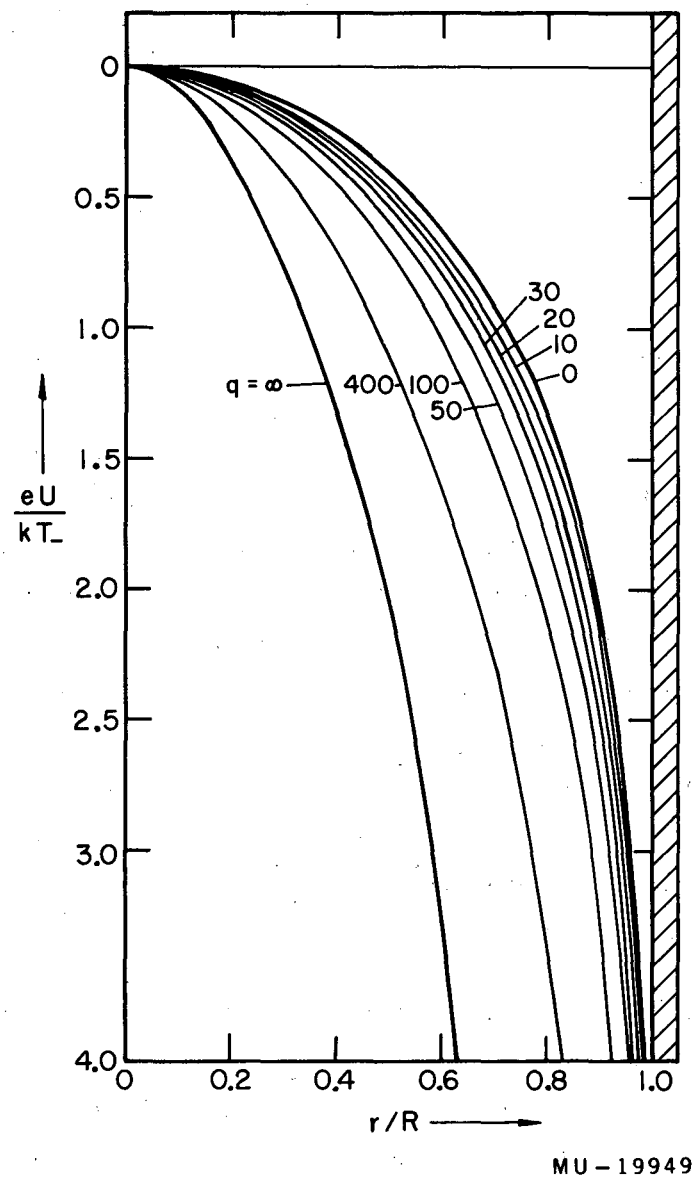

Fig. 3. The radial potential distribution for Simon diffusion from the theory of Ecker[29] plotted vs the relative radial distance r/R for values of the parameter $q = \mu_+^2 B^2 \cdot \sigma_{0+} + \sigma_{0-} = 5$; $T_-/T_+ = 10$.

where

$$g' = \left(\frac{\kappa m_+}{T_-}\right)^{1/2} \frac{T_+ + T_-}{e} \cdot \frac{\mu_{+1}\mu_{-1}}{\mu_{+1}+\mu_{-1}} \cdot \frac{J_1\left(\frac{2.4r'}{R}\right)}{J_0\left(\frac{2.4r'}{R}\right)} . \tag{II-12}$$

Here $\mu_{\pm 1}$ are the mobilities at 1 mm Hg and p is the neutral gas pressure. The primed quantities are to be evaluated at the sheath edge, a circumstance which introduces some uncertainty into the value of g'.

Hoh postulates that when Bohm's criterion is not satisfied, an instability of the sheath develops which then transports charged particles across the field at a rate in excess of ordinary collisional diffusion. The mechanism by which such a possible sheath instability develops to affect the macroscopic behavior of the plasma is not discussed. The expression for B_c (Eq. II-11) is quite sensitive to assumptions regarding the ionic species, but depends relatively weakly on the electron temperature T_-. Hall has criticized this approach to stability considerations by pointing out that Bohm's criterion is not applicable in the case of the positive column, as the potential drop across the sheath is only of the order of a few $\frac{\kappa T_-}{e}$.[30] The nonsatisfaction of Bohm's criterion is interpreted as an argument to re-examine and modify the model used in the derivation of Eq. (II-10), rather than an indication of a true instability.

Kadomtsev and Nedospasov approach the stability problem by a perturbation analysis of the positive column. Their treatment is focused upon a region of the magnetic fields where $\Omega_- \tau_- >> 1$ and $\Omega_+ \tau_+ << 1$, where $\Omega_\pm$, $\tau_\pm$ are the ion and electron cyclotron frequencies and the mean times between collisions with neutrals. Such an approximation is quite valid, for our experimental conditions, in the vicinity of the critical magnetic field. Further it is assumed that the conditions in the unperturbed state are governed by ambipolar diffusion and single-stage ionization; two-step processes and end effects are neglected. The equations of motion and continuity

$$\frac{\kappa T_{\mp}}{m_{\mp} n} \nabla n = \mp \frac{e}{m_{\mp}} \vec{v}_{\mp} \times \vec{B} \pm \frac{e}{m_{\mp}} \nabla V - \frac{\vec{v}_{\mp}}{\tau_{\mp}} ,$$

(II-13a)

$$\frac{\partial n}{\partial t} + \nabla (n \vec{v}_{+}) = \frac{\partial n}{\partial t} + \nabla (n \vec{v}_{-}) = \nu_i n$$

can then be simplified and combined to yield

$$\frac{\partial n}{\partial t} + \frac{\mu_-}{\Omega_- \tau_-} \vec{b} \cdot \nabla V \times \nabla n - \frac{D_-}{(\Omega_- \tau_-)^2} \nabla^2 n + \frac{\mu_-}{(\Omega_- \tau_-)} \nabla \cdot (n \nabla_\perp V) +$$

$$+ \frac{\partial n}{\partial z} \left(\mu_- n \frac{\partial V}{\partial z} - D_- \frac{\partial n}{\partial z} \right) = \nu_i n \; ; \; \vec{b} = \frac{\vec{B}}{B} ;$$

(II-13b)

$$\frac{\partial n}{\partial t} - \mu_+ \nabla \cdot (n \nabla V) = \nu_i n .$$

Perturbations of the form $J_1 (3.83r/R) \exp [i(m\Phi + kz - \omega t)]$, where Φ is the aximuthal angle, are now introduced into the potential as well as the density distribution, so that

$$n(\vec{r}, t) = n_0 J_0 (2.4/R) + n_1 J_1 (3.83r/R) \exp [i(m\Phi + kz - \omega t)] .$$

(II-14)

When Eq. (II-14) and its equivalent for $U(\vec{r})$ are substituted into Eq. (II-13b), a dispersion relation giving ω as a function of k is obtained. From the condition that $\mathrm{Im}(\omega) < 0$, the requirements for stability under such a perturbation can then be determined. The behavior of Eqs. (II-13b) under perturbations of general form $n_1(r)$, $U_1(r)$ is not discussed. The choice of the form of the perturbation,

$J_1(3.83r/R)$, is arbitrary; the effect of the second term on the right of Eq. (II-14) is to introduce an asymmetry into the density distribution.

The qualitative physical picture thus consists of studying the time dependence of perturbations in the plasma. In the absence of a magnetic field, a disturbance in the particle density will soon disappear because of a rapid diffusion of particles from the region of high charge density. The presence of a sufficiently strong magentic field, however, will retard the diffusion, and the perturbation in density and the associated kink in the current will persist for some time. An off-center current channel can thus develop, which together with $\vec{j} \times \vec{B}$ forces, will cause the initial disturbance to grow.

For stability, therefore,

$$\mathrm{Im}(\omega) = \left(\frac{3.83}{R}\right)^2 \frac{D_-}{y(\Omega_- \tau_-)^2} \frac{1}{\left[\left(\frac{0.33}{\Omega_- \tau_-} m \frac{\mu_-}{\mu_+}\right)^2 + \left(\frac{1+y}{y} + \frac{k^2}{0.79} \frac{\mu_-}{\mu_+} \frac{R}{3.83}\right)^2\right]}$$

$$\left\{ - \frac{(1.28+y)}{0.8(y+1)} x^4 - (2+y)x^2 - 0.12 \frac{\mu_-}{\mu_+} \frac{ym^2}{y+1} - 0.6\,(1+y) + 0.2\,xyv^* \frac{\mu_-}{\mu_+} \right\} < 0 , \qquad \text{(II-15)}$$

where

$$x = \frac{k\Omega_- \tau_- R}{3.83} , \quad v^* = \frac{v_{-z} R}{2.4\, D_-} , \text{ and } y = \frac{\mu_+}{\mu_-} (\Omega_- \tau_-)^2 .$$

Since the sign of Eq. (II-15) depends only on the terms in curly brackets, the conditions for stability can be simplified to

STUDENT & ALUMNI PLACEMENT CENTER
7TH PHD BULLETIN
MARCH 3 - 7, 1969

Campus interviews with employers will be completed effectively by April. (Camp Recruiting does not normally continue during the Summer quarter). Those candidates who are on file, and who may not have resolved their employment situation, should remain in close contact with their placement interviewers in order to take advantage of opportunities listed directly by employers.

It would be appreciated if all offers, acceptances of offers, address changes, be reported promptly to the Placement Center.

* * * * *

The following companies will interview at the Placement Center March 3 - 7. U citizenship is required for all firms unless marked with a single asterisk (*) which indicates that the company will interview candidates who are U.S. citizens or are possessing a permanent resident visa AT THIS TIME, or a double asterisk which indicates that there are no citizenship requirements unless specifically noted. SUMMER opportunities will be specifically noted below the description of the company.

* * * * *

The Directory of Canadian Employers 1968-1969 edition is available for distribution to students who are Canadian citizens. Interested students can obtain a copy from the Career Division of the Placement Center.

* * * * *

MON Mar 3 — *LITTON INDUSTRIES, ADVANCED MARINE TECHNOLOGY DIVISION, Culver City, California—PhD: Marine Engr, Naval Arch, Math (OR)

This division was established for the purpose of applying system techniques to marine design and operation. Primary effort is made military and commercial marine systems. Additional studies are under way or have been recently completed for the Department of Transportation, the Maritime Administration, and the U.S. Navy (on the subject of Standardized Propulsion Systems). Current assignments in System Analysis, Hull Structural Design, Marine Engineering and Naval Architecture.

MON
Mar 3

PHYSICS INTERNATIONAL, San Leandro, Calif.--PhD: EE, ME, Aero E, Mat Sci, Physics (Geophysics, solid state, and high energy).

Research and development in areas of pulsed power and electron beam technology, dynamic high-pressure studies, mechanical response of materials and structures to high amplitude short duration loads, strong shock phenomena in gases, plasma interactions of ultra high current electron beams, interactions of electrons and photons with solids, etc.

MON
Mar 3

SYSTEMS, SCIENCE AND SOFTWARE, La Jolla, Calif.--PhD: Physics, EE ME, Engr Sci.

A relatively recently formed research organization with major research efforts in applied theoretical physics on defense-related problems as well as other non-defense areas. Positions for applied physicists to work in the areas of nuclear radiation, transport electronic and electromagnetic phenomena; for Electronic Engineers to perform analysis, design and testing of circuits and systems operation in nuclear radiation environment; for Solid State Physicists to investigate radiation effects in semi-conductor components and electronic circuits; for Hydrodynamicists to conduct applied research in high-temperature hydrodynamic phenomena, geophysics, shock waves in solids, explosive devices, etc.

NON-TUE
Mar 3,4

HUGHES AIRCRAFT COMPANY, Southern California locations

Engaged in the research, design and development of a broad line of electronic and electro-mechanical components and systems. Positions as follows:

1) Aerospace Engineering Divisions, Culver City--engaged in the design and development of a line of electronic and electro-mechanical components and systems--(PhD: EE)

2) Ground Systems Group, Fullerton--positions in applied research design, development and field support of advanced electronic information systems and hardware--(PhD: EE)

3) Electron Dynamics Division, Torrance--Applied research and development of advanced electron devices--PhD: EE, Physics;

4) Research Laboratories, Malibu, Calif.--Applied research in such programs as semiconductor physics, ion physics, propulsion research, surface interaction, laser technology, quantum electronics, etc.--(PhD: EE, Physics)

TUE
Mar 4

NASA - MANNED SPACECRAFT CENTER, Houston, Texas--PhD: EE, ME (incl Aero), Math, Physics

The functions of the Center include conceptual design, basic research, test, development and evaluation of spacecraft and their systems. Additional functions include spacecraft flight control, mission planning, mission analysis, recovery operations and flight crew training, including the development of operational requirements for flight crew personnel. Engineering positions assisting in the first and subsequent lunar landings. Employment will begin in July.

THUR
Mar 6

*CORNING GLASS WORKS, Sunnyvale, Calif.; Provo, Utah; and Nationwide

Major manufacturer of integrated circuits. Positions with Corning Glass and its subsidiary, Signetics, in Circuit Design and Development--(PhD: EE or Physics); Process Design and Development--(PhD: Chem, Physics, EE); Research and Development--(PhD: EE, Chem, Physics, Material Sci).

THUR-FRI
Mar 6,7

LITTON INDUSTRIES, LITTON SYSTEMS, INC., GUIDANCE AND CONTROL SYSTEMS DIVISION, Woodland Hills, Calif.--PhD: EE, ME, IE, Comp Sci.

One of the leading developers of navigation systems and special purpose computers utilized on military and commercial aircraft, probes, etc. Positions for Engineers to design and develop microelectronic inertial guidance navigation systems and control systems, including digital and analog computers, and complete support equipment lines.

FRI
Mar 7

**BURR-BROWN RESEARCH CORP., Tuscon, Arizona--PhD: EE

Manufacturer of complex electronic components. Positions in design and development engineering in areas of operational amplifiers & circuitry.

FRI
Mar 7

RESEARCH ANALYSIS CORPORATION, McLean, Virginia--PhD: Math, Stat, IE (OR), Engineering, Computer Sciences, Physics

An independent and nonprofit organization performing advanced operations and systems analysis on various government contracts. Position as members of the technical staff applying operations research and systems analysis techniques to solve military and social problems.

FRI
Mar 7

**TEKTRONIX, Beaverton, Oregon--PhD: Physics, Chem, Chem E, Mat Sci.

Manufactures precision laboratory oscilloscopes & related equipment. Positions in circuit design & instrument evaluation, mechanical design, materials investigation & manufacturing process development for display devices.

UNIVERSITY OF CALIFORNIA
STUDENT & ALUMNI PLACEMENT CENTER
BUILDING T-6
BERKELEY, CALIFORNIA 94720

0284

MARTIN HALSETH
BLDG 16
LRL BERKELEY
CAMPUS

$$Kx^4 + Fx^2 + G > 0.16\ mv^* x\ (\mu_-/\mu_+)\ , \tag{II-16}$$

where

.886

$$K = \frac{1.28 + y}{y(y+1)}\ ;\ F = \frac{0.8(y+2)}{y}\ ;\ G = \frac{0.48(1+y)}{y} + 0.1\ \frac{\mu_-}{\mu_+}\ \frac{m^2}{1+y}\ .$$

Hence only for $m > 0$ will the plasma be unstable. Note also that an electron drift velocity v_{-z} is necessary. A current is required, but its magnitude does not affect the calculations of the characteristics of the instability. The form of Eq. (II-15) is presented in Fig. 4. Since at B_c, $\partial \mathrm{Im}(\omega)/\partial k = 0$ as well as $\mathrm{Im}(\omega) = 0$, Eq. (II-16) can be reduced to an expression independent of k:

5.65

$$x^2 = \frac{-F + (F^2 + 12KG)^{1/2}}{6K}\ ; \quad 0.08\ v^* = \frac{\mu_+}{m\mu_-}\left\{2Kx^2 + F\right\}\ x\ . \tag{II-17}$$

5.74 3.96 2.31

Eq. (II-17) can then be solved for B_c in terms of the parameters of the discharge.

In the presence of azimuthal density gradients and an azimuthal electric field the radial particle flux takes the form[23]

$$\Gamma_{+r} = \Gamma_{-r} = -\frac{D_a(0)}{1+\mu_+\mu_- B^2}\ \frac{\partial n}{\partial r} + \frac{\mu_+\mu_- B}{1+\mu_+\mu_- B^2}\left\{nE_\phi + \frac{1}{\mu_+ + \mu_-}\ \frac{1}{r}\ \frac{\partial}{\partial \phi}\left[(D_- - D_+)n\right]\right\}. \tag{II-18}$$

When averaged over time, the oscillations of density and potential contribute to $\Gamma_{\pm r}$ and thus give rise to an increased effective mobility across the magnetic field. The anomalous losses are then reflected in an increase of the longitudinal electric field for constant current.

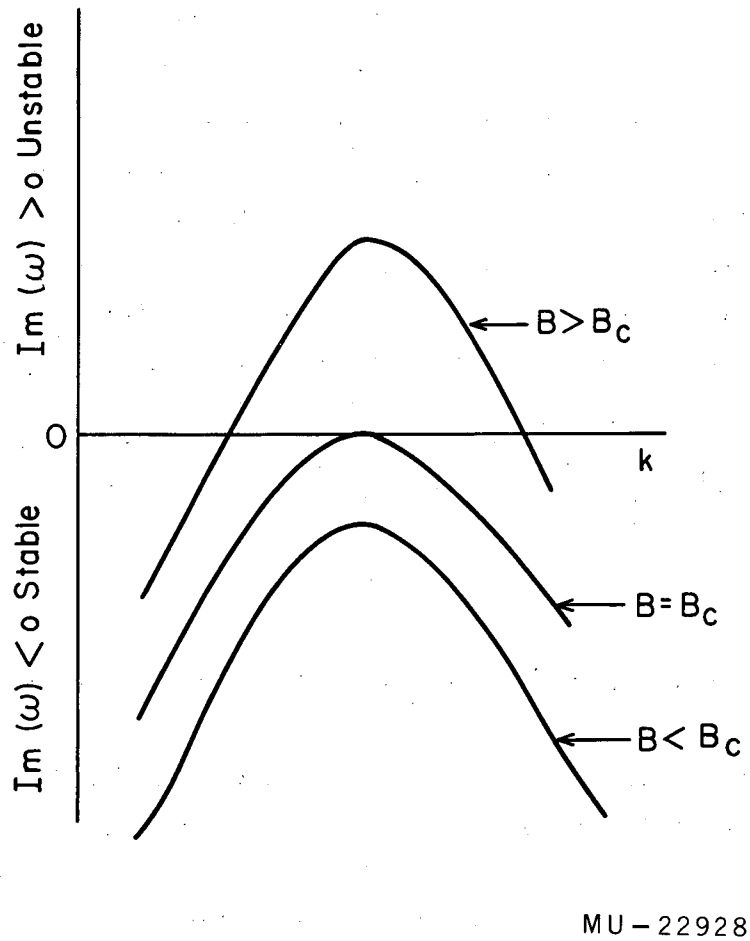

Fig. 4. The form of Eq. (II-15); Im(ω) vs k for several values of B (qualitative).

III. APPARATUS AND PROCEDURE

Two independent experimental arrangements were employed during this work. The layout of the primary system is shown in Fig. 5. In order to minimize the possibility of the end effects, a tube geometry of large length-to-radius ratio was used. The criterion developed by Simon[9] for the transverse diffusion to be ambipolar in a plasma column of radius R and immersed in a magnetic field of length L is

$$\frac{L}{R} > \left(\frac{q}{R}\right)^{1/2} \Omega_- \tau_- , \qquad \text{(III-1)}$$

where $\frac{1}{q} = \frac{1}{n} \frac{dn}{dr}$, n is the electron density, Ω_- is the electron cyclotron frequency, and τ_- the electron-neutral collision time. For example, in a column of helium at a pressure of 0.1 mm Hg, with R = 3 cm and L = 200 cm and $\frac{q}{R} \approx \frac{1}{2}$, the magnetic field must be less than 1000 gauss in order for the plasma to be free from end effects. Similar results are obtained for other gases, and as the largest tube radius used was 2.75 cm, the above calculation represents a pessimistic estimate.

Discharges in pyrex tubes 300 cm long and 0.9, 1.27, and 2.75 cm in radii were studied. Both electrodes were attached to the main body of the tube by ground glass joints and sealed with Apiezon wax. Such an arrangement permitted a number of electrode types and configurations to be employed interchangeably. Discharge currents from 50 to 500 ma dc were drawn from a hot tungsten cathode, although a dispenser-type cathode was also used for some measurements. The current was applied by an electronically regulated power supply with a maximum output of 6 kv at 600 ma. A rectangular current pulse up to 10 amp high, up to 10 msec long, and with a variable repetition rate, drawn from a small capacitor bank, permitted transient study of discharges at considerably higher particle densities.

The magnetic field was provided by ten 9-in. i.d. water-cooled coils 6 in. wide and spaced 2-1/4 inches apart. The field configuration,

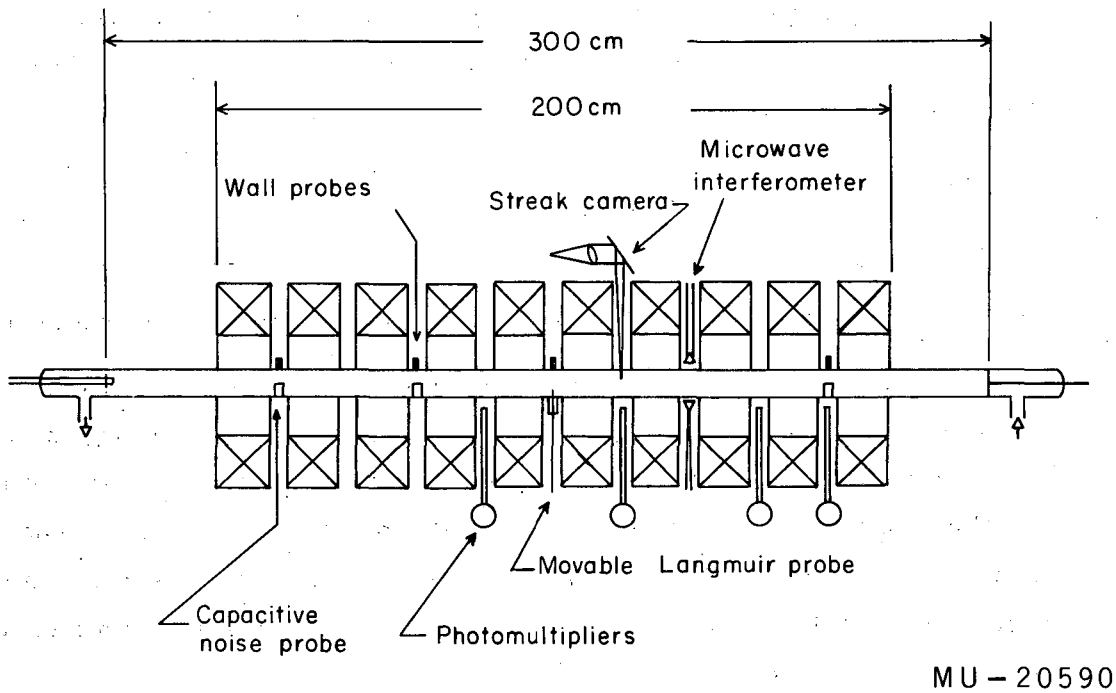

Fig. 5. The primary experimental arrangement ("long tube" system).

measured by a flip coil, is presented in Fig. 6. Available power supplies were capable of providing dc field strengths up to 7 kilogauss. To study the time-resolved behavior of the plasma, the magnet could be pulsed up to 1 kilogauss, again by means of a small condenser bank, the field rising sinusoidally to a maximum in 10 msec; the magnet is then short-circuited and the field decays exponentially with a e-folding time of 100 msec.

The region of uniform magnetic field was determined by visually following the progress of a number of low-pressure discharges in a tube of larger diameter. Well-defined beams traveled from a cathode, which consisted of an array of tungsten points placed at a radius slightly smaller than the radius of the discharge tube, to an anode almost filling the tube.[31] The effects of the radial components of the field due to the gaps between magnet coils were not visible to the eye. The radial field components should cause a line of force to be shifted by about 0.5 mm at $r = 2$ cm as it travels from the center of a coil to a gap; 0.5 mm is comparable to the tolerance on the tube radius.

A number of Langmuir-type probes were spaced along the tube in order to obtain measurements of the longitudinal electric fields. The probes were made of glass-coated 0.5-mm tungsten rod, ground flat at one end and protruding 3 to 5 mm from the tube wall. Midway between the electrodes, Langmuir probes of various shapes and types could be introduced into the tube and moved along a diameter by means of a micrometer screw. The following movable-probe types were used during the course of the experiment:

(a) Plane double and single probes made of 1.5-mm diam glass-coated tungsten, ground flat at the collecting end and with a 0.1-mm gap between glass and metal to prevent changes of the collecting area because of sputtering, with the collecting area perpendicular to the tube radius;

(b) Platinum cylindrical and spherical probes; collecting surfaces 2 mm in diameter; and

(c) Plane probes of 0.25-mm diam anodized aluminum wire shaped as shown in Fig. 7. The anodizing process provides a dielectric coating of excellent quality 0.025 mm thick.

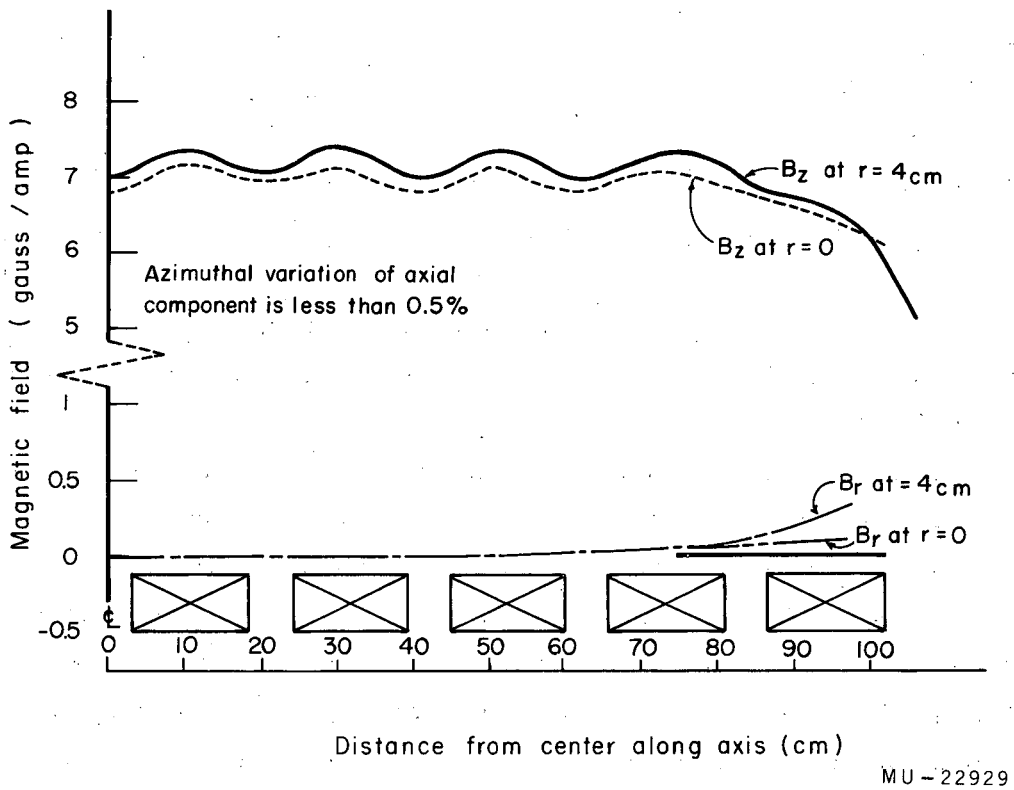

Fig. 6. Radial and longitudinal magnetic-field profiles.

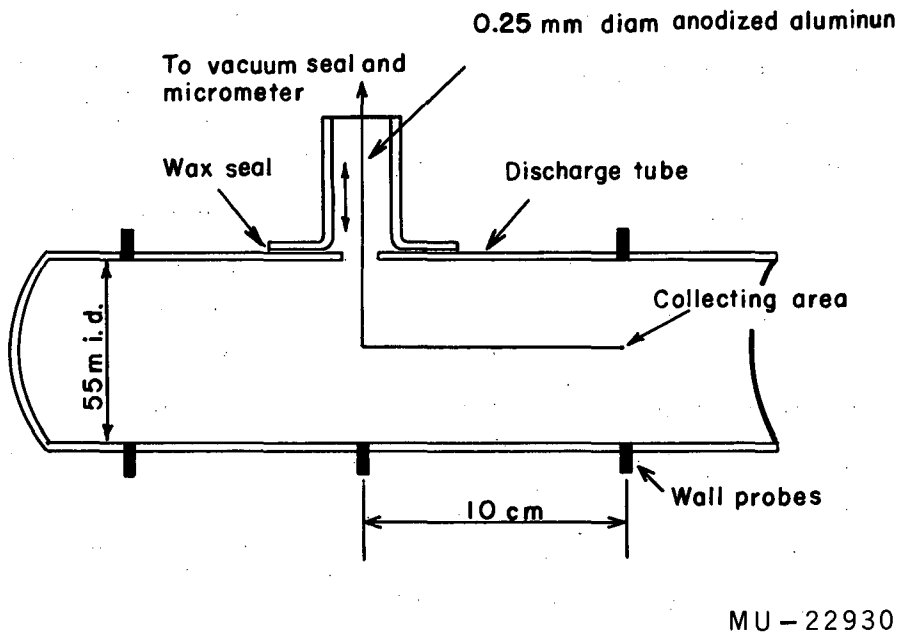

Fig. 7. Details of probe arrangement in "long tube" system.

The region of the tube in the vicinity of the radially movable probes was provided with several probes mounted flush with the tube wall. The perturbing effect of the radial probe on the plasma fields could thus be monitored to some extent.

The gaps between the coils of the magnet, together with a periscopic arrangement of front-surface mirrors, permitted a number of well-collimated magnetically shielded photomultipliers to view the discharge tube along its entire length. Signals were displayed on Tektronix-551 or -555 oscilloscopes and photographically recorded. A rotating-mirror streak camera yielded space-and-time-resolved data on the light fluctuations in the tube. The space resolution could be extended to two dimensions through the arrangement shown in Fig. 8. The maximum-design streak speed of the entire system was 30 μsec/cm, but because of the limited light intensity, 100 μsec/cm was the maximum operating speed using Polaroid 3000 film. In discharges of low light intensities, such as argon, a bank of photomultipliers (Fig. 8) substituted effectively for the streak camera. This device also permitted the detailed examination of short time intervals during the growth of the instability.

The electrical signals associated with the plasma were frequency-analyzed by using a series of radio detectors covering the frequency range from 5 kc to 250 Mc, and 1 to 10 kMc.[32] The detectors were coupled to the plasma either through wall probes or through capacitative pickups outside the tube.

When the plasma density could be made sufficiently high, an 8-mm microwave interferometer was used to study the behavior of the electron density. The arrangement in Fig. 9 permitted densities as low as $5 \times 10^{10}/cm^3$ to be resolved.

An oil diffusion pump with a refrigerated baffle system and a trap kept at liquid nitrogen temperature gave the system a base pressure of the order of 10^{-7} mm Hg. During an experimental run, gases were continuously bled through the system. Other methods of gas handling were used, such as a charcoal trap kept at liquid nitrogen

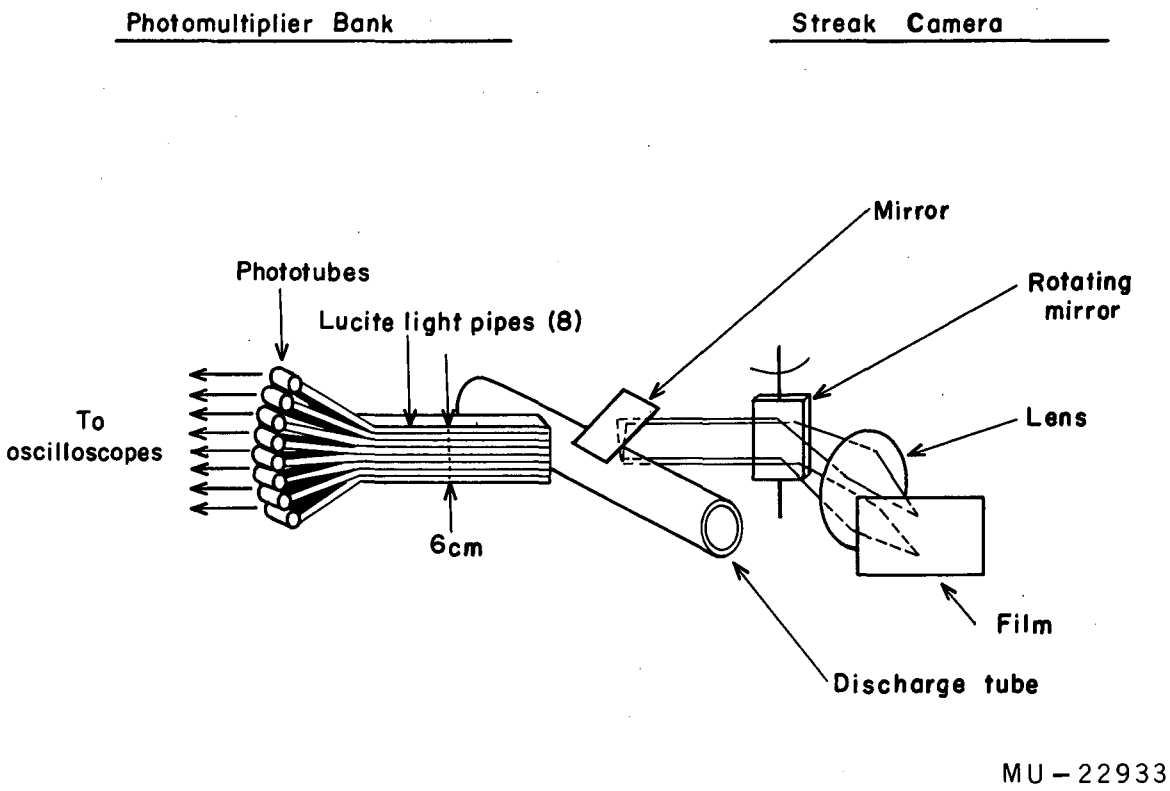

Fig. 8. Schematic of optical diagnostics.

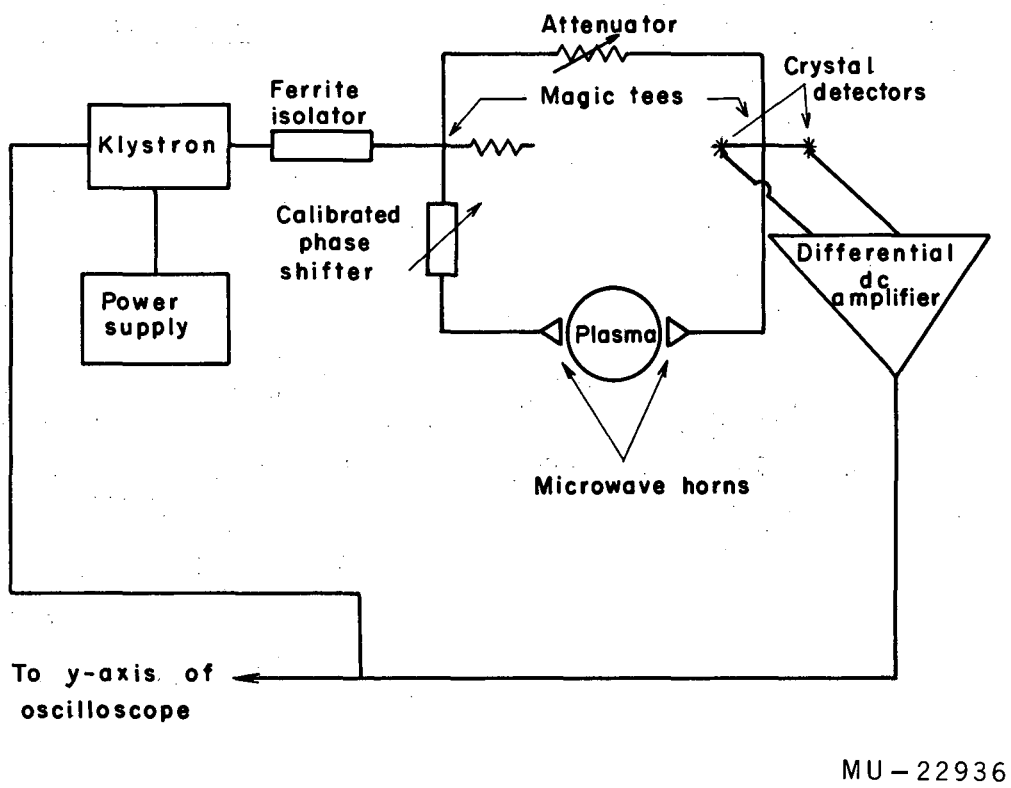

Fig. 9. Schematic of 8-mm microwave interferometer bridge.

temperature, but with no effect on the experimental results. The neutral gas pressure was measured by an oil-filled manometer or an Autovac gauge calibrated with the manometer. The neutral gas temperature could be estimated from measurements with thermocouples inside and outside the glass tube as well as from pressure changes when the tube was isolated and the discharge turned on. All measurements with a varying magnetic field were taken at constant current, data being recorded on an x-y or strip-chart recorder.

The experimental arrangement of the secondary system is shown in Fig. 10. The purpose of this subsidiary experiment was to perfect techniques of measuring the radial potential distribution in the positive column and also to study the behavior of the column in a "short tube" geometry. The radial probe arrangement (Fig. 10) was designed to minimize end effects of the probes themselves and to provide a geometry possessing a high degree of symmetry. Anodized aluminum wires, 0.25 mm in diameter with a 1-mm-long bare spot as the collecting area were used. A port was provided in the discharge tube for the insertion of other types of probes. The diagnostic tools described in the previous sections could be readily transferred to this system. The vacuum was of comparable quality; however, a mercury diffusion pump was used here.

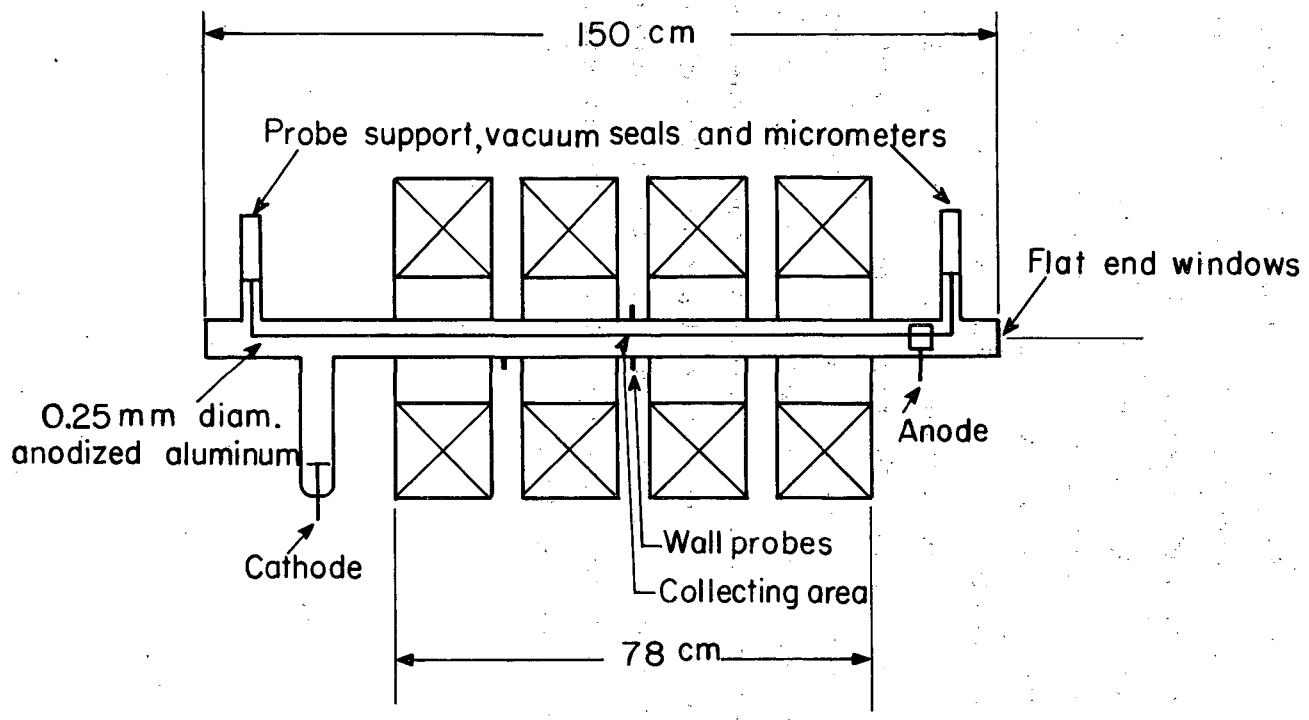

MU-22939

Fig. 10. Secondary, "short tube" system. The anodized aluminum wire was movable along a diameter for radial potential measurements.

IV. RESULTS

A. The Longitudinal Electric Field and the Critical Magnetic Field

We have investigated the behavior of the longitudinal electric fields, measured between wall probes, in tubes of 0.9, 1.27, and 2.75 cm radius, using discharges of hydrogen, deuterium, helium, neon, and argon. Typical experimental measurements of the fields as functions of the applied magnetic field at constant discharge currents are presented in Fig. 11 and in Appendix A. In agreement with the experiments of Lehnert and Hoh,[13] we find that the axial electric field decreases with increasing magnetic field up to some critical field B_c. At B_c the slope of E_z-vs-B curve changes sign; E_z in general increases with increasing B above B_c, although in some regimes of pressures, gas, and tube radius, further undulations of the curve may occur. The exact form of the curves at pressures below about 0.2 mm Hg depends slightly upon whether the magnetic field was increased or decreased during a run.

The shapes of the curves and the values of B_c were not affected by varying electrode materials and geometries or external circuit parameters. Modest misalignment of the discharge tubes with respect to the axis of the magnetic field changed the shapes of the E_v-vs-B curves above B_c but did not change the value of B_c. Placing one or both electrodes inside the magnetic field left B_c unchanged except at rather low pressures (Fig. 12). A series of measurements taken in the "short tube" system (Fig. 10) yielded results consistent with the curves from the primary system (Tube 300 cm long), again with the exception of low pressures. The deviations observed at low pressures in short-tube geometries are probably caused by the shortening of the positive column at low pressures and the encroachment of the Faraday dark space into the region of measurement.

We have calculated the longitudinal electric field (Eq. II-5) as a function of the magnetic field for several sets of typical discharge parameters, and plotted these curves with the experimental

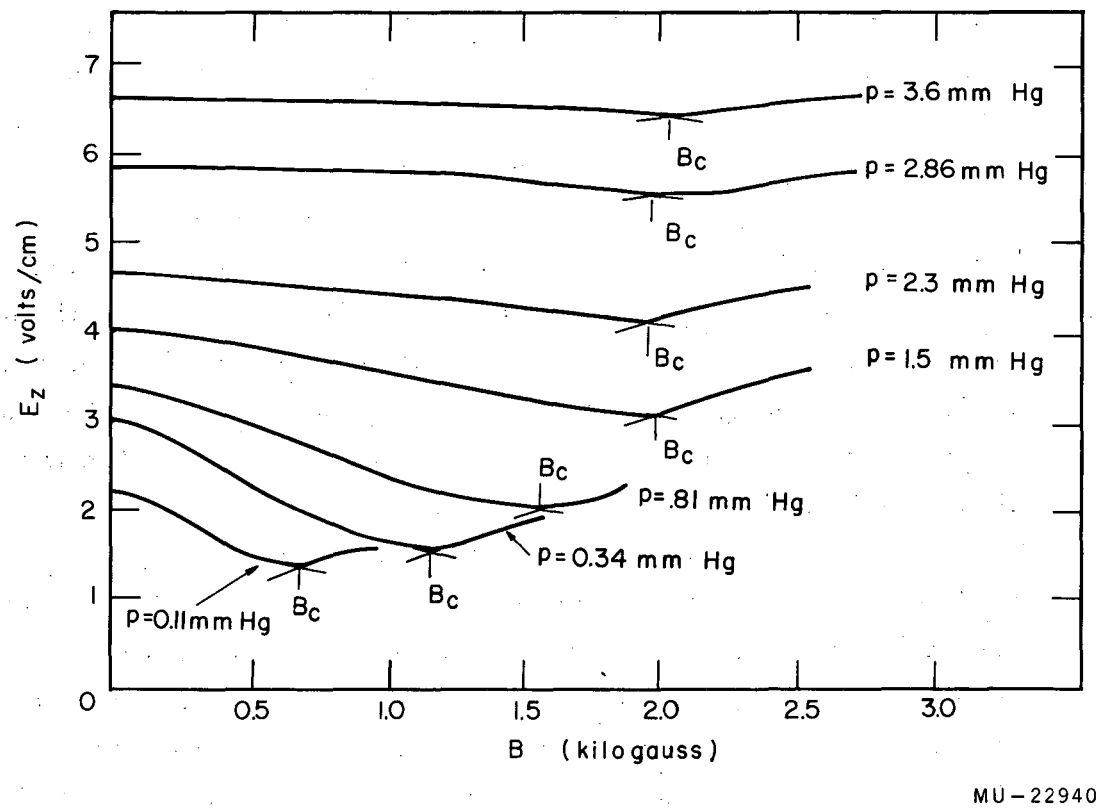

Fig. 11. E_z vs B: He gas, R = 1.27 cm, I = 400 ma.

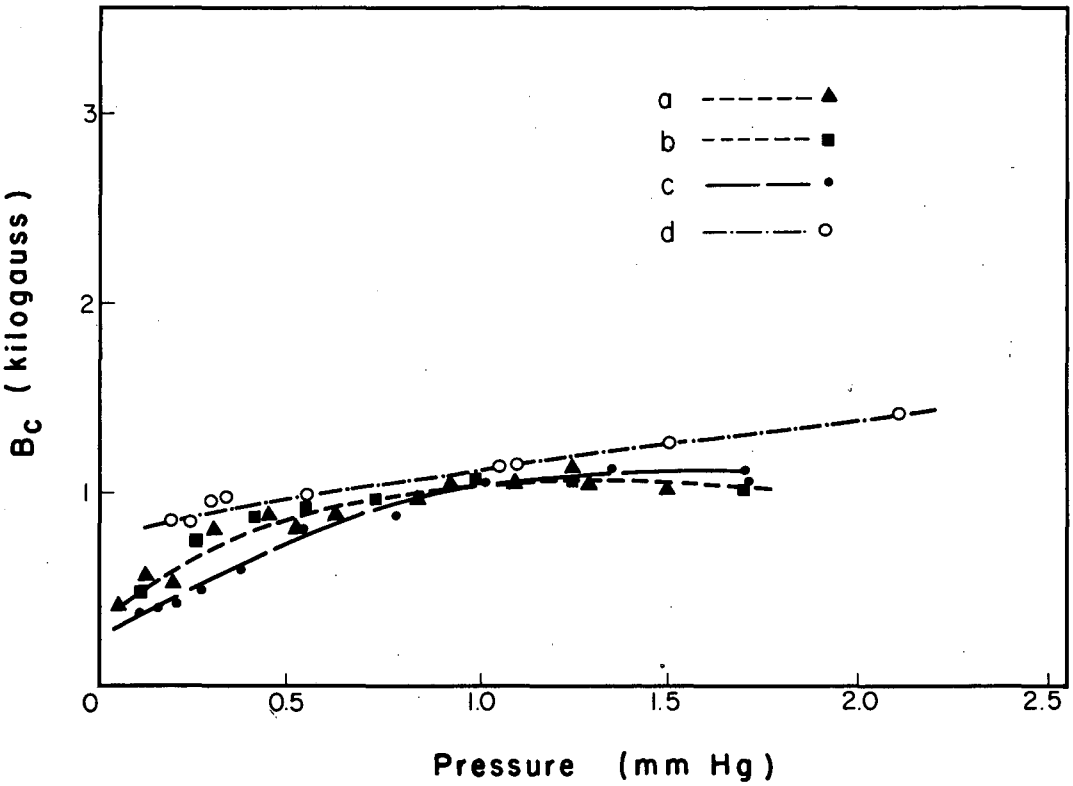

MU-18965

Fig. 12. B_c vs pressure for various electrode configurations: He gas, R = 2.75 cm. (a) and (d); electrodes outside magnetic field (normal condition); (b) anode in magnetic field; (c) both electrodes in magnetic field; (a), (b), and (c) at 50 to 300 ma dc, (d) at 5 amp pulsed.

results, Fig. A-3, for comparison. Qualitative agreement between theory and experiment is good up to B_c. At higher magnetic fields the experimental curves deviate markedly from the theoretical calculations; specifically, the classical theory of the positive column does not predict any deviation from the monotonic decrease of the axial electric field with increasing applied magnetic field.

Optical observations of the light from the discharge by means of photomultipliers and a stereo streak camera have shown that at B_c the column loses its azimuthal symmetry and becomes a constricted, rotating luminous helix (Fig. 23, a, b). We shall defer until a later section detailed discussion of the properties of this phenomenon; we find that the apparently enhanced diffusion from the column, characterized by a longitudinal field considerably in excess of theoretical predictions, is the result of an instability which develops at B_c and transforms the uniform column into a constricted helical column.

The behavior of B_c as a function of gas, gas pressure (reduced to $0^{\circ}C$), and tube radius is presented in Figs. 13 through 21, together with the B_c-vs-p curves calculated from the theories of Hoh[20] and Kadomtsev and Nedospasov.[21] The experimental points represent results obtained over a period of months with a variety of tubes of a given radius and various methods of gas handling. Preceding any set of measurements the discharges were repeatedly flushed and allowed to run for 2 to 6 hours until no significant impurity lines were detectable spectroscopically. Appreciable admixture of an impurity (99% He, 1% A; 99%A, 1% N_2) yielded E_z-vs-B curves from which it was impossible to deduce a critical field.

The scatter of the experimental points is probably the result of several effects: (a) in an unbaked system such as ours the impurity level is certainly not constant over long periods of time; (b) our calibration techniques permitted determination of the average magnetic field between probes to ± 2%; and finally, (c) in some cases the determination of B_c was difficult because of the very gradual transition to the anamolous state.

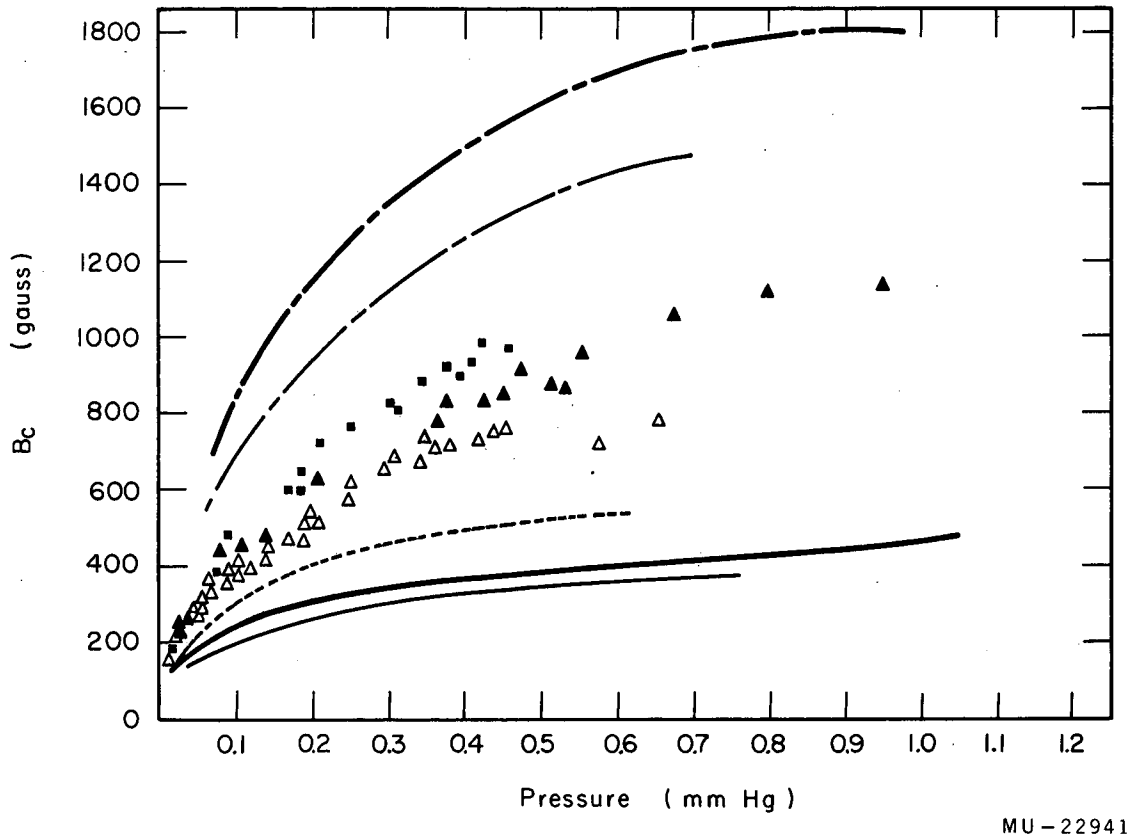

Fig. 13. B_c vs pressure (R = 0.9 cm): △ H_2, I = 200 ma; ▲ D_2, I = 200 ma; ■ D_2, I = 400 ma; —— H_2^+, (200 ma) theory of K and N; —— D_2^+ (200 ma), theory of K and N; - - - - D_2^+ (400 ma), theory of K and N; —·—H_2^+, theory of Hoh; —··—D_2^+, theory of Hoh.

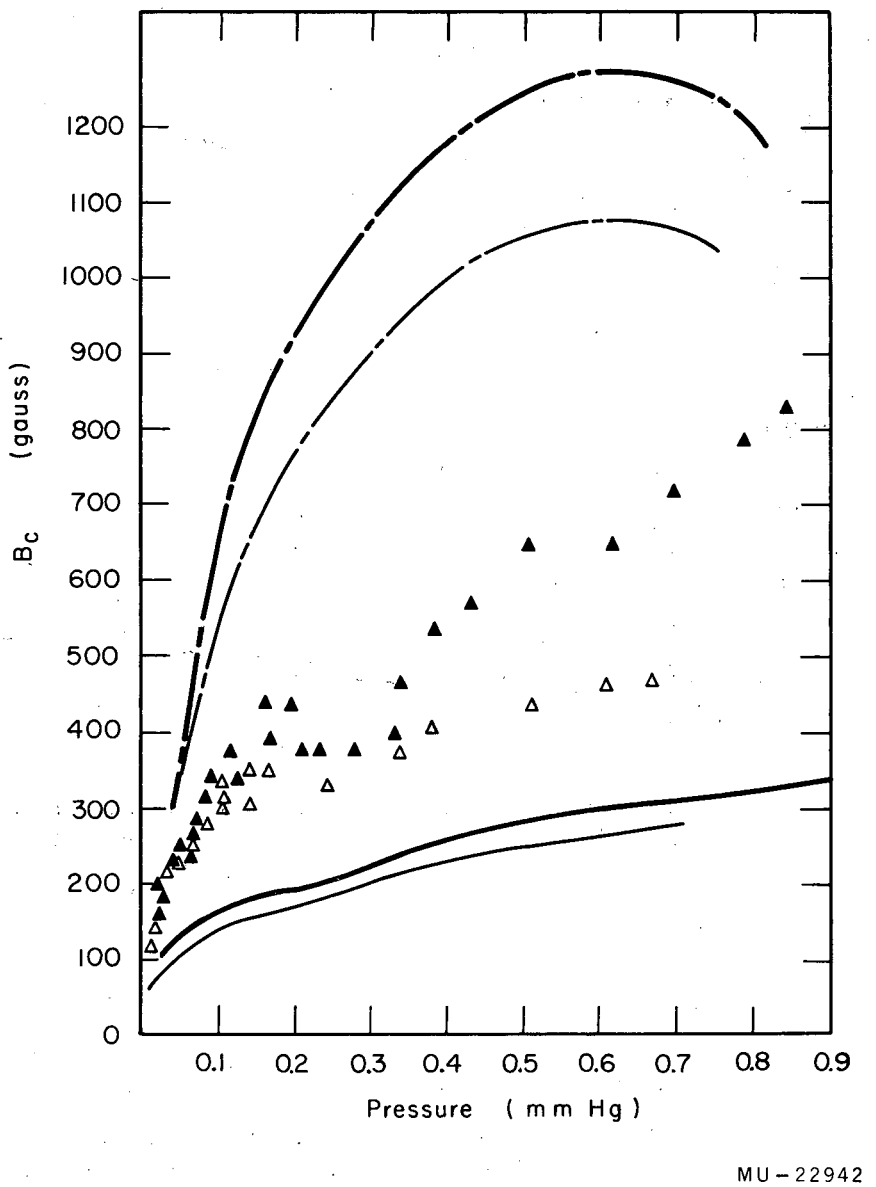

Fig. 14. B_c vs pressure (R = 1.27 cm): △ H_2, I = 200 ma; ▲ D_2, I = 200 ma; —— H_2^+, theory of K and N; ▬ D_2^+, theory of K and N; — - — H_2^+, theory of Hoh; ▬ - ▬ D_2^+, theory of Hoh.

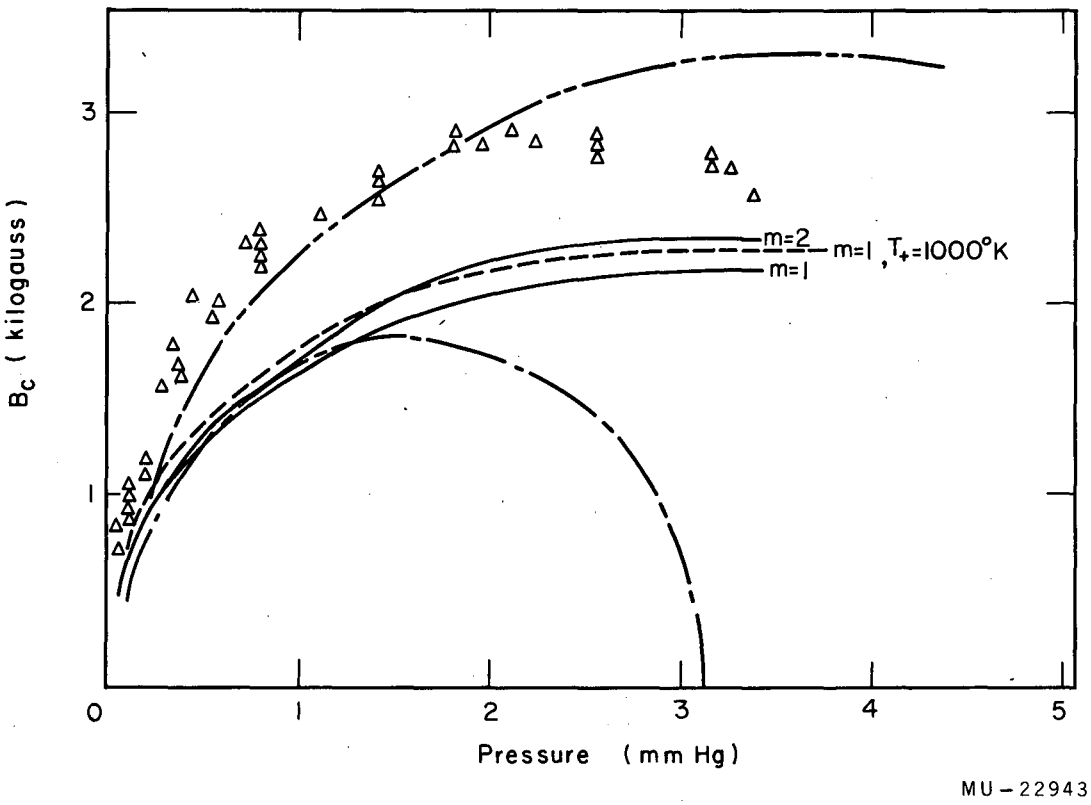

Fig. 15. B_c vs pressure — R = 0.9 cm, He gas, I = 200 ma: —— theory of K and N (He^+ only); —— - —— theory of Hoh, He^+ only; —— -- —— Theory of Hoh, He_2^+ only; — — — theory of K and N (He^+ only), T_+ = 1000°K.

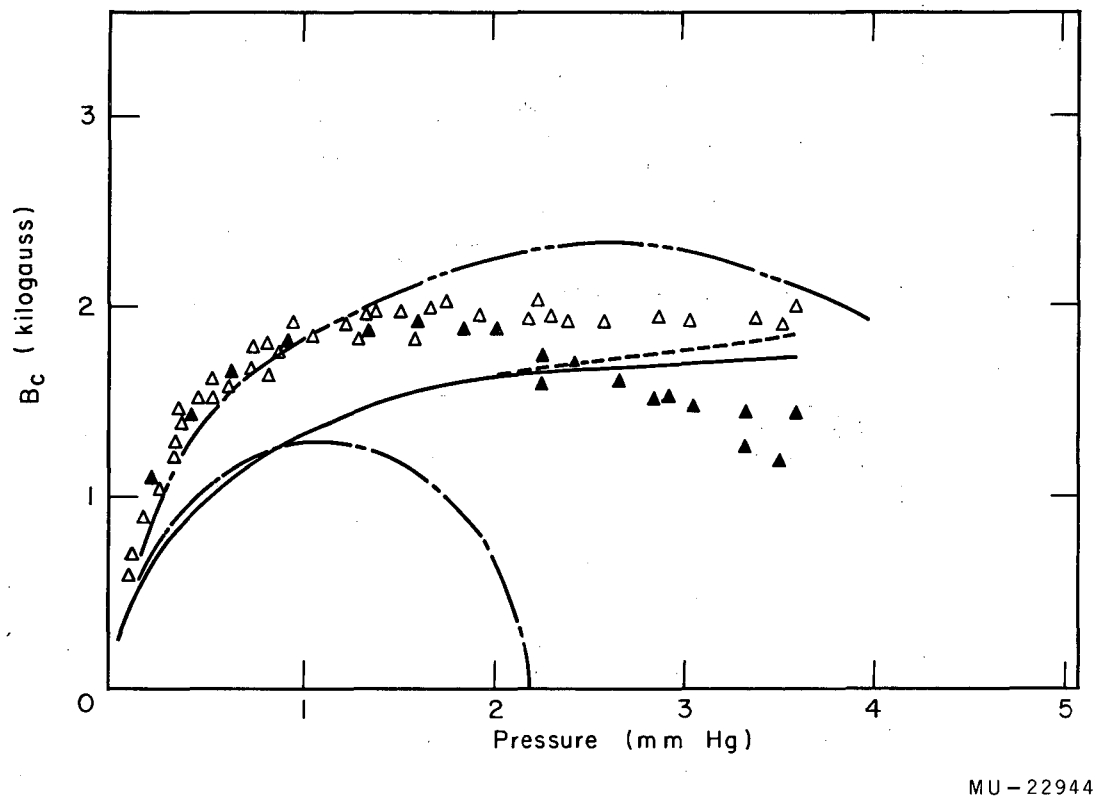

Fig. 16. B_c vs pressure,(R = 1.27 cm): ▲ He, I = 200 ma; △ He, I = 400 ma; —— theory of K and N, 200 ma, He^+ only; – – – – theory of K and N, 400 ma, He^+ only; —·— theory of Hoh, He^+ only; — — — theory of Hoh, He_2^+ only.

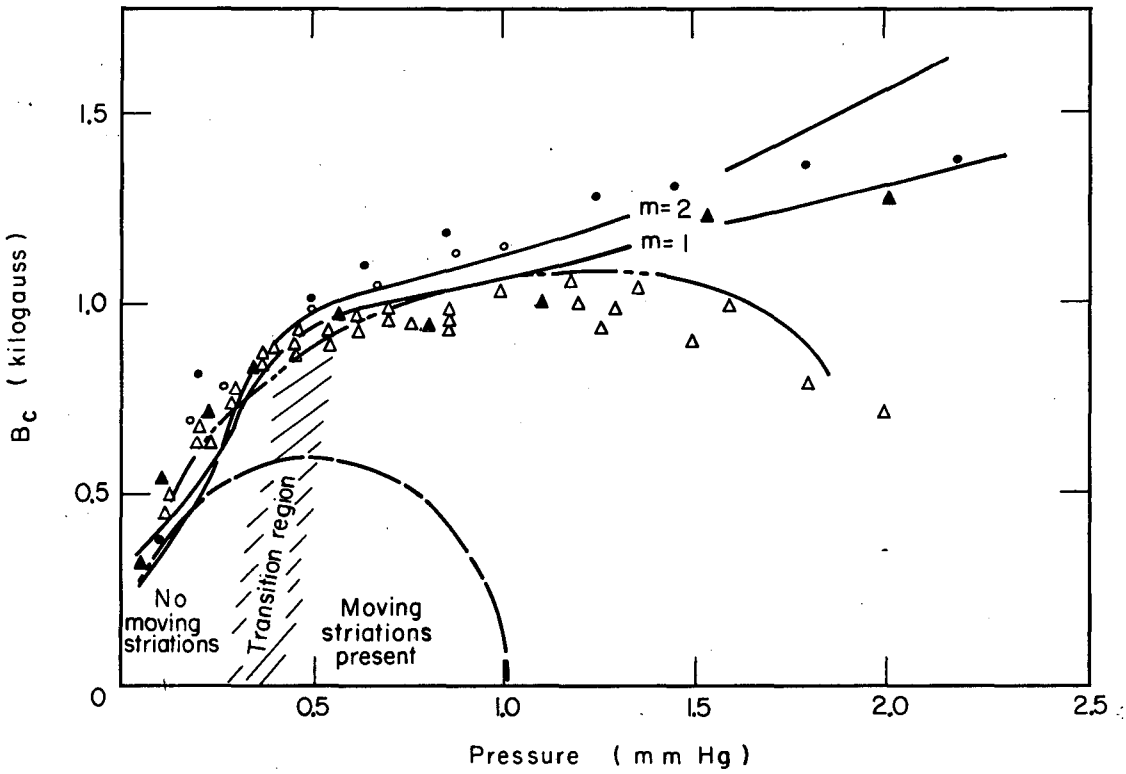

MU-22945

Fig. 17. B_c vs pressure, (R = 2.75 cm, He gas): △ I = 200 ma, and ▲ I = 500 ma, "long tube" system; ○ I = 200 ma, ● I = 400 ma, "short tube" system; —— theory of K and N, He^+ only; — - — theory of Hoh, He^+ only; — - - — theory of Hoh; He_2^+ only.

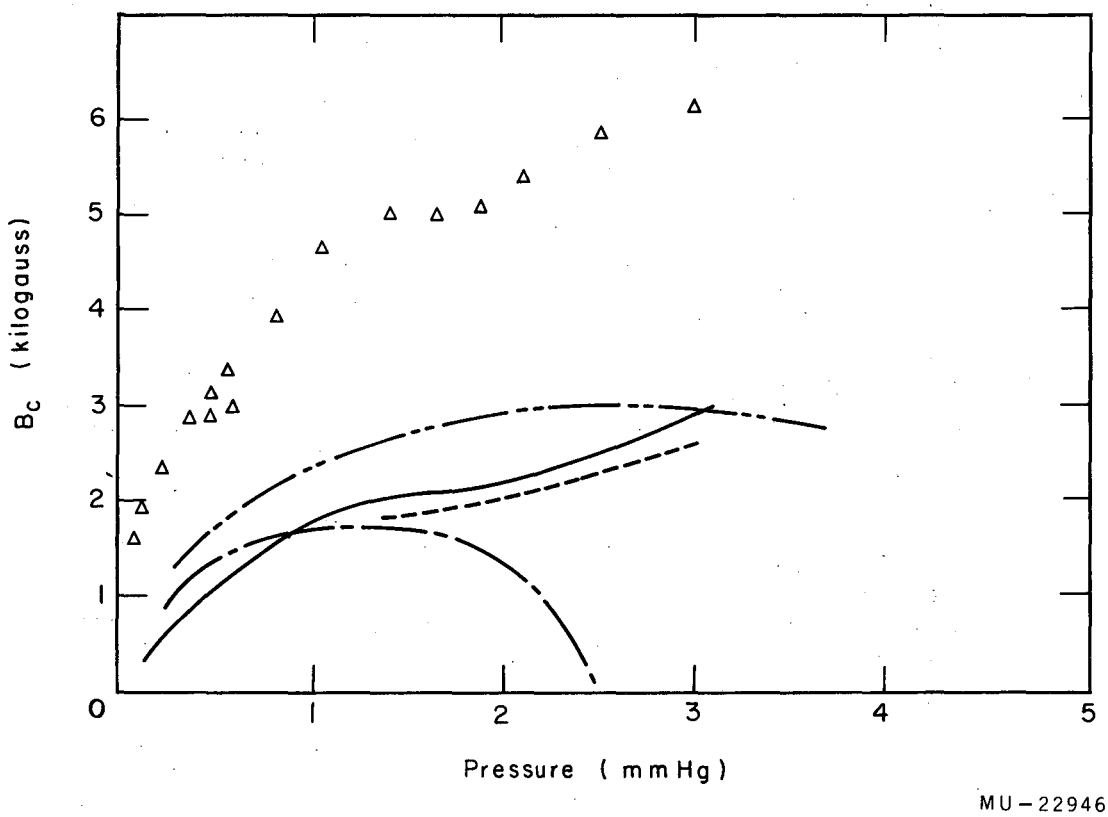

Fig. 18. B_c vs pressure — R = 0.9 cm, Ne gas; 200 ma: ——— theory of K and N, Ne^+ only; — — — theory of K and N, Ne_2^+ only. —— - —— theory of Hoh, Ne^+ only; —— - - —— theory of Hoh, Ne_2^+ only.

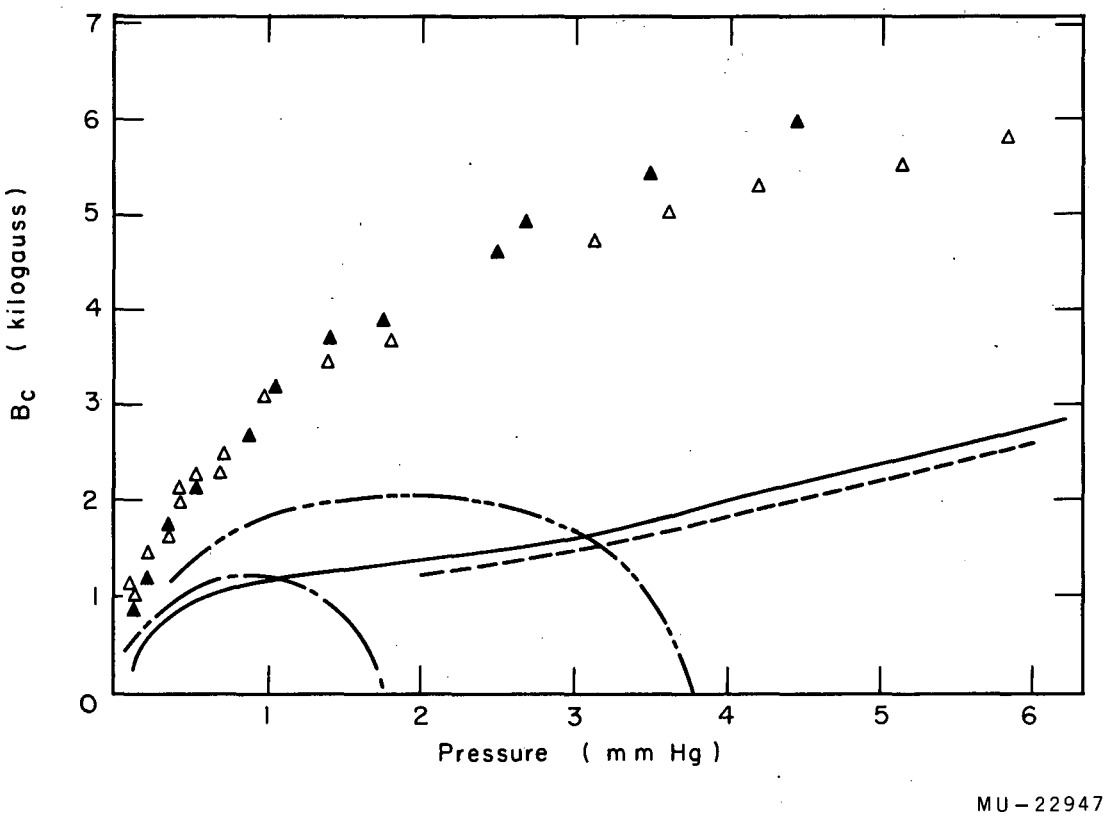

Fig. 19. B_c vs pressure — R = 1.27 cm, Ne gas; △ 200 ma and ▲ 400 ma: —— theory of K and N, 200 ma, Ne^+ only; – – – – theory of K and N, 200 ma, Ne_2^+ only; —·—theory of Hoh, Ne^+ only; —·-·— theory of Hoh, Ne_2^+ only.

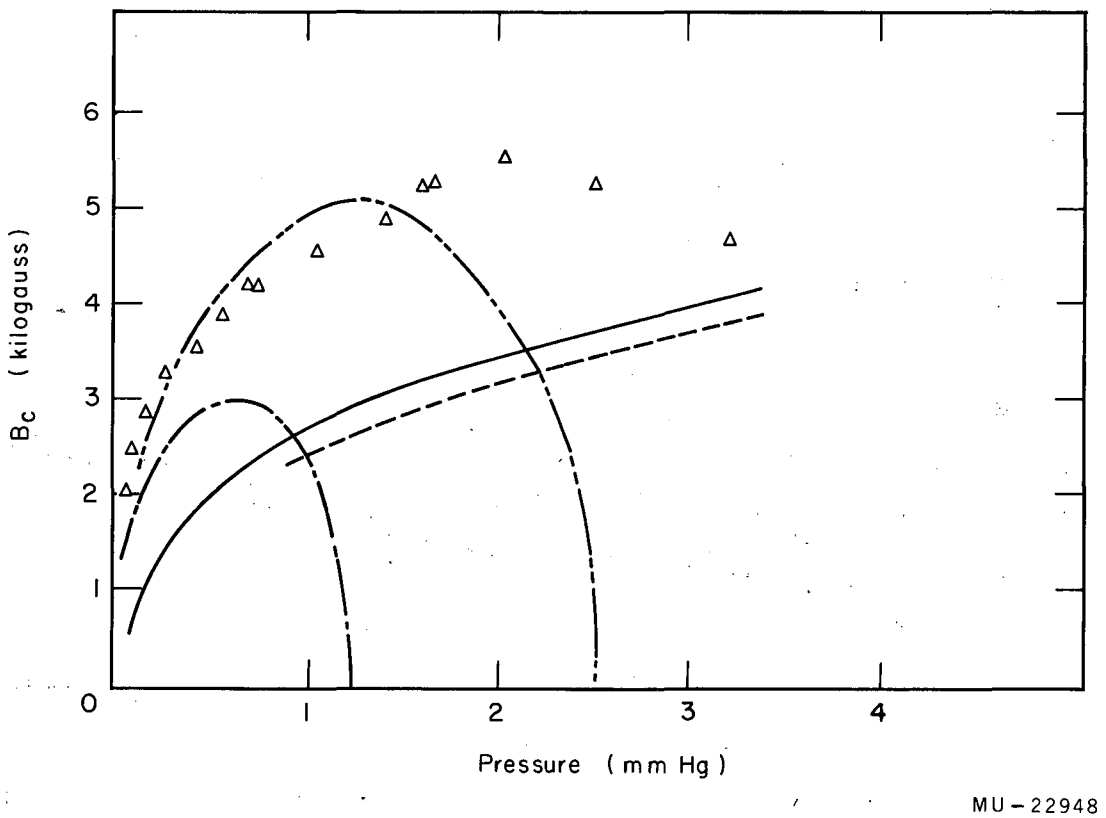

Fig. 20. B_c vs pressure — R = 0.9 cm, A gas, 200 ma: ———theory of K and N, A^+ only; - - - - theory of K and N, A_2^+ only. — - — theory of Hoh, A^+ only; — - - — theory of Hoh, A_2^+ only.

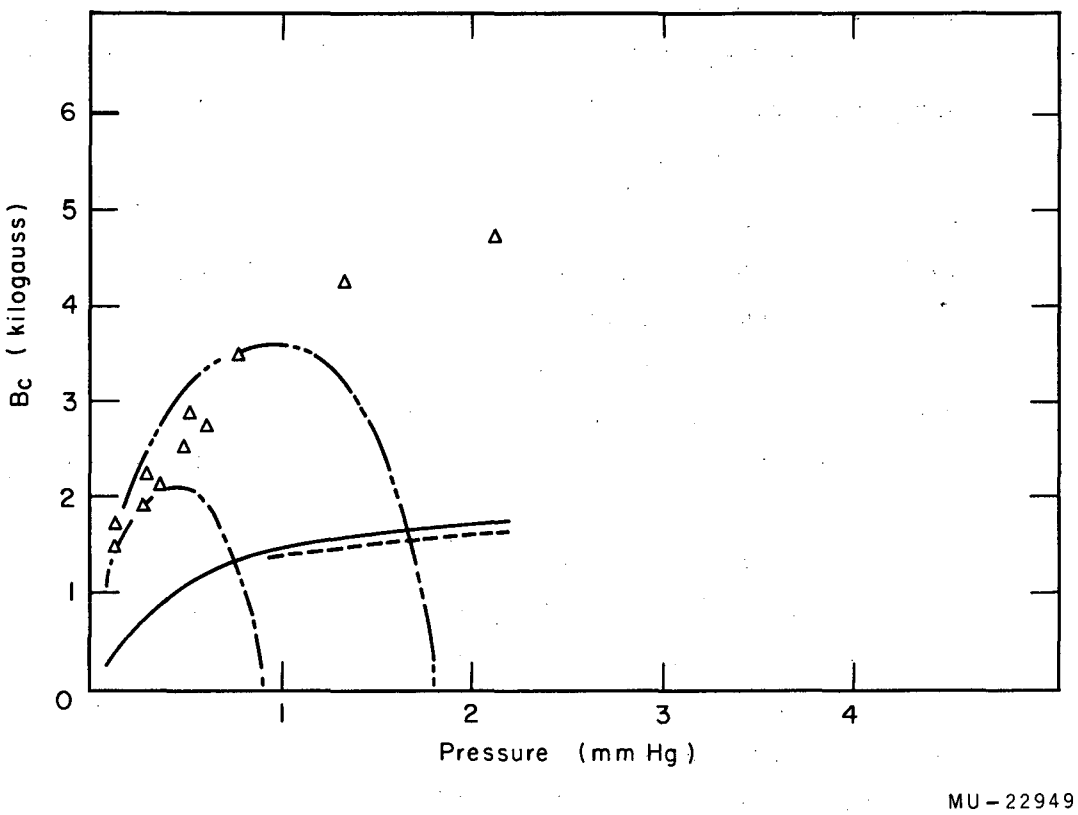

Fig. 21. B_c vs pressure — R = 1.27 cm, A gas, 200 ma: ——— theory of K and N, A^+ only; — — — theory of K and N, A_2^+ only; —— — —— theory of Hoh, A^+ only; ——— - - ——— theory of Hoh, A_2^+ only.

An IBM 650 was used to solve Eq. (II-17) with $m = 1$ (theory of Kadomtsev and Nedospasov) by successive approximations. Here we have used the experimentally determined longitudinal electric field at the critical magnetic field as an input parameter. The electron temperature was calculated from the modified Schottky theory,[11] assuming $T_+ = 400^\circ K$. A calculation with $T_+ = 1000^\circ K$ is shown in Fig. 15 to illustrate the dependence of B_c on the ion temperature. In calculating the values of B_c as predicted by the sheath-instability theory we have assumed, with Hoh[20] $T_-/V_i = 1200^\circ$ K/volt and $J_0\left(\frac{2.4r'}{R}\right) = 0.013$. Atomic data from the compilation by Brown[33] were used; the value for the mobility of H_2^+ was taken from the work by Chanin.[34]

Considerable uncertainty exists as to the actual conditions in the positive column, e.g., both atomic and molecular ions are known to be present.[35] Since the theory of Hoh, although depending weakly on T_-, is particularly sensitive to assumptions regarding the ion species, we have calculated and plotted curves for the two limiting compositions. The theory of Kadomtsev and Nedospasov, on the other hand, is relatively insensitive to changes in the ion mobility. Here the assumption that only molecular ions are present at a given pressure decreases the calculated critical magnetic field slightly from the value obtained by using atomic ion mobilities (Figs. 18 through 21). However, the electron temperature T_- enters these calculations in an important way; for a given pressure B_c varies roughly as T_-. The effect of the moving striations on T_- is not known; we find, however, that the experimental B_c-vs-p curve passes smoothly from the striated to the unstriated regime. Values of the electron temperature, as determined from Langmuir probe measurements, Fig. 22, were also in reasonable agreement with theoretical calculations, at least up to B_c. Above B_c the experimental results are of doubtful value. The electron temperature increases with increasing particle losses. In addition, the marked oscillations of the current channel result in oscillations of the

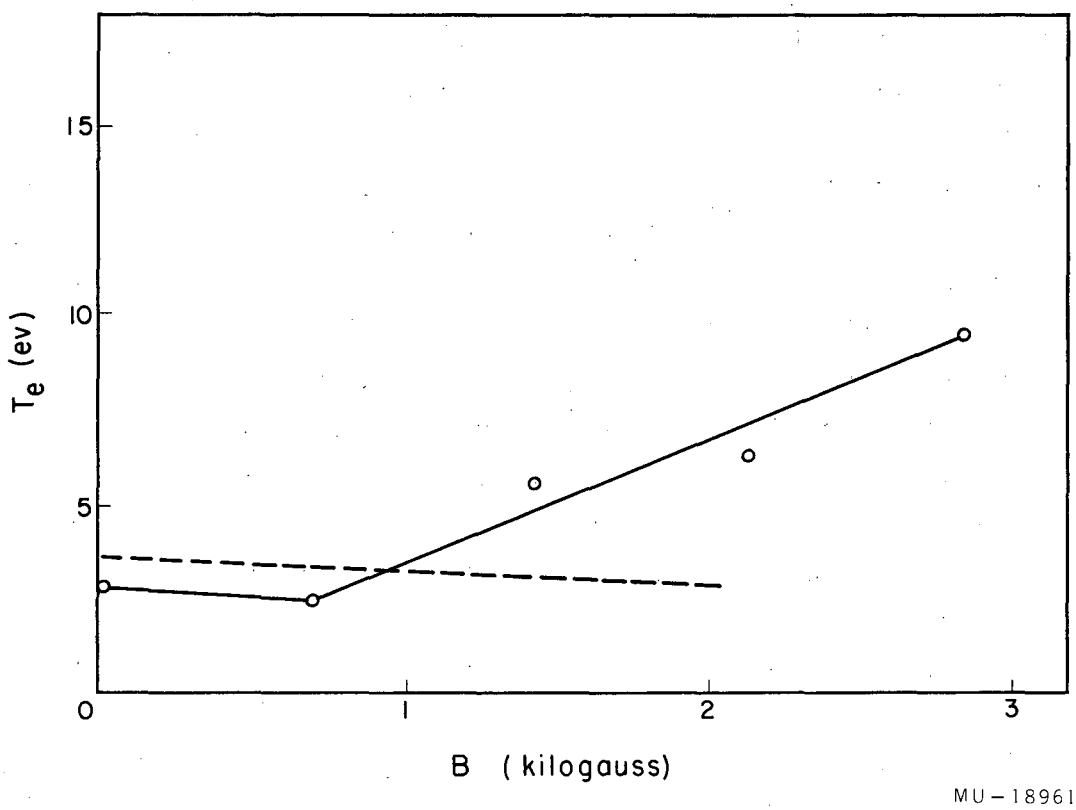

Fig. 22. Apparent electron temperature as measured with Langmuir probe near tube center (R = 2.75 cm) vs B; p = 0.22 mm Hg and I = 200 ma, He gas. Dashed line is theoretical curve.

potential of the plasma about some average value at the probe. Because of the nonlinearity of the probe characteristics, the potential oscillations create an average probe characteristic which indicates an apparently higher electron temperature.

The value of B_c increases slowly with increasing discharge current (Figs. 12, 13, 19). The effect is more pronounced at relatively hight pressures (Fig. 16). At high current densities and at pressures above a few millimeters, an appreciable fraction of the ionizations may occur from excited atomic levels, especially if long-lived metastable states are present,[27] with a consequent decrease of the longitudinal electric field. This in turn, according to the K and N theory, will result in a higher B_c. As shown in Fig. 16, there is qualitative agreement between this theory and experiment.

At high values of the pressure-radius product pR, the positive column constricts into a filament of current; Fowler[35a] finds that appreciable constriction is present in helium discharges with $pR \approx 10$ cm/mm Hg. The causes of pressure constriction are not well understood; it is not predicted by the Schottky theory. It has been suggested that the constriction of the positive column comes about as a consequence of a rapid decrease of electron temperature with increasing pressure and a subsequent piling up of the electrons in the center of the discharge.[36] A temperature lower than predicted by the Schottky theory would decrease our theoretical B_c values at a given pressure, as calculated from the theories of Hoh and Kadomtsev and Nedospasov. The decrease of the experimental helium B_c-vs-p curves starting at $pR \approx 4$ may thus be connected with the beginning of pressure constriction in the column; a similar argument may also apply to other gases.

B. The Radial Potential Distribution

Earlier attempts to measure the radial potential distribution of the positive column in a longitudinal magnetic field have shown that, in agreement with theory, the radial field is lowered by the magnetic field.[11] A measurement of the radial field describes the type of diffusion operating in the column (ambipolar, "Simon") and in addition is relatively sensitive indicator of the presence of collective phenomena, such as microinstabilities.[29]

It has proven surprisingly difficult to develop a reliable and believable scheme for radial potential measurements. Our early attempts employed probes penetrating radially into the plasma. Measurements at zero magnetic field yielded results consistent with expectations. At fields larger than a few hundred gauss asymmetries developed in the U(r)-vs-r curves, quite similar to those reported by Bickerton and von Engel (Ref. 11). We believe that, in the presence of a longitudinal B field, probes penetrating radially into the plasma perturb the fields markedly. To overcome this problem, we have devised the systems shown in Figs. 7 and 10. A series of curves taken with these configurations is presented in Appendix B.

The results are in all cases relatively symmetric. Curves of Figs. B-1 through B-4 show a general tilt, probably the effect of the radial stem of the dogleg probe. The small humps present at d = 55 are most likely caused by interactions of the sheaths. Near d = 0 the hole through which the probe is inserted exerts a more pronounced perturbation. These minor perturbations are eliminated if the probe system of Fig. 10 is employed. Unfortunately, problems of sag and insulation precluded the use of this type of probe in the 300-cm tube.

Several general conclusions can be drawn from the above-mentioned figures:

(a) In all cases considered we are dealing with diffusion of the ambipolar type. "Simon" diffusion would leave the potential distribution unaffected by the magnetic field. We have not found deviation from ambipolar diffusion even in cases where the Simon criterion (Eq. III-1)

is clearly not satisfied. This suggests that in a glow discharge, measurements are more likely to be confused by too short a positive column at low pressures than by non-ambipolar diffusion.

(b) Above the critical magnetic field B_c the curves represent a time average of some peculiar potential distribution. In some cases this average is symmetric about the center of the tube— we find this to be connected with a rather regular helical mode. The distorted potential curves may be connected with the peculiar electrode arrangement in the short-tube system (Fig. 10).

(c) There is no detectable minimum in the U(r)-vs-r curves at fields below the critical field, hence no detectable "enhanced interaction" as considered by Ecker.

C: Properties of the Instability

The striking optical behavior of the column at the critical magnetic field has already been mentioned briefly. Luminous helices of the clarity shown in Fig. 23 (a) were observed only for special combinations of gas, pressure, and tube radius. In general the appearance was more chaotic, often moving striations were superimposed on the spirals (Fig. 23 b). The transition to the helical state is quite abrupt, and especially so if there are no moving striations present. The presence of moving striations (Fig. 39 b) thus complicates analysis of the behavior of the column. We have therefore attempted, unsuccessfully, to remove the moving striations from the column by adjusting external circuit parameters and by operating an auxiliary discharge at the anode. The latter scheme was meant to provide a source of ions; the oscillations of the anode fall are believed by Pupp to be the source of one species of moving striations.[37] At some discharge conditions, however, we found that the longitudinal magnetic field was able to suppress the striations: a column striated at $B = 0$ can become uniform as the field is raised, and then at B_c makes the transition to the helical mode.

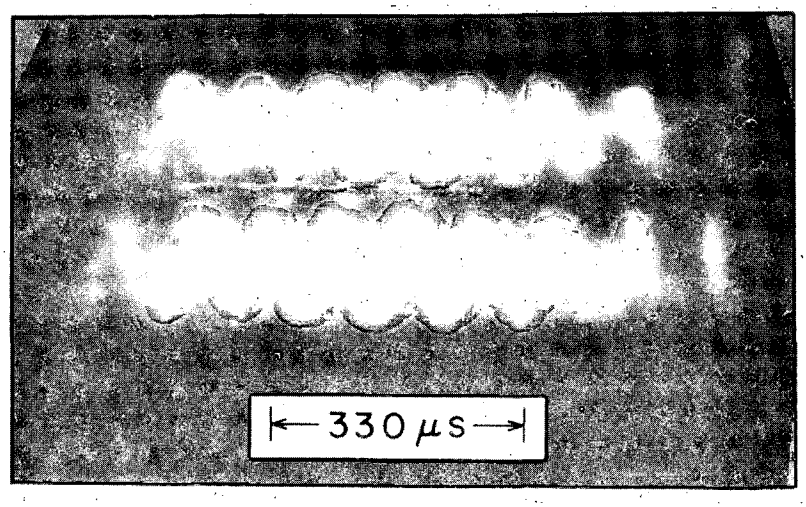

(a)

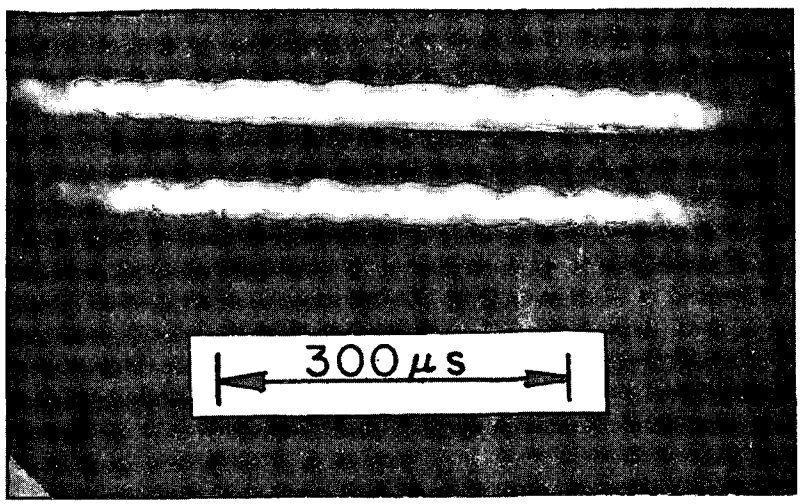

(b)

ZN-2714

Fig. 23. 90 deg. stereo streak photographs of helical constriction in He. Traces show variation of light intensity with time and radius as seen through a slit perpendicular to axis of discharge tube: (a) R = 2.75 cm, p = 0.23 mm Hg, B = 710 gauss, and (b) R = 0.9 cm, p = 0.5 mm Hg, B = 1990 gauss. Note that these are not photographs of helices; the helicity has been established by wavelength measurements with photomultipliers.

The helical nature of the constriction has been determined by studies with a series of photomultipliers placed along the discharge tube. Wave lengths of the luminous current channel could thus be found by studying the phase differences of the photomultiplier signals. The pitches of the spirals were such that $\vec{j} \times \vec{B}$ was directed toward the tube walls. In Figs. 24 through 28 we show experimental measurements of this wave length as a function of the neutral pressure.

The perturbation analysis by Kadomtsev and Nedospasov predicts the growth rate of the instability to be a strong function of the wave length of the instability (Eq. II-15, Fig. 4) Bearing in mind that the above theoretical analysis is based on a small-amplitude theory while our experimental measurements were carried out on the fully developed helix, the new, azimuthally nonsymmetric, steady state, we have computed curves similar to Fig. 4 for the discharge parameters of the experimental points in Figs. 24 through 28. If we assume that the maxima in the Im(ω)-vs-k curves represent that wave length which will grow fastest and dominate as the behavior of the column becomes nonlinear, we can arrive at the theoretical values for the instability wave length. We present these theoretical values (m = 1), together with experimental results, in Figs. 24 through 28. Higher values of m shift the maximum of the Im(ω)-vs-k curves toward shorter wave lengths. The agreement between theory and experiment is excellent in the case of helium and satisfactory in the cases of hydrogen, deuterium, and neon. However, even for the latter, the form of the theoretical curves is consistent with experimental results. Measurements in helium could usually be made at magnetic fields not more than 40 gauss above B_c. For H_2, D_2, and Ne it was necessary to raise the magnetic field up to 10 to 20% above B_c in order to find a spiral reasonably free from striation; this may also account for the reversal of experimental and theoretical dependences on ion mass in Fig. 24. During a given measurement the column was monitored with the streak camera and the photomultipler bank, Fig. 8.

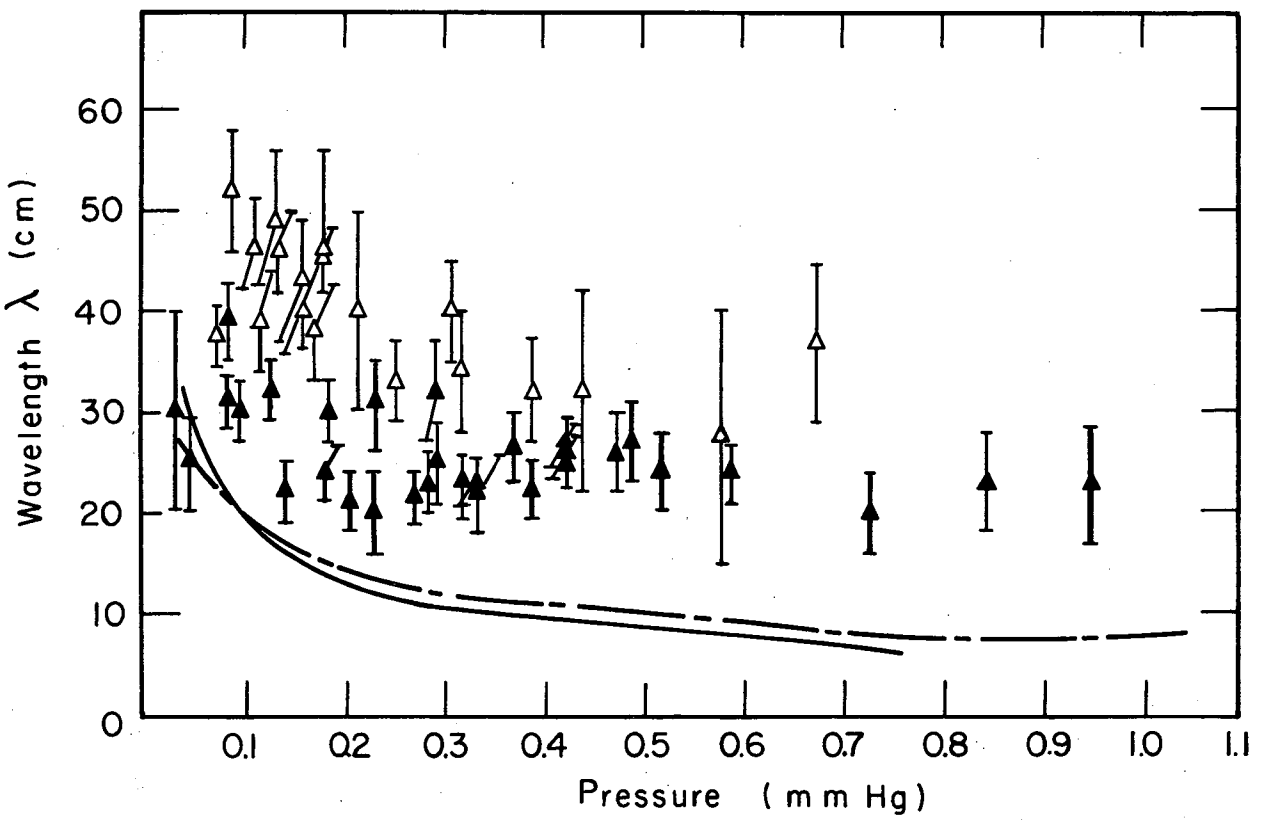

MU-22950

Fig. 24. Spiral wave length λ vs pressure. For R = 0.9 cm, I = 400 ma: △ H_2 experimental; ——— H_2 theory. For ▲ D_2 experimental: — - — D_2 theory.

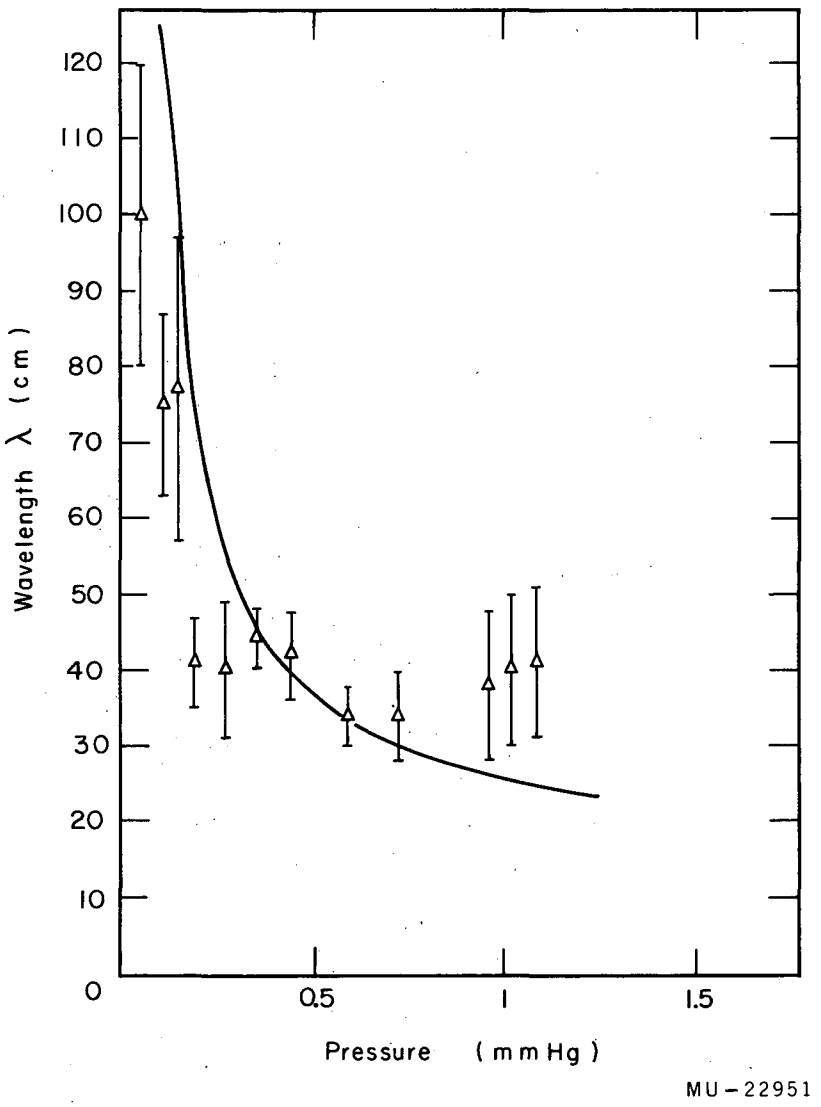

Fig. 25. λ vs pressure: R = 0.9 cm, I = 400 ma, He gas. Solid line is theoretical curve.

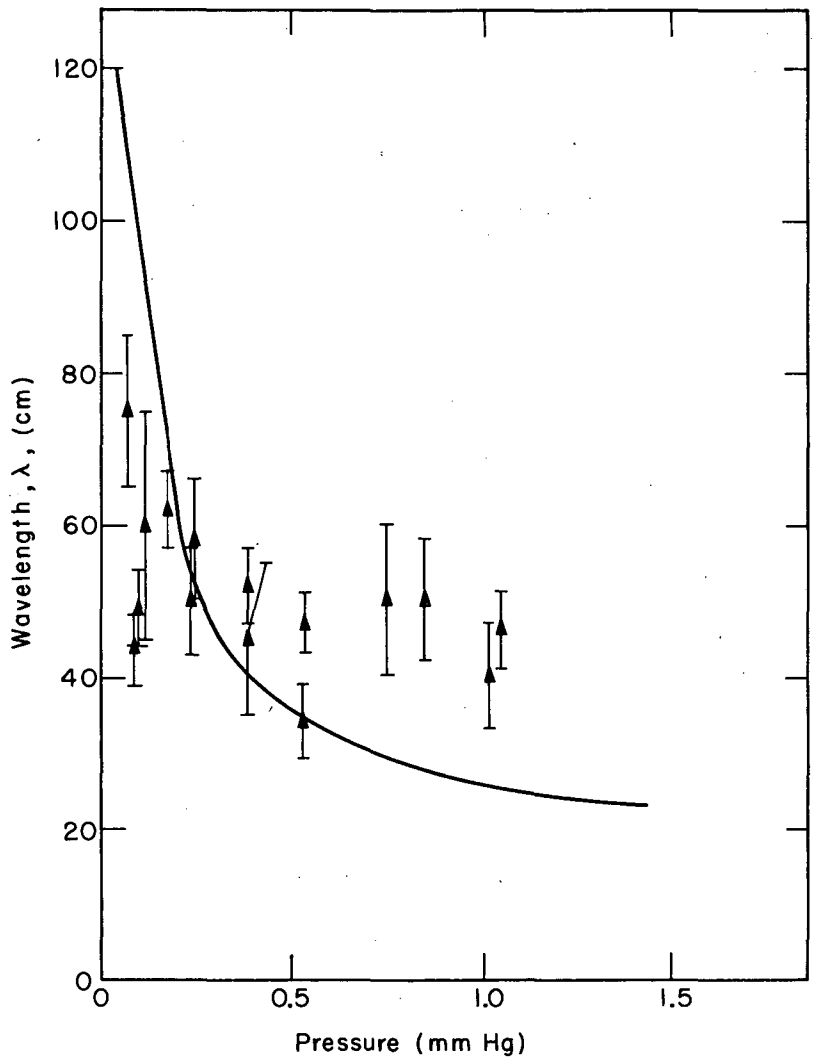

Fig. 26. λ vs pressure : R = 1.27 cm, I = 400 ma, He gas. Solid line is theoretical curve.

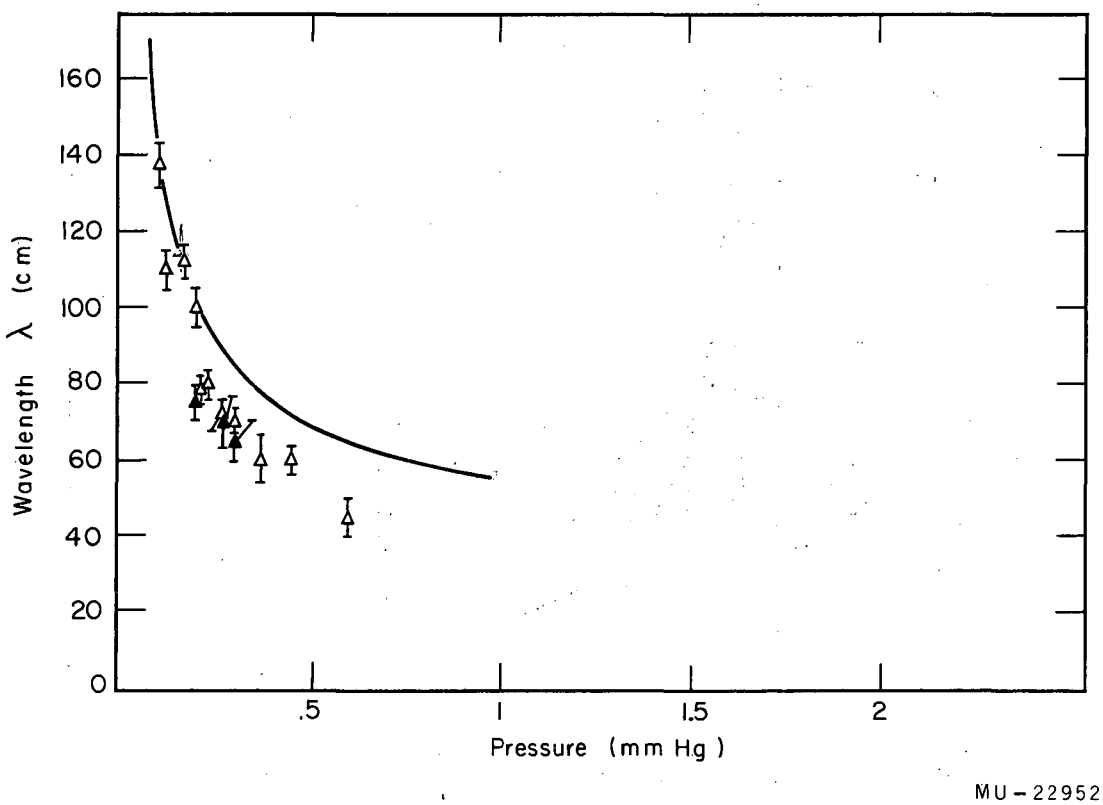

Fig. 27. λ vs pressure: R = 2.75 cm, He gas; ▲ 200 ma and △ 400 ma. Solid line is theoretical curve.

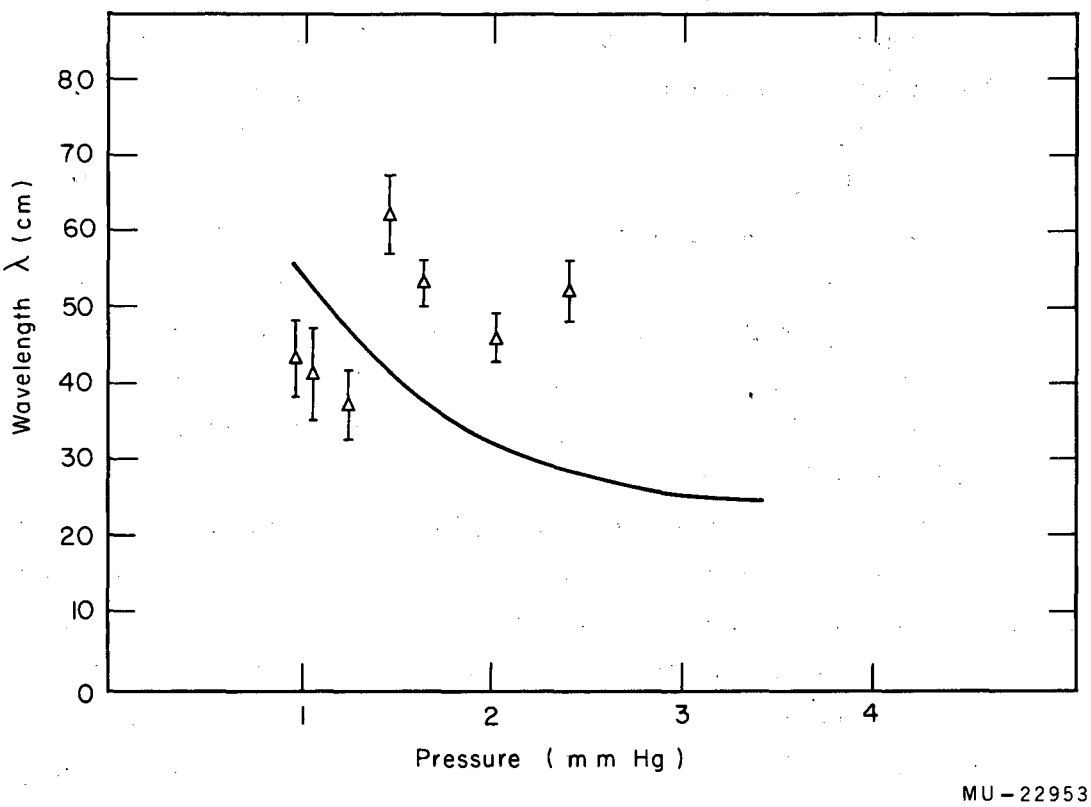

Fig. 28. λ vs pressure: R = 1.27 cm, Ne gas, I = 200 ma. Solid line is theoretical curve.

The effect of changes in the length of the magnetic field on the wave length is presented in Fig. 29 for several values of the neutral pressure and the discharge current. We have studied the $R = 2.75$ cm tube, as here the L/R ratio is most unfavorable. As Fig. 29 indicates, λ approaches an asymptotic value as the length of the magnetic field is increased. The "long tube" approximation becomes increasingly valid with increasing neutral pressures at $L/R = 72$.

We have attempted to determine the wave length λ at the earliest possible moment in its development. The small capacitor bank supplying a sinusoidally rising magnetic field was so charged that $B_{max} \approx B_c$; i.e., the magnetic field changed by only a small amount during the time of measurement. A typical set of photomultiplier traces is presented in Fig. 30, together with the schematic positions of the various photomultipliers. The general decrease in the light intensity, because of the falling electron temperature with increasing magnetic field, is followed at B_c by the development of oscillations in the light output. The disturbance does not develop simultaneously at all points along the column. The instability is seen to arise initially in the vicinity of $z = 56$ cm, i.e., away from the ends of the magnet coil, and to propagate in both directions. There is some evidence, however, that at low pressure ($p < 0.1$ mm Hg) the disturbance arises first at the anode end of the magnetic coil. The theory of Kadomtsev and Nedospasov predicts that the instability should arise everwhere along the column at the same time; our experimental results, on the other hand, indicate the spiral grows from a localized disturbance. The phase relationships between photomultiplier traces remain constant as time increases and can be fitted with a wave length of about 90 cm. This compares well with $\lambda = 100$ cm obtained from the fully developed steady-state spiral.

An estimate of the growth rate, $\mathrm{Im}(\omega)$, can also be obtained from the above measurements, although an accurate measurement is difficult. We find $\mathrm{Im}(\omega) \approx 10^5$ sec^{-1}, in rough agreement with

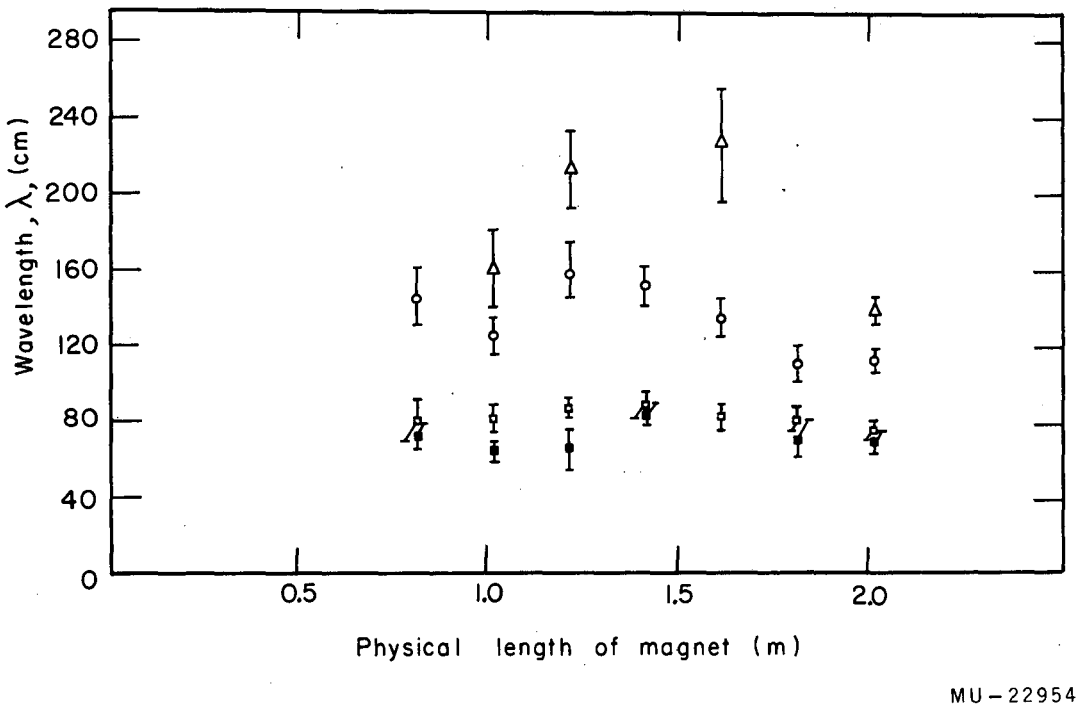

Fig. 29. Spiral wave length λ vs length of magnet coil: R = 2.75 cm, He gas: △ p = 0.11 mm Hg, 400 ma; ○ p = .17 mm Hg, 400 ma; ■ p = 0.27 mm Hg, 200 ma; □ p = 0.27 mm Hg, 400 ma.

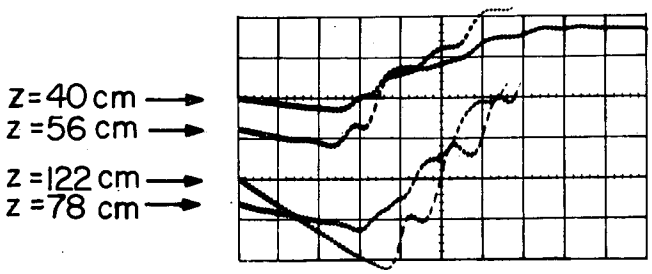

(a)

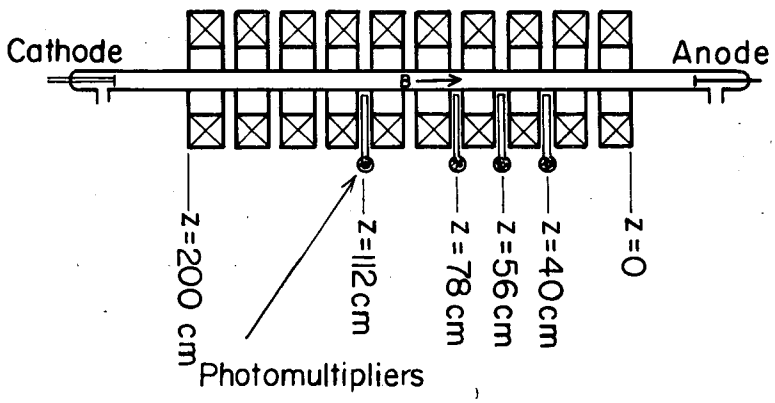

(b)

MU-22955

Fig. 30. Photomultiplier traces showing development of light oscillations. Position of photomultipliers are indicated in lower portion of figure. At 0.2 mm Hg He discharge, 400 ma: R = 2.75 cm, $B \approx B_c \approx 650$ gauss. Sweep speed is 100 μsec per large division. Time increases from left to right.

calculations. This instability thus develops rather slowly compared with the type observed in pinch discharges.[38]

The dispersion relation derived by Kadomtsev and Nedospasov in considering the stability of the column can also be solved for ω_r, the real frequency of oscillation of the luminous current channel. Under the condition that $B \approx B_c$, the expression for ω_r takes the simple form

$$\omega_r \approx \frac{3\mu_+ D_- \beta_1^2}{\mu_- (\Omega_- \tau_-)} \left[.6 + x^2 \right], \quad x = \frac{k\Omega_- \tau_-}{\beta_1}, \quad \beta_1 = \frac{3.83}{R} . \tag{IV-1}$$

The growth of the instability is driven by $\vec{j} \times \vec{B}$ forces that twist a kink in the current channel into a helix in close contact with the tube walls. From Eq.s (IV-1) and (II-17) we can arrive at an approximate expression for the phase velocity of the perturbation:

$$v_{ph} = \frac{\omega_r}{k} \approx \frac{1.15\, mv_{-z}}{\{2F + \sqrt{F^2 + 12KG}\}} + \frac{68}{R^2} \left\{ 2F + \sqrt{F^2 + 12KG} \right\} \left(\frac{\mu_+}{\mu_-} \right)^2 \frac{D_-^2}{mv_{-z}} . \tag{IV-2}$$

The second term on the right of Eq. (IV-2) is, for our experimental conditions, usually less than a 30% correction. Typically $\{2F + \sqrt{F^2 + 12KG}\} > 3$, thus $v_{ph} < v_{-z}$.

The luminous helical structure, traveling in the direction of the electron drift, will appear to an observer at some cross section along the tube as a rotating column. This picture has been verified by experimental measurements of the pitch and direction of rotation of the spiral; we present a sketch of the situation in Fig. 31. In the steady state with $B > B_c$ the luminous column revolves about the tube axis, this rotation being clockwise when the column is

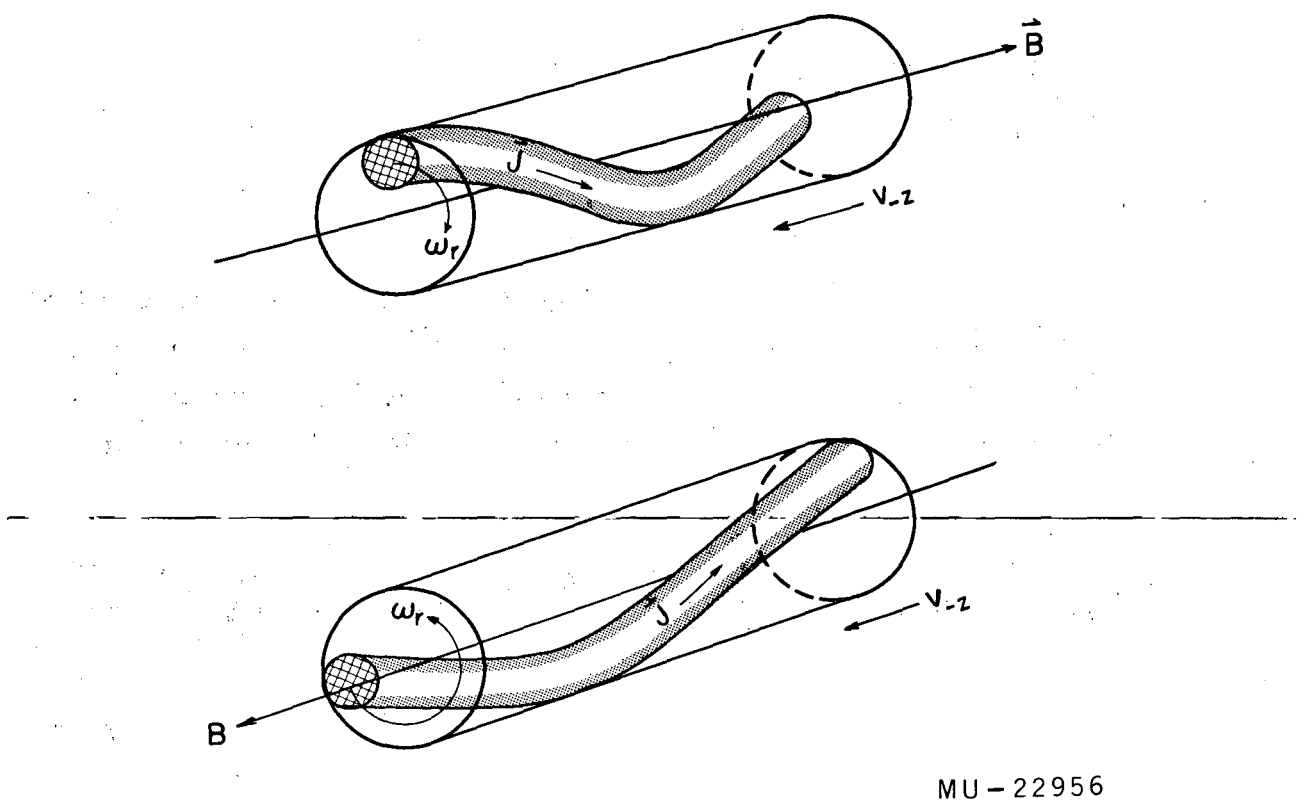

Fig. 31. Pitch and direction of rotation of helix as a function of the direction of the magnetic field.

viewed in the direction of the magnetic field. In Fig. 32 we present the instantaneous density profile across the column taken with a radially movable Langmuir probe.

The measurements of the frequency of rotation of the luminous current channel are presented in Figs. 33 through 38. The photomultiplier bank, together with the rotating mirror, permitted identification of the spiral mode; under certain conditions the time-resolved light-wave form of axially moving stirations is similar to the near-sinusoidal wave form of the azimuthally moving column. Each experimental point in the above figures represents an average of 6 to 12 photomultiplier traces, each trace about 10 periods long. Again remembering that Eq. (IV-1) was derived by considering small-amplitude disturbances, we have plotted ω_r as a function of pressure with the experimental results in Figs. 33 through 38. The observed general decrease of ω with increasing pressure is confirmed theoretically, with good quantitative agreement between experiment and theory for helium.

Measurement of the time development of the wave length of the instability, as described earlier, also yielded information regarding the changes occurring in the frequency. Using a 400-ma He discharge in a tube of $R = 2.75$ cm, we obtain the following values for the frequency (rad/sec) at $t \approx 0$ and $t = \infty$:

p (mm Hg)	$t \approx 0$ $(B = B_c)$	$t = \infty$ $(B \approx B_c)$
0.2	5.9×10^4	5.0×10^4
0.37	4.3×10^4	3.8×10^4

As the magnetic field was increased somewhat above B_c, the luminous spiral degenerated into irregular fluctuations of light, Fig. 39 (a). In some cases, this transition was preceded by the appearance of frequencies which modulated ω_r, and abrupt changes in ω_r ; sometimes,

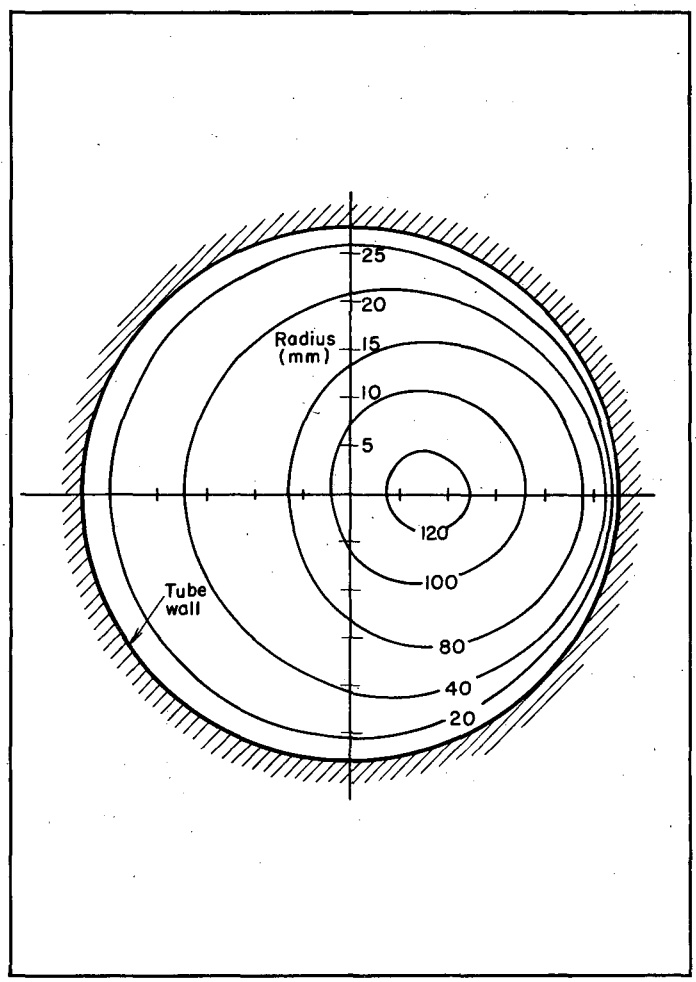

MU-22957

Fig. 32. Ion current distribution (μa) across tube as collected by negative probe; R = 2.75 cm, He gas; p = 0.23 mm Hg, I = 300 ma, B = 767 gauss.

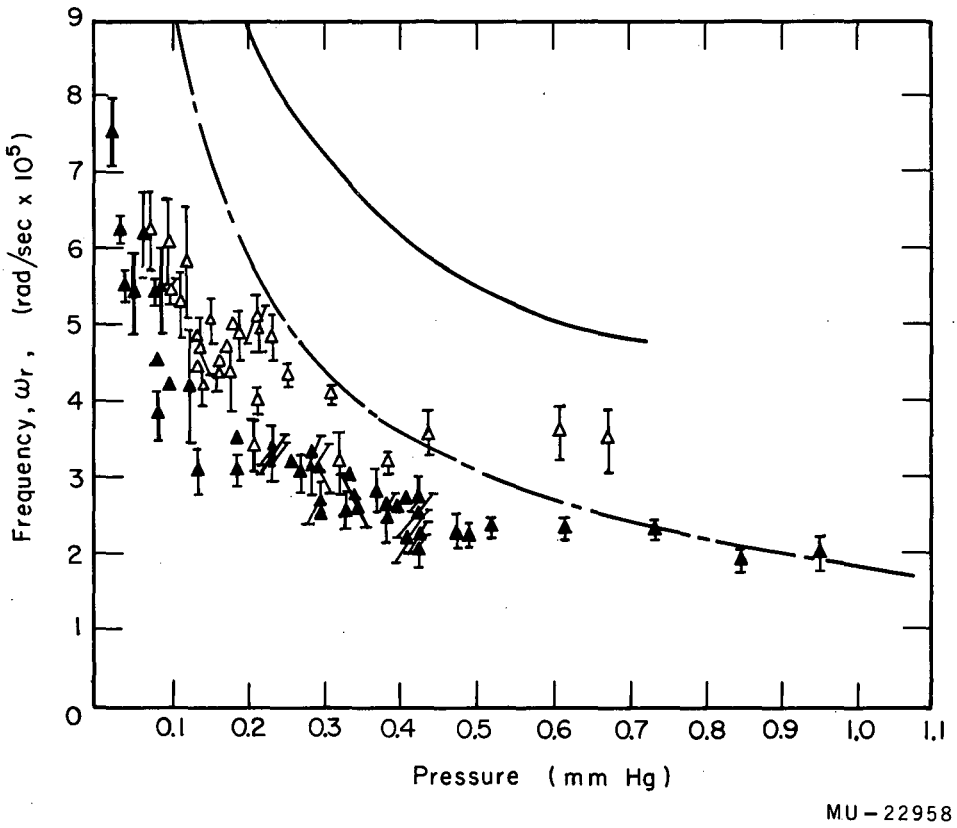

Fig. 33. Frequency of rotation of luminous channel, ω_r, vs pressure: △ H_2 experimental, —— H_2 theory; ▲ D_2 experimental, — - — D_2 theory; R = 0.9 cm, I = 400 ma.

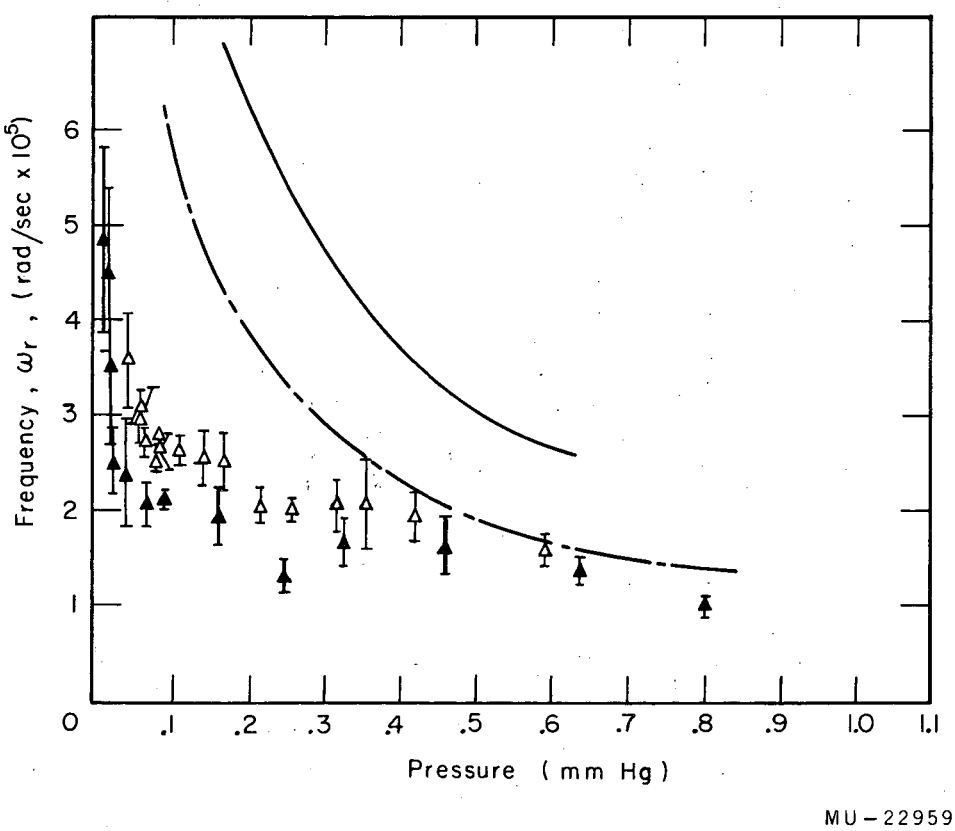

Fig. 34. ω_r vs pressure — R = 1.27 cm, I = 400 ma; △ H_2 experimental, —— H_2 theory; ▲ D_2 experimental, — - — D_2 theory.

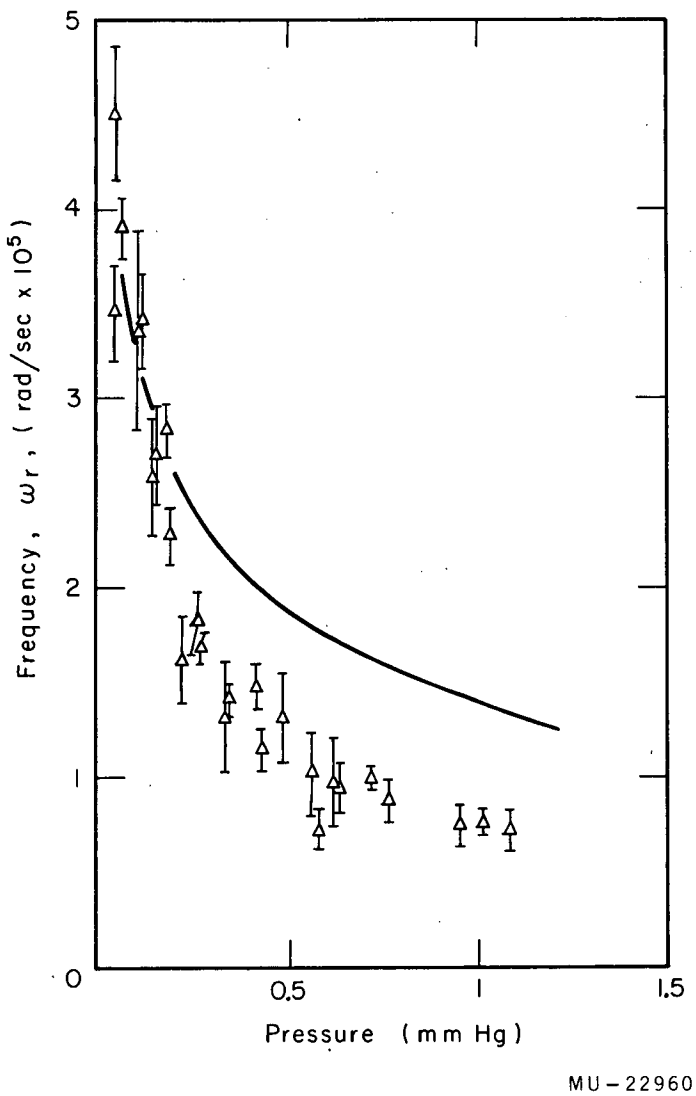

Fig. 35. ω_r vs pressure; R = 0.9 cm, He gas, I = 400 ma. Solid line is theoretical curve.

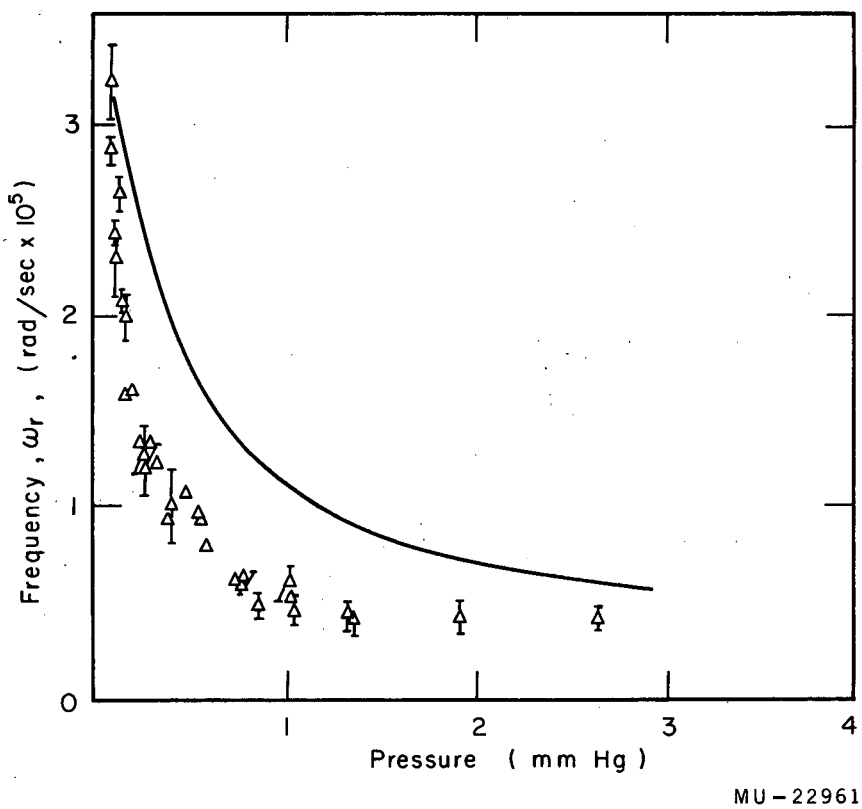

Fig. 36. ω_r vs pressure: R = 1.27 cm, He gas, I = 400 ma. Solid line is theoretical curve.

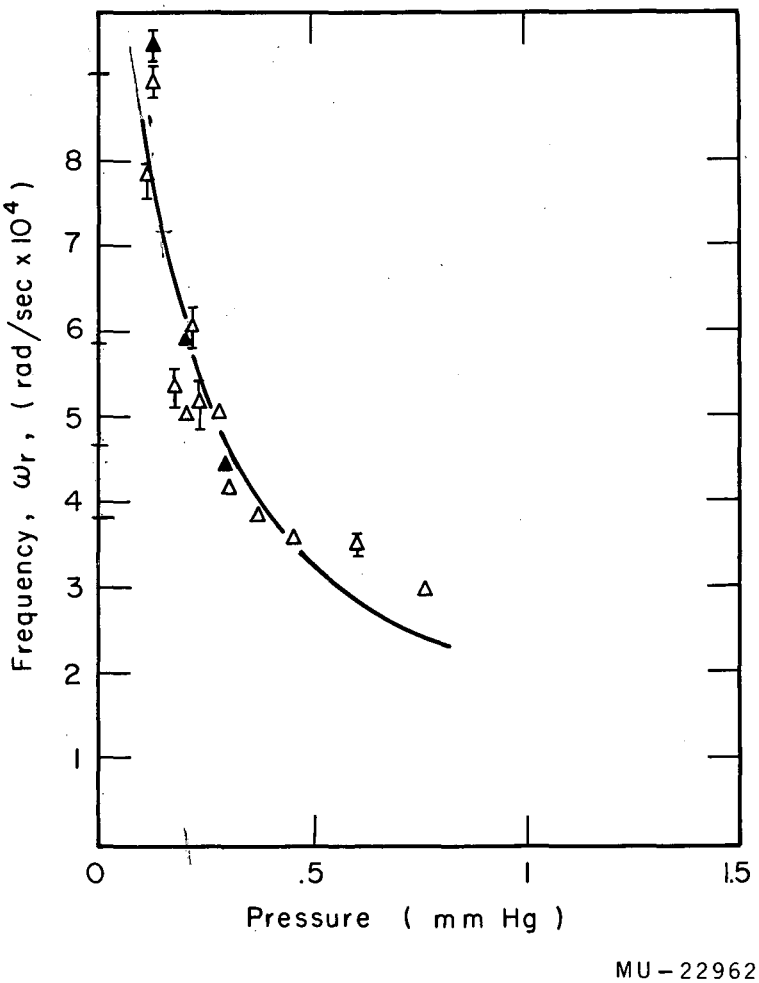

Fig. 37. ω_r vs pressure (R = 2.75 cm); Δ 400 ma He and ▲ 200 ma He. Solid line is theoretical curve.

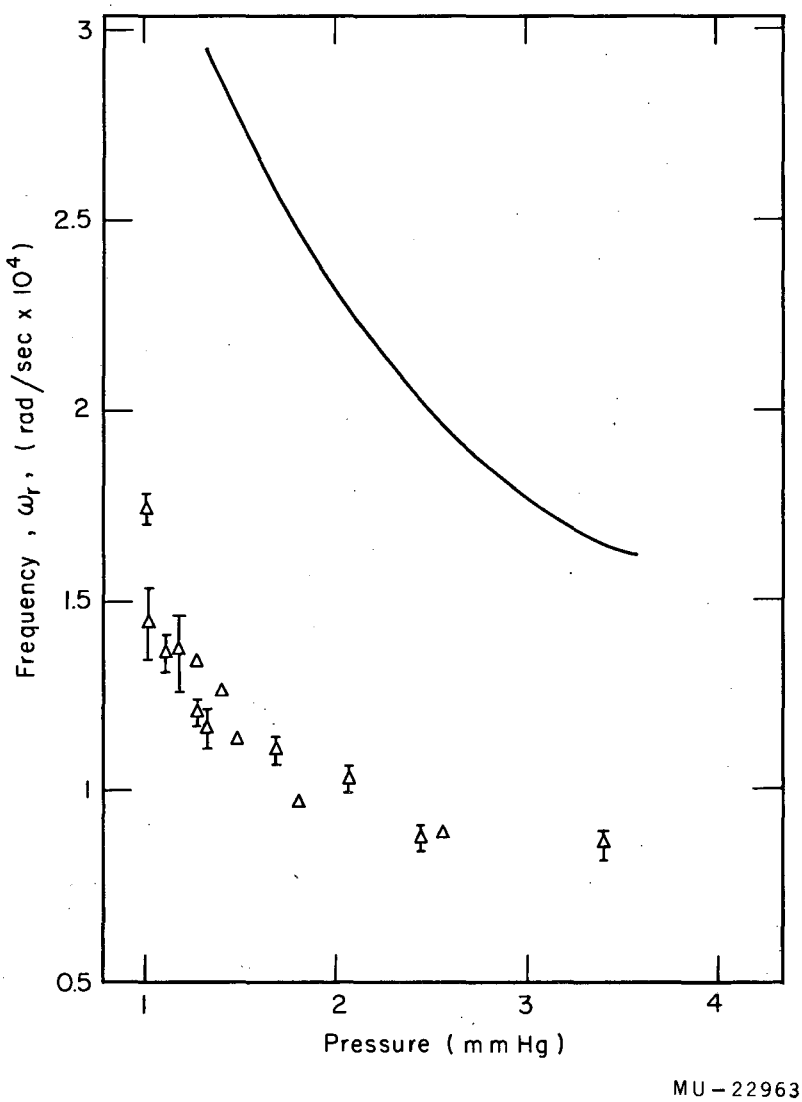

Fig. 38. ω_r vs pressure: R = 1.27 cm, I = 200 ma, Ne gas. Solid line is theoretical curve.

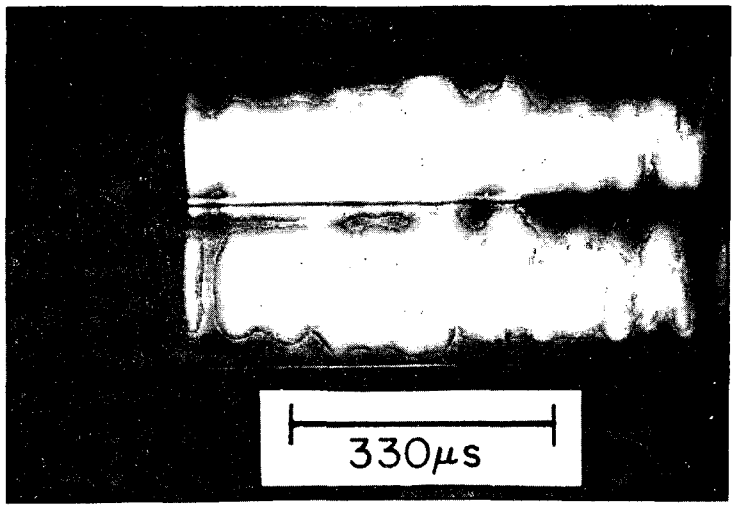

(a)

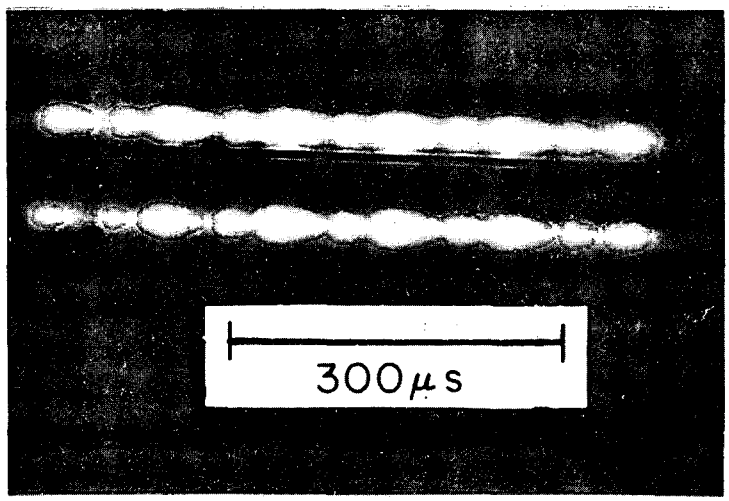

(b)

ZN-2713

Fig. 39. 90 deg. stero streak photographs. Traces show variation of light intensity with time and radius in helium discharges: (a) R = 2.75 cm, p = 0.23 mm Hg, B = 979 gauss; and (b) R = 0.9 cm, p = 0.2 mm Hg, B = 994 gauss $< B_c$ (moving striations).

as in the case of helium, the color of the spiral as seen with the rotating mirror underwent a change, indicating changes in the electron temperature. We have found that the various transitions just described are intimately connected with the undulations of the E_z-vs-B curves at $B > B_c$.

The above discussion suggests that modes higher than $m = 1$ may be present in the plasma under these circumstances. Indeed, if we calculate B_c-vs-p curves from the theory of Kadomtsev and Nedospasov and let $m = 2$ (Figs. 13 and 17), we find that the higher mode can appear at fields only slightly higher than B_c. At low pressures we may even have $B_c\ (m = 2) < B_c\ (m = 1)$. Experimentally, however, we have been unable to distinguish or identify a symmetric $m = 2$ mode in the confused state of the plasma above B_c.

The chaotic state of the plasma above the critical magnetic field is reflected in the radial electron density distribution, Fig. 40. The time-average density distribution is noticeably flattened; visually we observed that the luminous column now appears to fill the tube more completely than at $B = 0$.

The microwave interferometer (Fig. 9) permitted time-resolved measurements of the electron density to be made. We have studied the rate of loss of electrons from the column as a function of the pressure and the magnetic field. A 5-amp rectangular pulse of current yielded densities of approximately $4 \times 10^{12}/cm^3$ for times of the order of 10 msec. The termination of the current flow left a plasma in the tube whose density then decreased with time. The e-folding times for the roughly exponentially decaying density are shown as functions of pressure and magnetic field in Fig. 41. The rather consistent results at low magnetic fields are followed by widely scattered points at $B > 1$ kilogauss, corresponding approximately to the transition to the spiral state. Analysis of these results is probably impossible — the behavior of afterglows is extremely complex and influenced by a variety of processes.[39] The nonsymmetric distribution of the plasma at fields greater than B_c would only serve to complicate the problem.

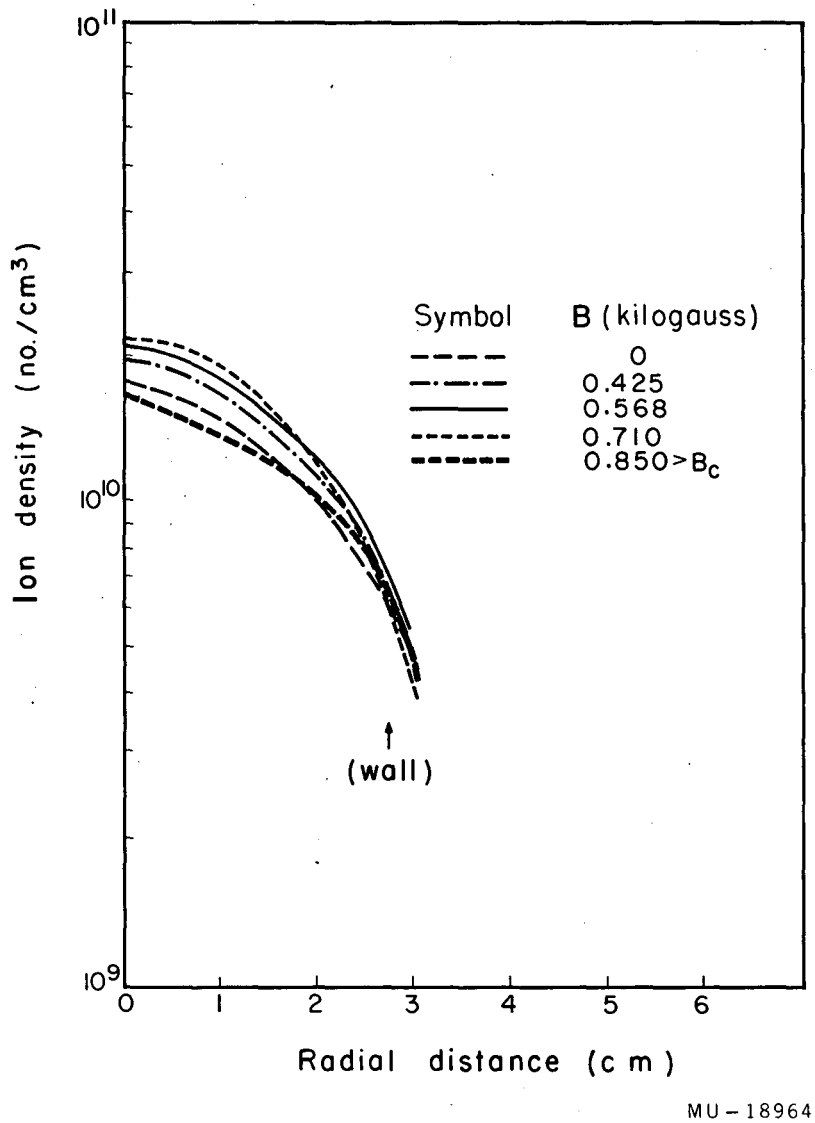

Fig. 40. Ion density vs radius and magnetic field; p = 0.22 mm Hg, I = 200 ma, He gas.

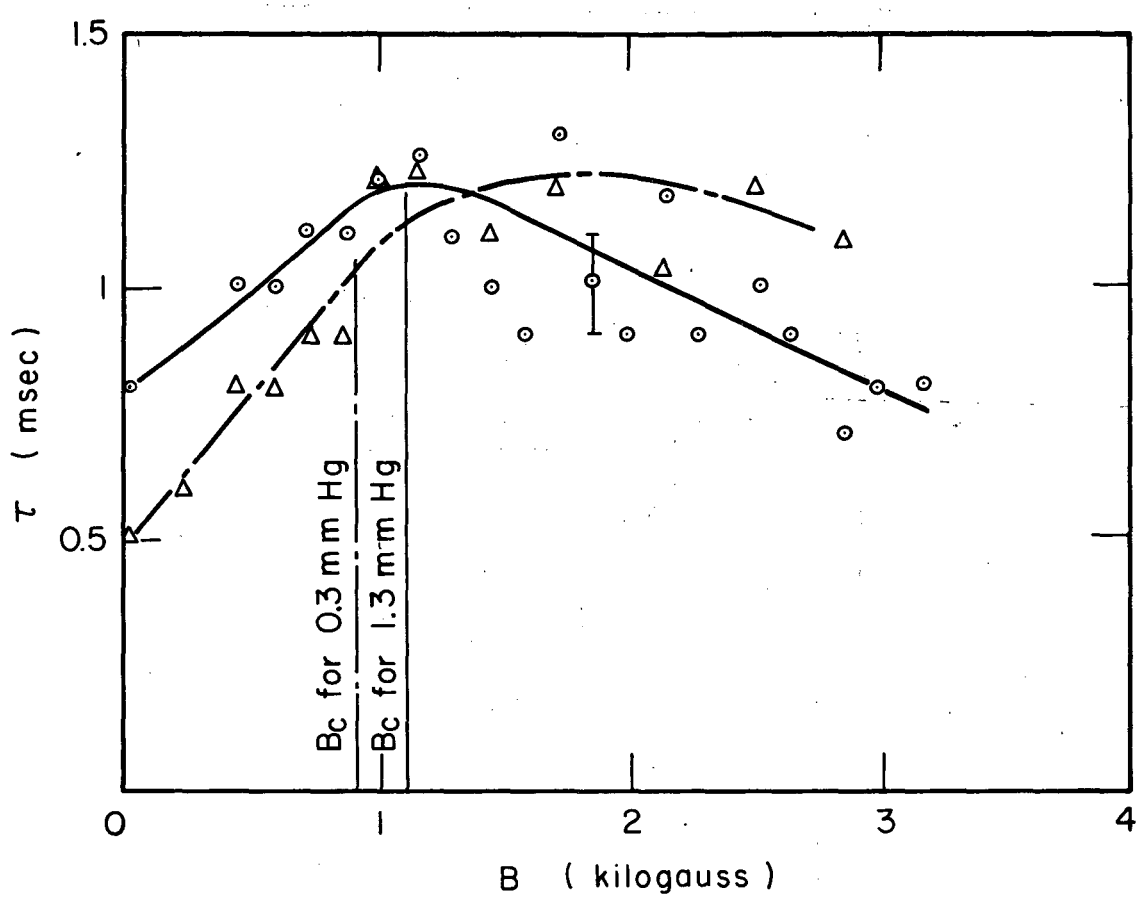

MU-22964

Fig. 41. Decay time of electron density vs pressure and magnetic field I = 5 amp, He gas: Δ 0.3 mm Hg and ⊙ 1.3 mm Hg. Curves indicate roughly the trend of experimental points; — - — 0.3 mm Hg and ——— 1.3 mm Hg.

We have analyzed the electromagnetic noise generated by the plasma in the frequency ranges 5 kc to 250 Mc and 1 to 10 kMc. In addition to frequencies associated with moving striations, we find frequencies that correspond to the frequency of the luminous spiral. A broad band of electromagnetic noise from 10 kc to about 2 Mc appears at fields slightly above B_c and is associated with the transition from the rather regular spiral mode to a chaotic state of the column, characterized by irregular fluctuations of light. We have not detected any oscillations that could be associated with either cyclotron or plasma frequencies of the electrons or ions.

V. SUMMARY AND CONCLUSIONS

The previously reported anomalous state of the positive column, characterized by a longitudinal electric field that rises with increasing magnetic field, is the result of an instability which appears at B_c. The critical magnetic field, B_c, describing the onset of the instability, varies approximately inversely as the tube radius and directly as the square root of the ion mass. The relatively slow-developing instability results eventually in a steady state in which the plasma density distribution has lost its azimuthal symmetry and formed a long-wave-length rotating spiral. Because of the absence of a net radial current, we believe rotation of the plasma density, as well as of the luminous structure, to be associated with the passing of a potential wave rather than an actual mass motion. The close contact between the luminous current channel and the walls of the tube increases the losses of charged particles and results in an electric field considerably in excess of classical predictions. As the magnetic field is increased to higher and higher values, the behavior of the column becomes increasingly more chaotic, characterized not only by irregular fluctuations of light, but also by a broad band of electromagnetic noise.

We have calculated the onset of the instability from the theories of Kadomtsev and Nedospasov[21] and Hoh.[22] The shapes of the experimental curves are perhaps more like the calculations from the K and N theory; the rapid decrease of B_c at high pressures by Hoh is not confirmed by the experimental results in neon and argon. Investigations of B_c at high pressures in helium have shown that B_c is here no longer independent of the discharge current. This suggests that both theories may need to be modified to include stepwise ionization and pressure constriction.

The wave length of the instability as well as its frequency of oscillation is predicted by the theory of K and N. The experimental frequencies and wave lengths were obtained from the fully developed steady-state helix. It is not obvious that they should be the same as the quantities calculated from a small-amplitude theory. Nevertheless we find qualitative, and sometimes quantitative, agreement between

theory and experiment: the wave lengths decrease with increasing pressure and decreasing radius; the frequencies increase with decreasing radius and decreasing pressure. The inverse relationship between frequency and pressure suggests a connection with the instabilities reported in PIG-type discharges.[16]

We have not been able to unequivocally distinguish between the theory of Hoh and the rather different approach of Kadomtsev and Nedospasov. Uncertainties about the ion species present in the discharge permit a latitude in the value of the ion mobility; with a proper choice either theory fits the experimental results reasonably well. Measurements of B_c at high pressures, where the predictions of these theories diverge markedly, are complicated by pressure constriction. The theory of Hoh, in contrast to the K and N theory, does not require a current for the development of the instability. A current-free plasma might thus in principle permit a distinction to be made between these theories. We are not certain that a meaningful experiment could be performed in the afterglow of a glow discharge. The particle-loss mechanisms are not yet understood in the $B = 0$ case.[39]

Our search for possible enhanced diffusion preceding the large-scale instability just described has yielded negative results. Measurements of the radial potential distributions for a number of conditions can be explained by the classical theory of the column; we have not found minima in the curves which would, according to the Ecker theory,[29] suggest the presence of enhanced diffusion. No electromagnetic radiation at the plasma or cyclotron frequencies has been found.

ACKNOWLEDGMENTS

It is a pleasure to thank Dr. Robert V. Pyle and Dr. T. Kenneth Allen for encouragement and guidance during the course of this work. I am grateful to J. Warren Stearns for helping with many of the measurements, to Y. T. Fung, Larry S. Hall, Dr. Wulf B. Kunkel, Dr. J. Bryan Taylor, and Dr. Gunter Ecker for valuable discussions of the theory and experiment and to Dr. C. M. Van Atta for the direction and encouragment of this research. The skillful and patient efforts of Harry Powell's glass shop and the mechanical shops headed by John Meneghetti and Louis Biagi were essential to the success of the experiment. Ferd Voelker and M. C. Horton constructed the microwave gear. The IBM 650 programs were written by Edna Williams and Elizabeth Meyers.

This research was done during the tenure of a National Science Foundation fellowship at the University of California.

I would like to dedicate this thesis to my wife, Joan Marie, in grateful recognition of her unfailing moral support.

Appendix A. Curves of Measurements of the Longitudinal Electric Field

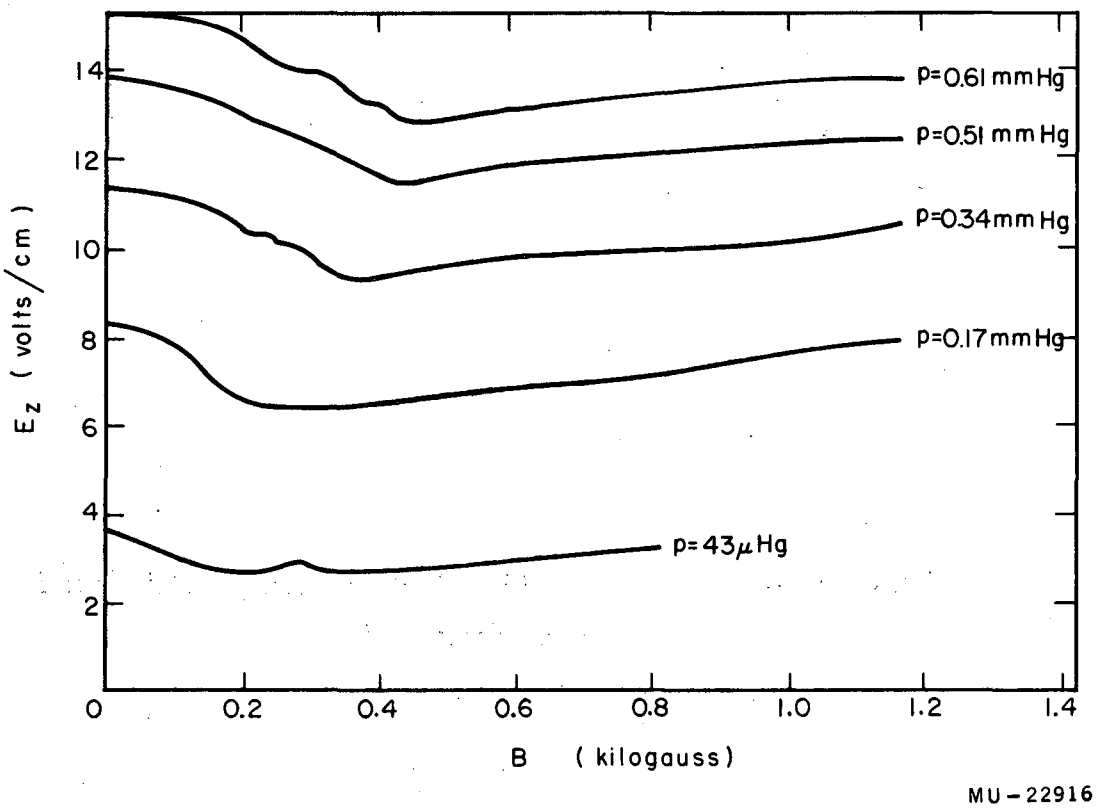

Fig. A-1. The longitudinal electric field E_z vs magnetic field B: H_2 gas, R = 1.27 cm, I = 200 ma.

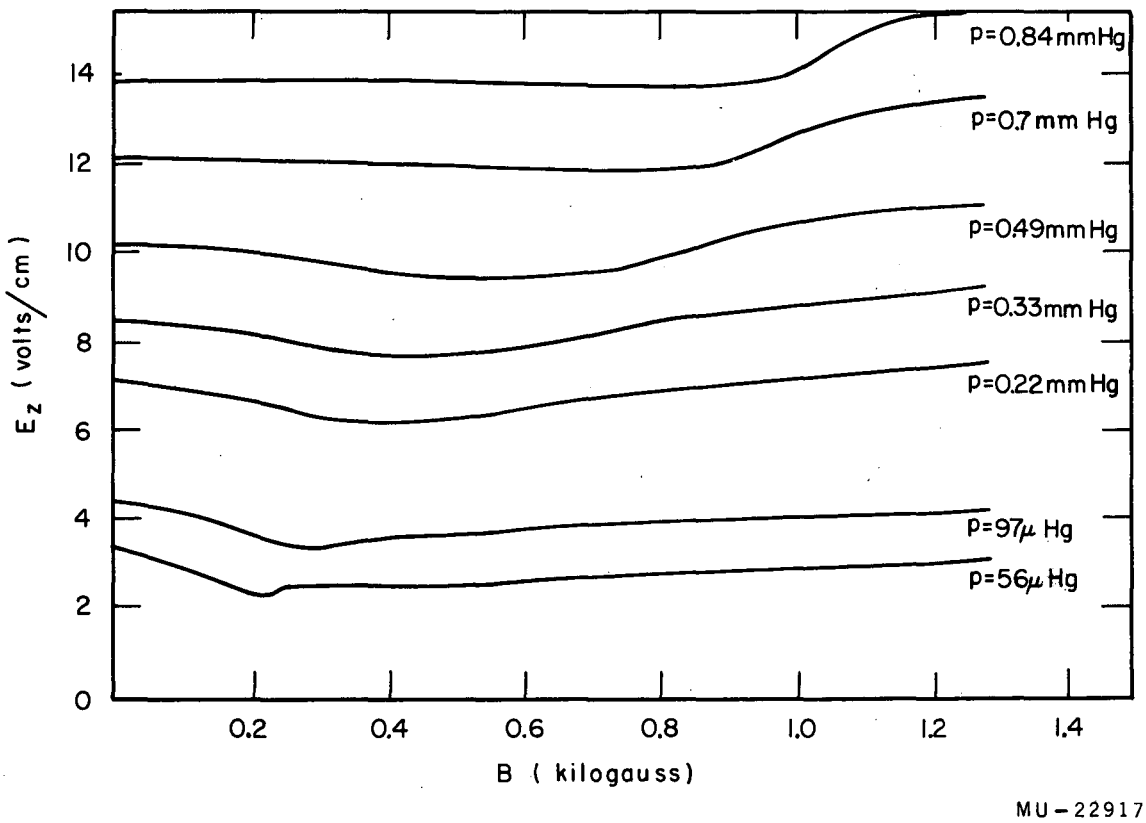

Fig. A-2. E_z vs B: D_2 gas, R = 1.27 cm, I = 200 ma.

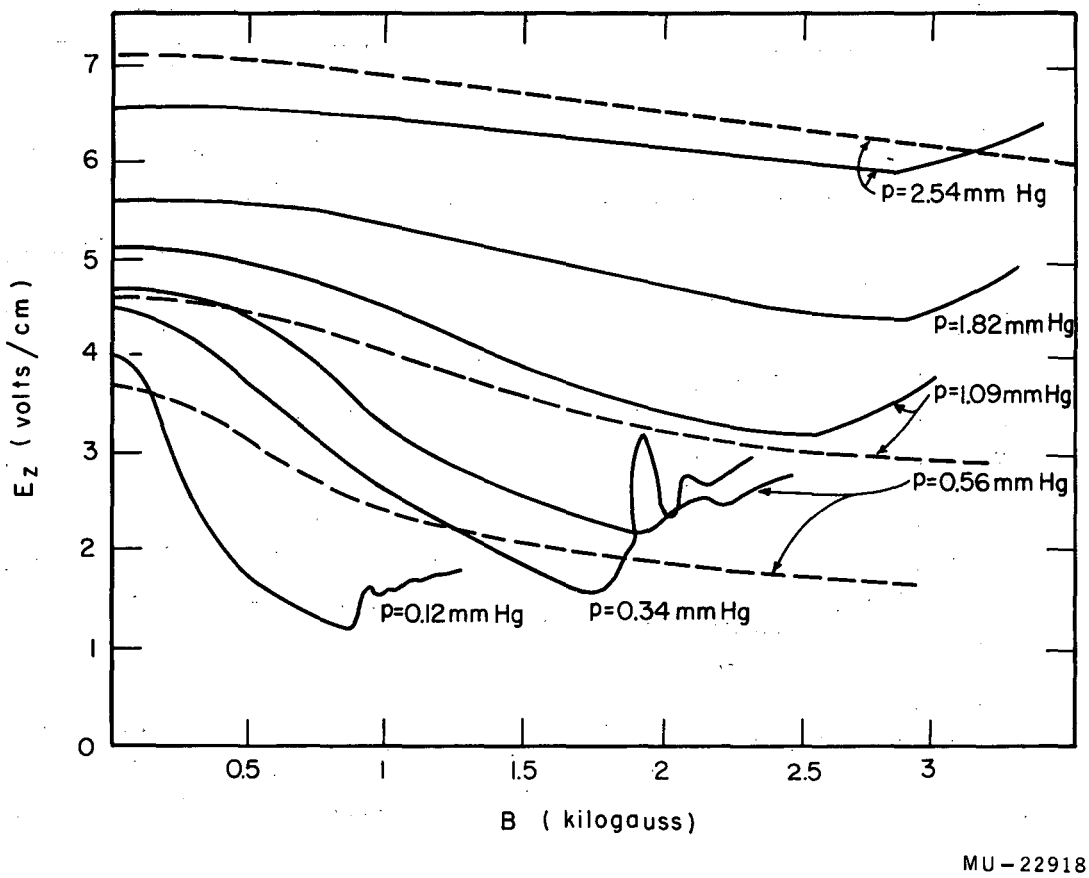

Fig. A-3. E_z vs B: He gas, R = 0.9 cm, I = 200 ma. Dashed lines represent theoretical calculations.

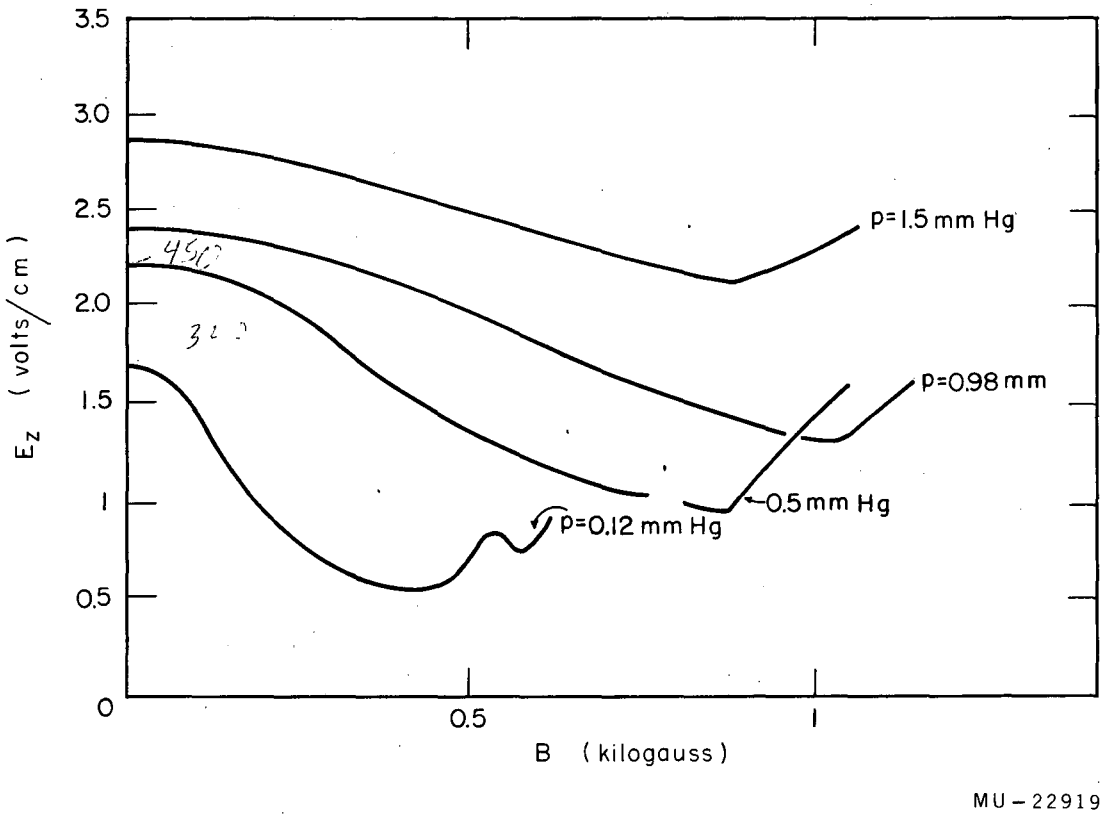

Fig. A-4. E_z vs B curves: He gas, R = 2.75 cm, I = 200

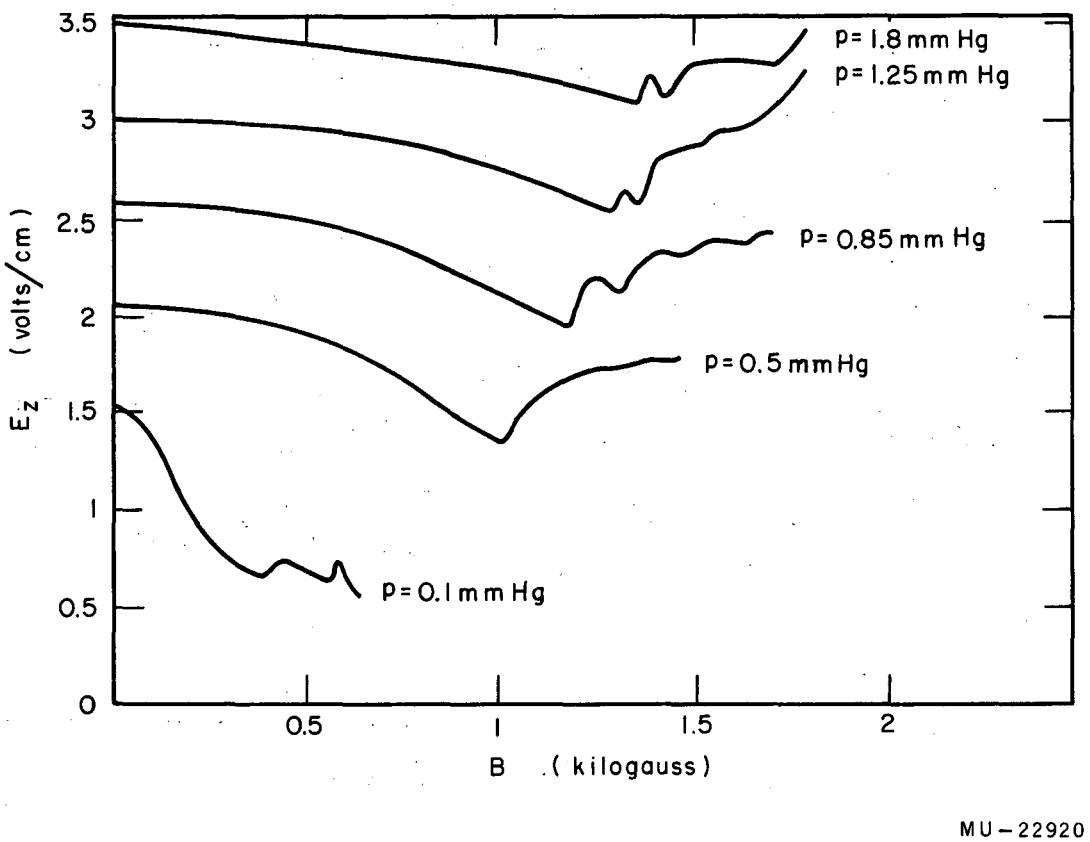

Fig. A-5. E_z vs B curves: He gas, R = 2.75 cm, I = 400 ma. "Short tube" geometry (Fig. 10).

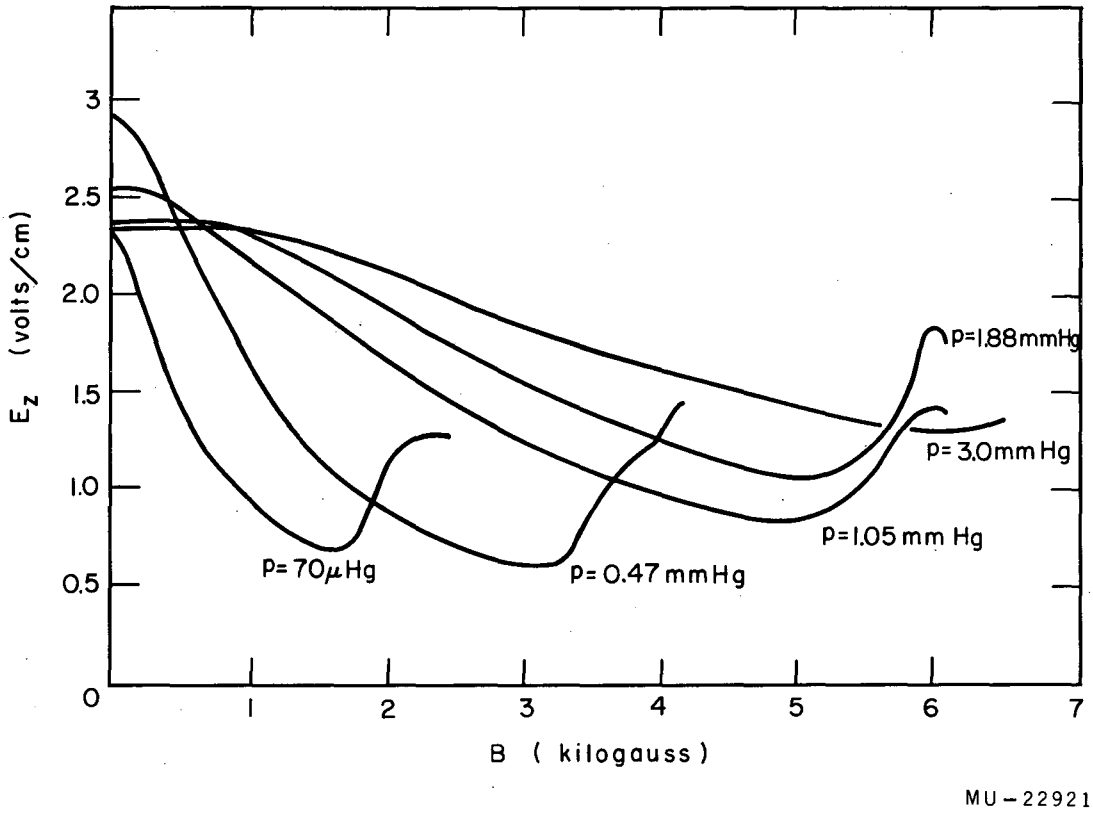

Fig. A-6. E_z vs B curves: Ne gas, R = 0.9 cm, I = 200 ma.

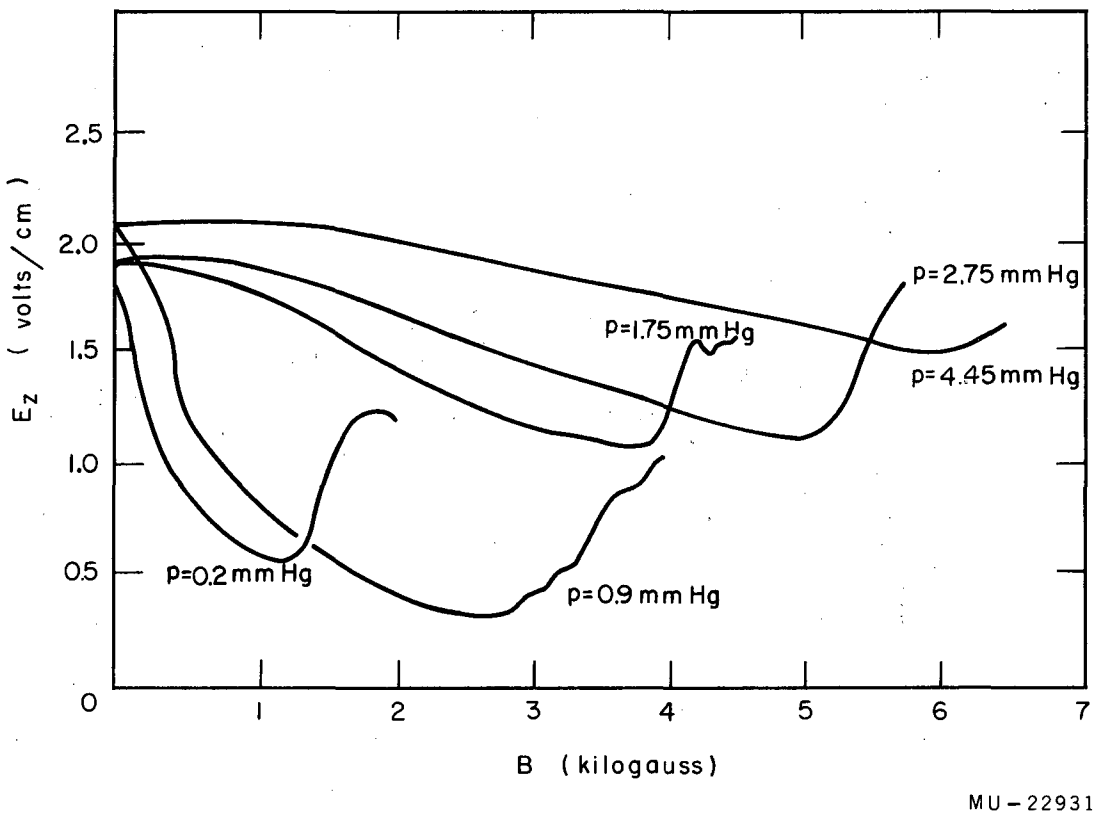

Fig. A-7. E_z vs B curves: Ne gas, R = 1.27 cm, I = 400 ma.

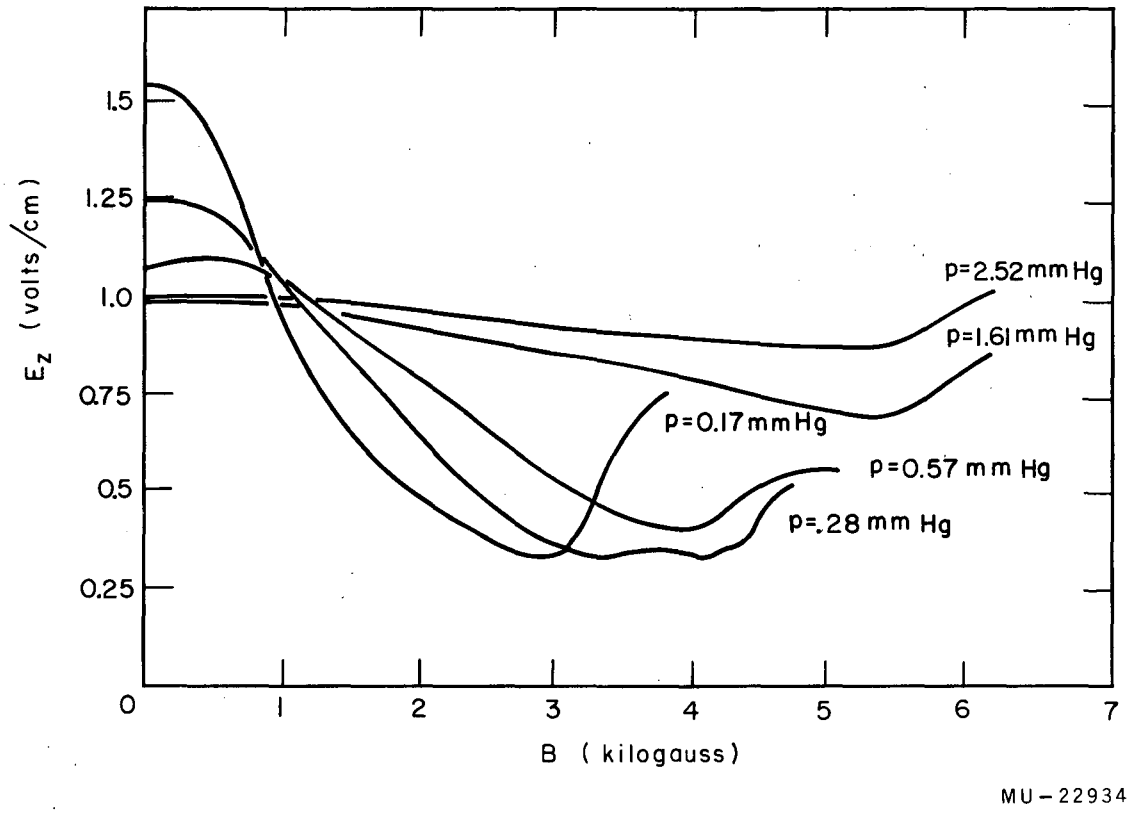

Fig. A-8. E_z vs B curves: A gas, R = 0.9 cm, I = 200 ma.

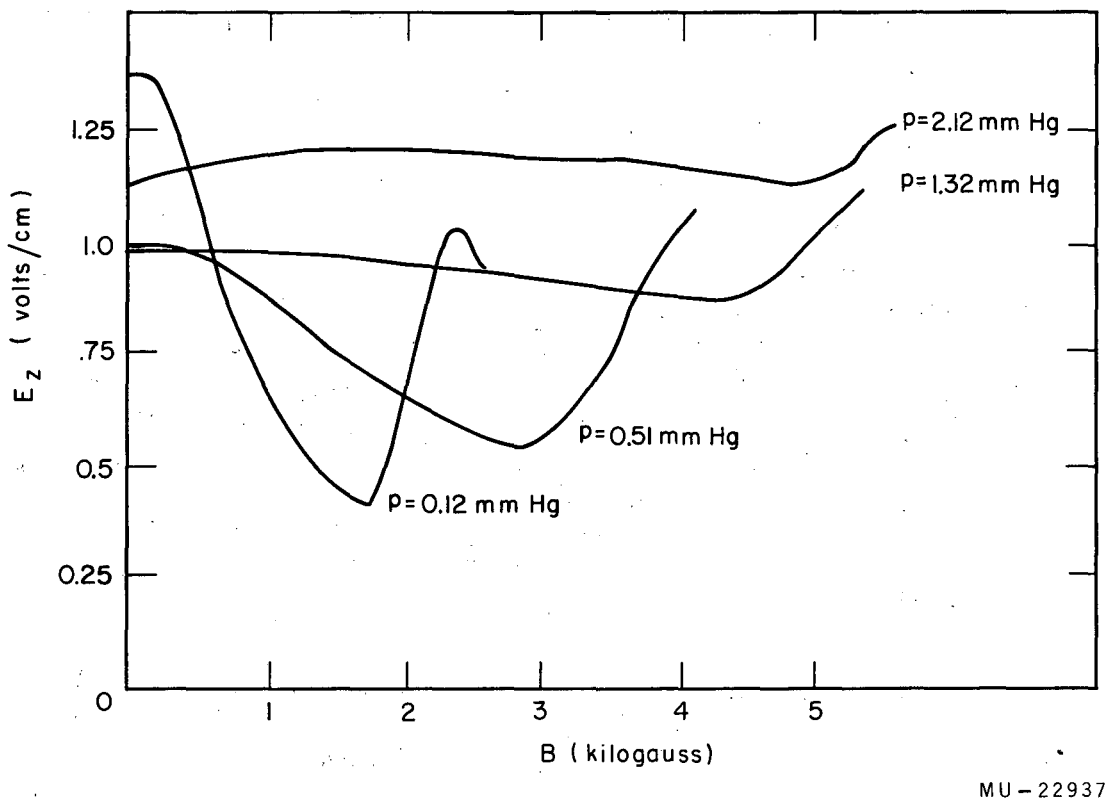

Fig. A-9. E_z vs B curves: A gas, R = 1.27 cm, I = 200 ma.

Appendix B. Curves of the Measurements of the Radial Potential Distribution

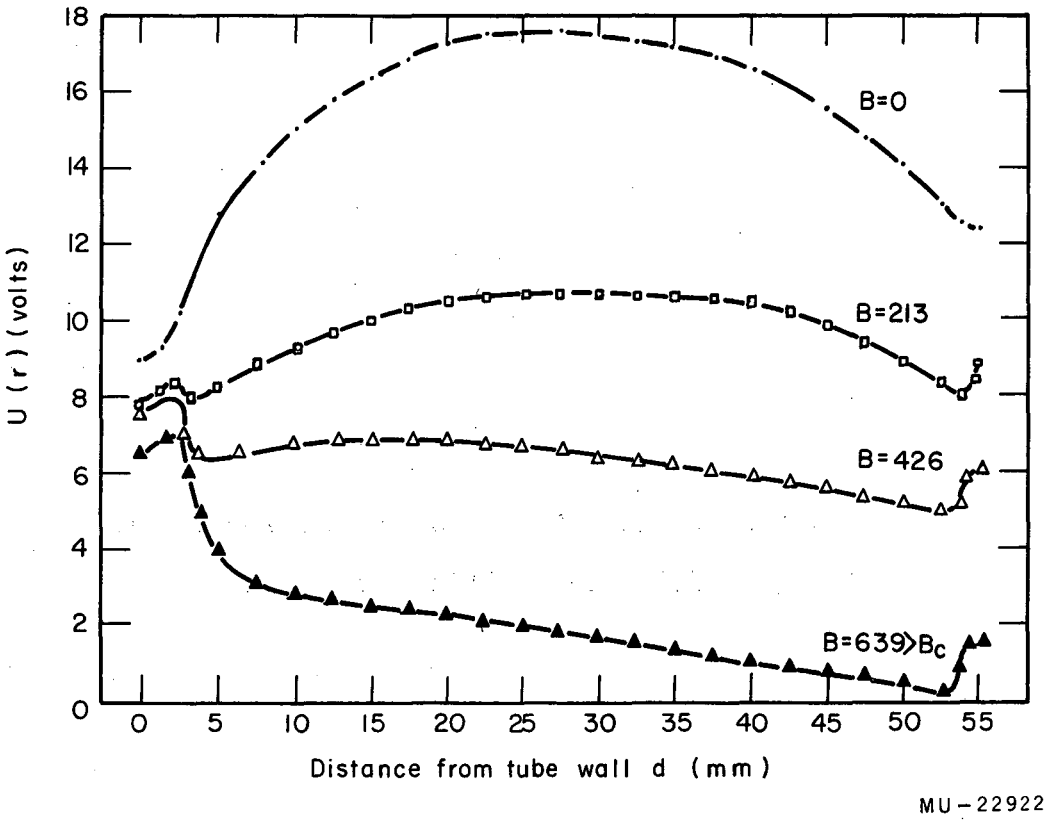

Fig. B-1. Radial potential U(r) vs distance from tube wall d; 0.1 mm Hg, He gas, I = 200 ma. "Dog leg" probe (Fig. 7) in 300 cm long tube , R = 2.75 cm. Magnetic field B is in gauss.

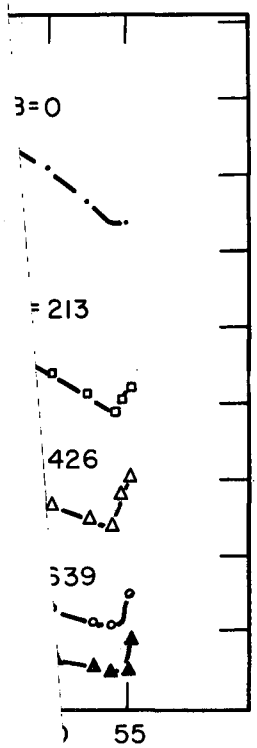

MU-22923

= 200 ma.
. B-1.

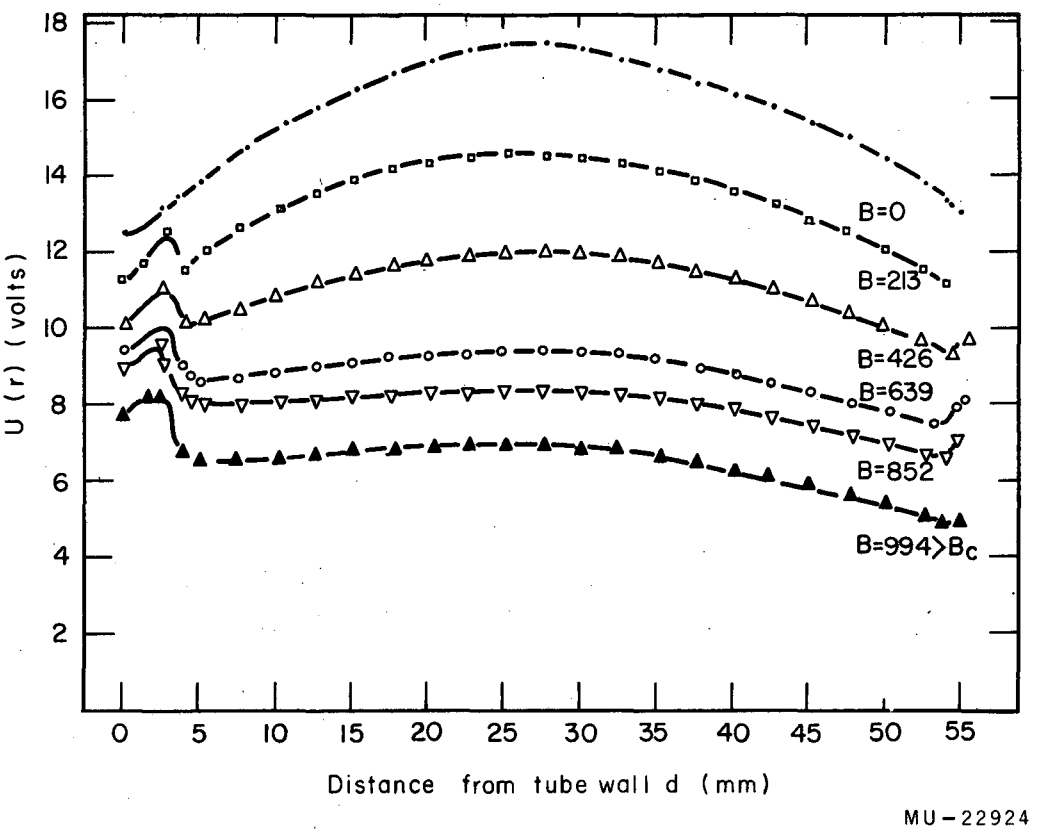

Fig. B-3. U(r) vs d curves; He gas, 0.6 mm Hg, I = 200 ma. Probe and tube geometry is identical with Fig. B-1.

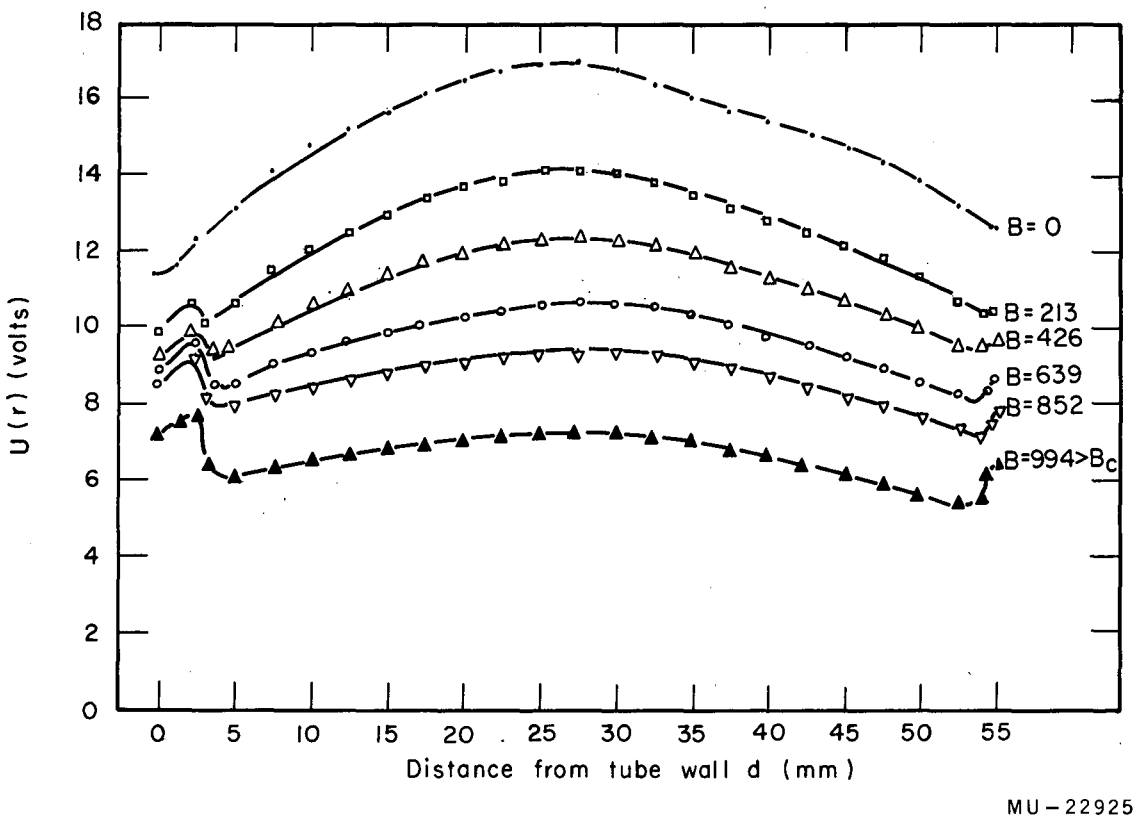

Fig. B-4. U(r) vs d curves; He gas, 0.9 mm Hg, I = 200 ma. Probe and tube geometry is identical with Fig. B-1.

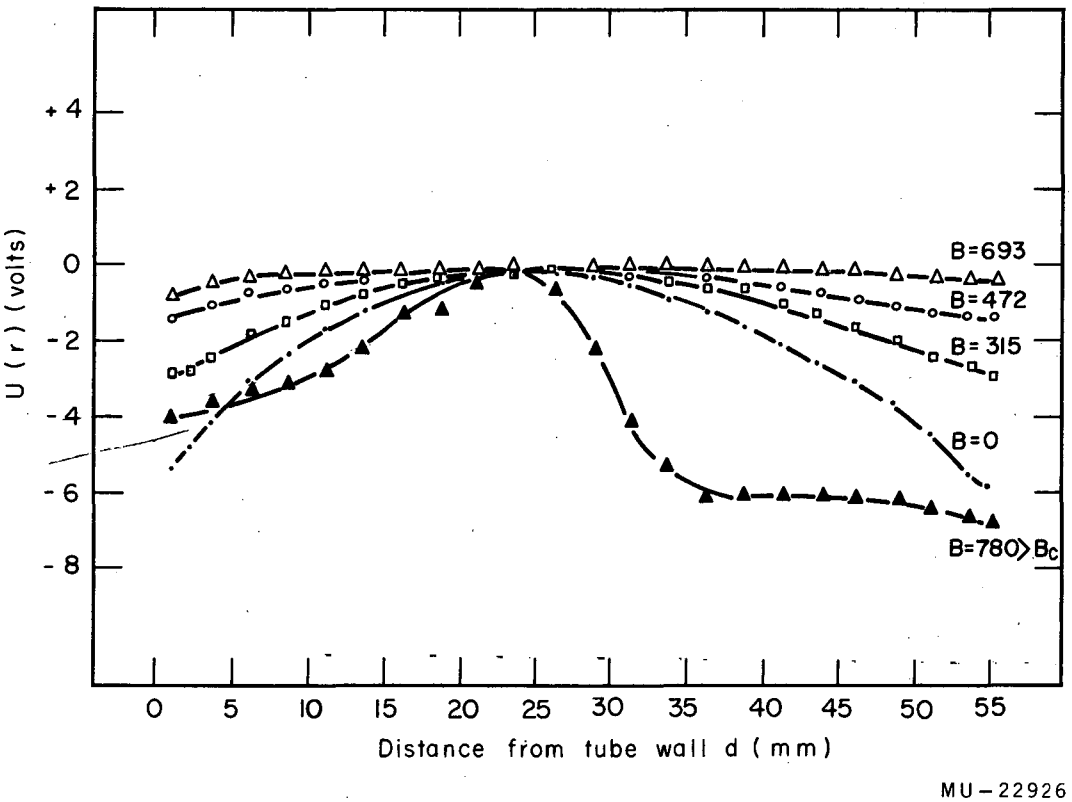

Fig. B-5. U(r) vs d curves; He gas, 0.2 mm Hg, I = 200 ma. probe and tube geometry as shown in Fig. 10; R = 2.75 cm.

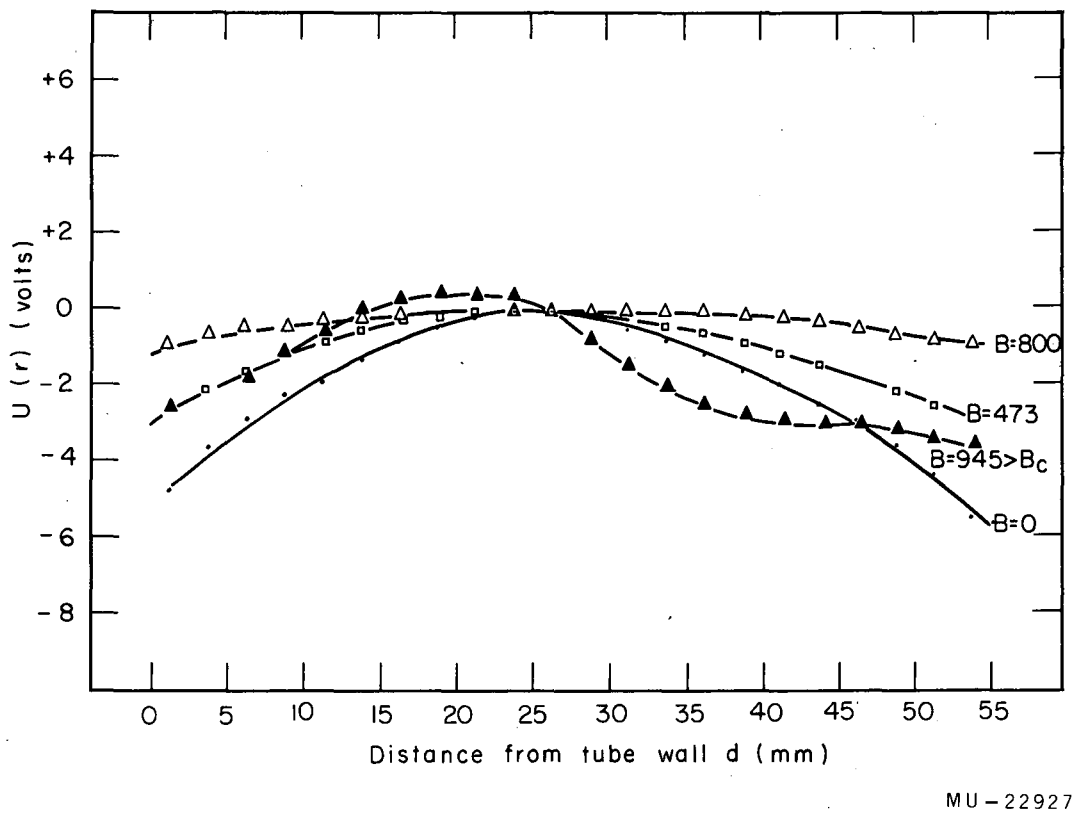

Fig. B-6. U(r) vs d curves; He gas, 0.4 mm Hg, I = 200 ma. Probe and tube geometry as shown in Fig. 10, R = 2.75 cm.

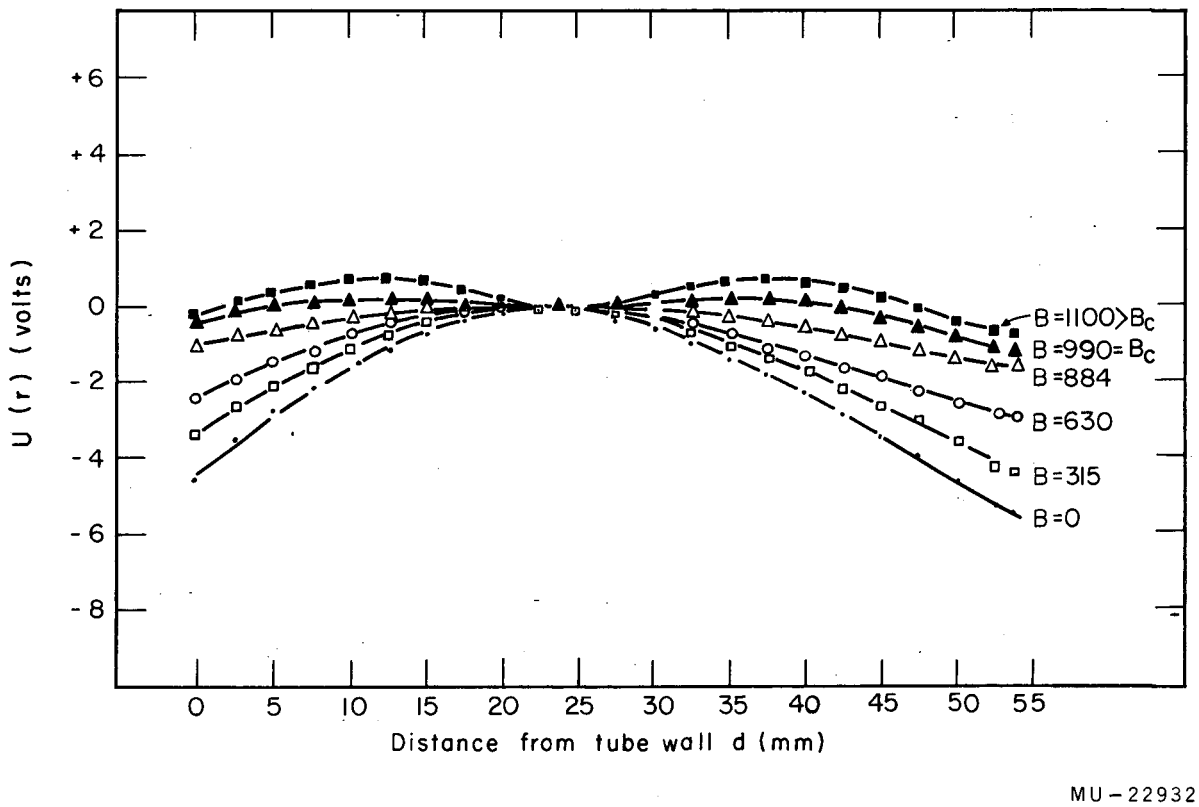

Fig. B-7. U(r) vs d curves; He gas, 0.6 mm Hg, I = 200 ma. Probe and tube geometry as shown in Fig. 10; R = 2.75 cm.

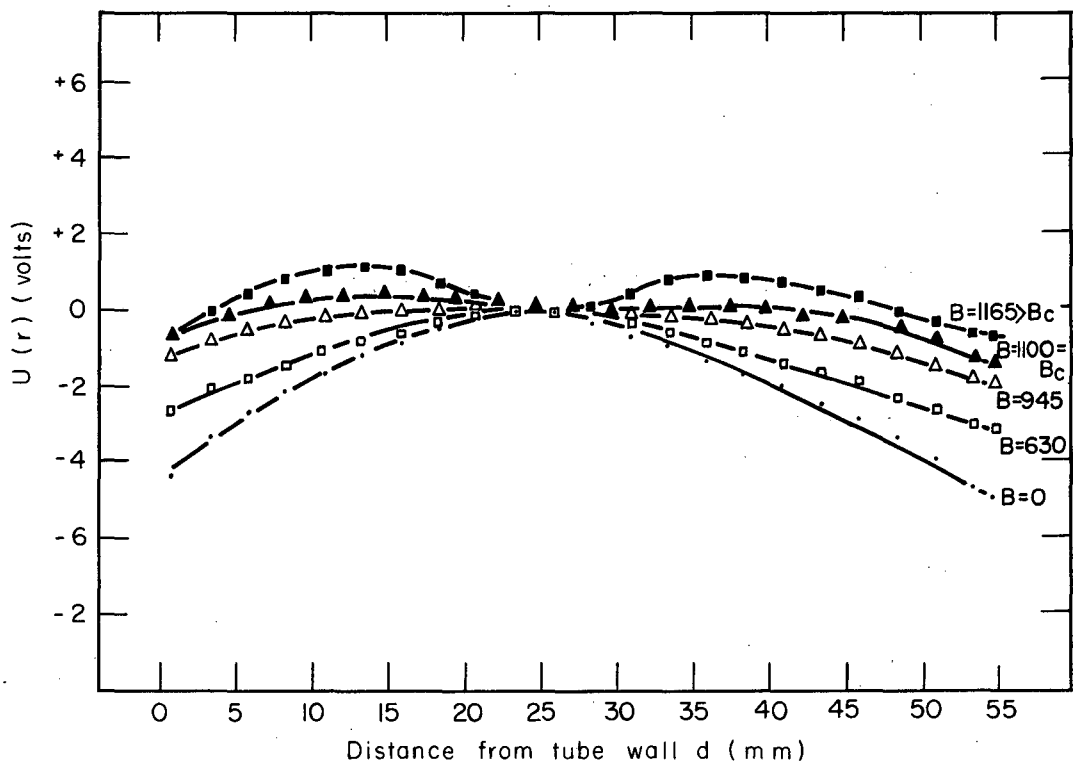

MU-22935

Fig. B-8. U(r) vs d curves; He gas, 0.9 mm Hg, I = 200 ma. Probe and tube geometry as shown in Fig. 10; R = 2.75 cm.

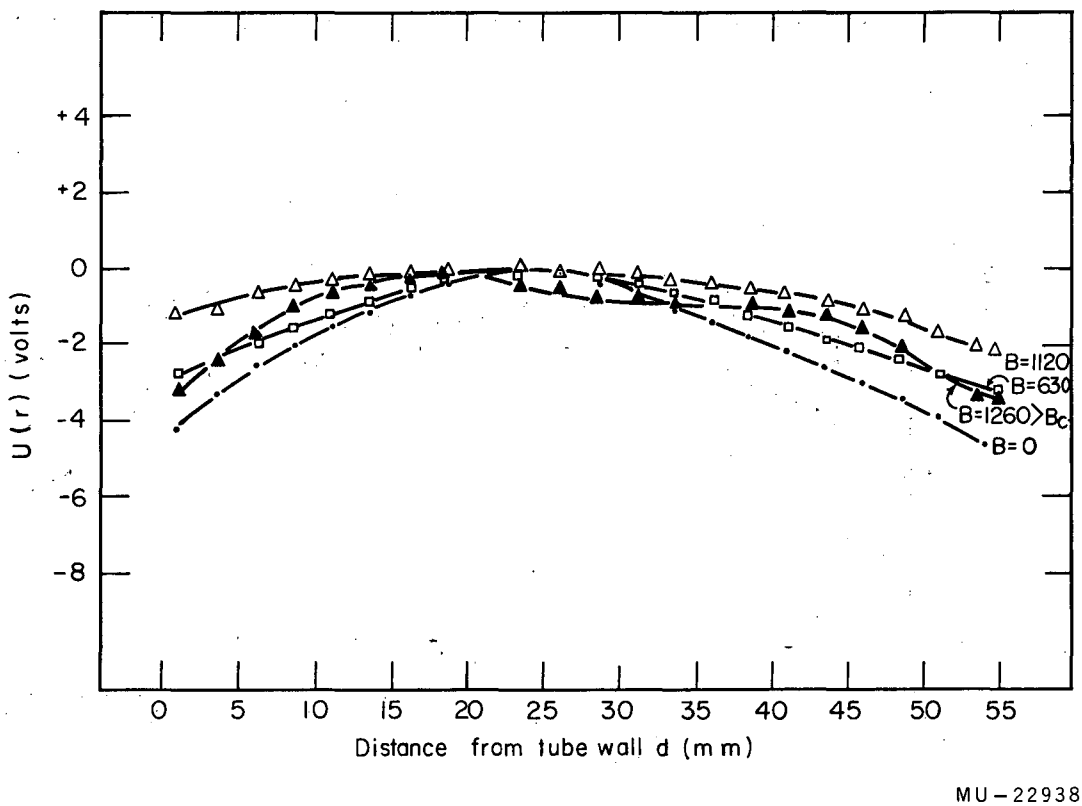

Fig. B-9. U(r) vs d curves; He gas, 1.35 mm Hg, I = 200 ma. Probe and tube geometry as shown in Fig. 10; R = 2.75 cm.

REFERENCES

1. G. Francis, in Handbuch Der Physik, Vol. 22 Ed. S. Flugge (Springer-Verlag, Berlin, 1956).

1a. L. Spitzer, Jr., Physics of Fully Ionized Gases (Interscience, New York, 1956).

2. C.S. Cummings and L. Tonks, Phys. Rev. 59, 517 (1941).

3. G.N. Rohklin, J. Phys. (USSR), 1, 347 (1939).

4. E. Reichrudel and G. Spivak, J. Phys. (USSR), 4, 211 (1941).

5. L. Tonks, Phys. Rev. 56, 360 (1939).

6. L. Tonks and I. Langmuir, Phys. Rev. 34, 876, (1929).

7. W. Schottky, Physik. Z. 25, 342 (1924).

8. D. Bohm, E.H.S. Burhop, H.S.W. Massey, and R.M. Williams, in The Characteristics of Electrical Discharges in Magnetic Fields, Eds. A. Guthrie and R.K. Wakerling (McGraw-Hill, New York, 1949).

9. A. Simon, Phys. Rev. 98, 317 (1955).

10. R.V. Neideigh, quoted by A. Simon in Proceedings of the Second United Nations International Conference on the Peaceful Uses of Atomic Energy, Vol. 32 (United Nations, Geneva, 1958), p. 343.

11. R.J. Bickerton and A. von Engel, Proc. Phys. Soc (London), B69 468 (1956).

12. B. Lehnert, in Proceedings of the Second United Nations International Conference on the Peaceful Uses of Atomic Energy, Vol. 32, (United Nations, Geneva, 1958), p. 349.

13. F.C. Hoh and B. Lehnert, Phys. Fluids 3, 600 (1960).

14. R.A. Ellis, Jr., L.P. Goldberg, and J.G. Gorman, Phys. Fluids 3, 468 (1960).

15. W.H. Bostick and M.A. Levine, Phys. Rev. 97 13 (1955).

16. J.F. Bonnal, G. Briffod, and C. Manus, Compt. rend. 250, 2859 (1960).

17. I.B. Bernstein, E.A. Frieman, R.M. Kulsrud, and M.N. Rosenbluth, Phys. Fluids 3, 136 (1960).

18. L. Spitzer, Jr., Phys. Fluids 3, 659 (1960).

19. L. B. Bierman and D. Pfirsch, Z. Naturforsch, 15a, 10, 14 (1960).
20. F. C. Hoh, Phys. Rev. Letters 4, 559 (1960).
21. B. B. Kadomtsev and A. V. Nedospasov, J. Nuclear Energy, Part C, 1, 230 (1960).
22. T. K. Allen, G. A. Paulikas and R. V. Pyle, Instability of the Positive Column in a Magnetic Field, Phys. Rev. Letters, 5, 409 (1960), and UCRL-9110, same title, (unpublished) (1960).
23. W. P. Allis and S. J. Buchsbaum, Notes on Plasma Dynamics, Summer Program (1959) MIT.
24. M. Pahl, Z. Naturforsch. 12a, 632 (1957).
25. R. L. F. Boyd and N. D. Twiddy, Proc. Roy. Soc. (London) A250, 53 (1959).
26. T. Donahue and G. H. Dieke, Phys. Rev. 81, 248 (1951).
27. E. Spenke, Z. Physik 127, 221 (1950).
28. A. von Engel, Ionized Gases (Oxford University Press, 1955).
29. G. Ecker, Phys. Fluids 4, 127 (1961).
30. L. S. Hall, On the Application of Bohm's Criterion for the Formation of a Sheath, Phys. Fluids (to be published).
31. A. W. DeSilva and J. M. Wilcox, Rev. Sci. Instr. 31, 455 (1960).
32. We are grateful to the U. S. Navy installation at Vallejo for loan of this equipment.
33. S. C. Brown, Basic Data of Plasma Physics (John Wiley and Sons, New York, 1959).
34. L. M. Chanin (Honeywell Research Center), private communication.
35. M. Pahl, Z. Naturforsch. 14a, 239 (1959).
35a. R. G. Fowler and L. W. Jones, Pressure Constriction in the Positive Column, 13th Annual Gaseous Electronics Conference, Monterey, California, Oct. 12-15, 1960.
36. R. G. Fowler, Proc. Phys. Soc. (London) B68, 130 (1955).
37. W. Pupp, Physik. Z. 34, 756 (1933).
38. O. A. Anderson, W. R. Baker, S. A. Colgate, J. Ise, Jr., and R. V. Pyle, Phys. Rev. 110, 1375 (1958).
39. D. E. Kerr, Transient Studies of Ionization and Deionization Processes in Gaseous Discharges, Johns Hopkins University, Department of Physics Report AFOSR-TR-60-110, 1959 (unpublished).

This report was prepared as an account of Government sponsored work. Neither the United States, nor the Commission, nor any person acting on behalf of the Commission:

A. Makes any warranty or representation, expressed or implied, with respect to the accuracy, completeness, or usefulness of the information contained in this report, or that the use of any information, apparatus, method, or process disclosed in this report may not infringe privately owned rights; or

B. Assumes any liabilities with respect to the use of, or for damages resulting from the use of any information, apparatus, method, or process disclosed in this report.

As used in the above, "person acting on behalf of the Commission" includes any employee or contractor of the Commission, or employee of such contractor, to the extent that such employee or contractor of the Commission, or employee of such contractor prepares, disseminates, or provides access to, any information pursuant to his employment or contract with the Commission, or his employment with such contractor.